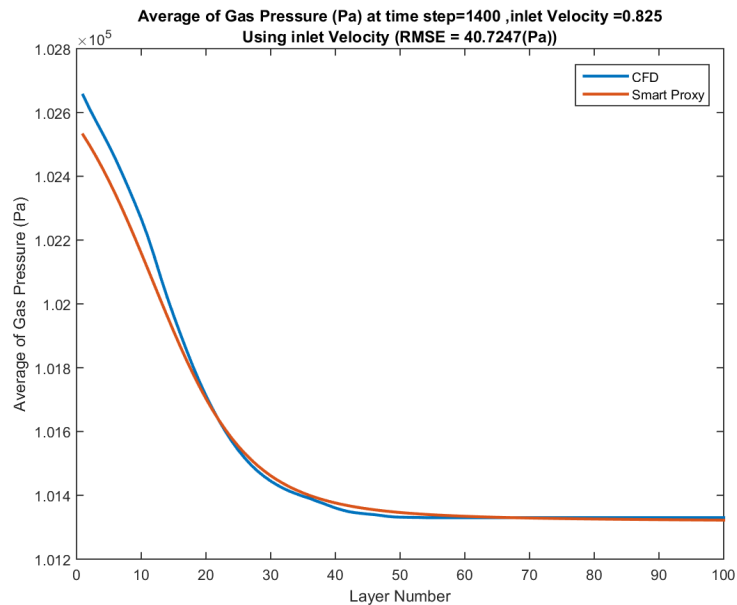




NATIONAL ENERGY TECHNOLOGY LABORATORY



## Data Driven Smart Proxy for CFD

Application of Big Data Analytics & Machine Learning in Computational Fluid Dynamics

Report Two: Model Building at the Cell Level

April 2018



U.S. DEPARTMENT OF  
**ENERGY**



NATIONAL  
ENERGY  
TECHNOLOGY  
LABORATORY

Office of Fossil Energy

NETL-PUB-21634

## Disclaimer

This report was prepared as an account of work sponsored by an agency of the United States Government. Neither the United States Government nor any agency thereof, nor any of their employees, makes any warranty, express or implied, or assumes any legal liability or responsibility for the accuracy, completeness, or usefulness of any information, apparatus, product, or process disclosed, or represents that its use would not infringe privately owned rights. Reference therein to any specific commercial product, process, or service by trade name, trademark, manufacturer, or otherwise does not necessarily constitute or imply its endorsement, recommendation, or favoring by the United States Government or any agency thereof. The views and opinions of authors expressed therein do not necessarily state or reflect those of the United States Government or any agency thereof.

**Cover Illustration:** Comparing the pressure drop at different layers of a fluidized bed generated by the Smart Proxy (red) with CFD results (blue).

**Suggested Citation:** Ansari, A., Mohaghegh, S., Shahnam, M., Dietiker, J. F., Li, T., *Data Driven Smart Proxy for CFD Application of Big Data Analytics & Machine Learning in Computational Fluid Dynamics, Part Two: Model Building at the Cell Level*; NETL-PUB-21634; NETL Technical Report Series; U.S. Department of Energy, National Energy Technology Laboratory: Morgantown, WV, 2017.

**Data Driven Smart Proxy for CFD**  
**Application of Big Data Analytics & Machine Learning in Computational Fluid Dynamics**  
**Part Two: Model Building at the Cell Level**

**Ansari, A.<sup>1</sup>, Mohaghegh, S.<sup>1,2</sup>, Shahnam, M.<sup>3</sup>, Dietiker, J. F.<sup>3,4</sup>, Li, T.<sup>3,5</sup>**

<sup>1</sup> **Petroleum & Natural Gas Engineering Department, West Virginia University**

<sup>2</sup> **ORISE Faculty Program**

<sup>3</sup> **Energy Conversion Engineering Directorate, Research and Innovation Center, U.S.  
Department of Energy, National Energy Technology Laboratory**

<sup>4</sup> **West Virginia University Research Corporation, Morgantown, WV**

<sup>5</sup> **AECOM, Morgantown, WV**

---

**NETL-PUB-21634**

April 2018

NETL Contacts:

Mehrdad Shahnam, Principal Investigator

Jonathan Lekse, Technical Portfolio Lead

David Alman, Executive Director, Research and Innovation Center

This page intentionally left blank

# Table of Contents

<b>EXECUTIVE SUMMARY .....</b>	<b>1</b>
<b>1. INTRODUCTION.....</b>	<b>2</b>
1.1 STRUCTURE OF THE WORK .....	3
<b>2. BACKGROUND .....</b>	<b>4</b>
2.1 MFiX.....	4
2.2 MACHINE LEARNING.....	6
2.2.1 <i>Artificial Neural Network</i> .....	7
2.3 PREVIOUS WORK .....	8
<b>3. METHODS .....</b>	<b>10</b>
3.1 CFD SIMULATION SETUP .....	10
3.2 PROBLEM DEFINITION .....	10
3.2.1 <i>Interpolating the inlet air velocity</i> .....	11
3.3 ARTIFICIAL NEURAL NETWORK SETUP .....	12
3.3.1 <i>Neural Network architecture</i> .....	12
3.3.2 <i>Input and output</i> .....	13
3.3.3 <i>Data partitioning</i> .....	13
3.3.4 <i>Blind test</i> .....	17
3.4 SOLUTION SCENARIOS .....	18
3.4.1 <i>Training for gas pressure using 7 static parameters</i> .....	19
3.4.2 <i>Training for gas pressure using 11 static parameters</i> .....	20
3.4.3 <i>Optimizing the ANN</i> .....	21
3.4.4 <i>Time and space average</i> .....	21
3.4.5 <i>Training for gas velocity and gas volume fraction using static parameters</i> .....	22
3.4.6 <i>Sequential modeling</i> .....	23
3.4.7 <i>Sequential modeling by considering tier system</i> .....	25
<b>4. RESULTS AND DISCUSSIONS.....</b>	<b>27</b>
4.1 PRESENTATION OF THE RESULT .....	27
4.2 TRAINING FOR GAS PRESSURE USING 7 STATIC PARAMETERS AT A SINGLE TIME STEP .....	28
4.3 TRAINING FOR GAS PRESSURE USING 11 STATIC PARAMETERS AT A SINGLE TIME STEP .....	34
4.4 OPTIMIZING THE ANN .....	43
4.5 TIME AVERAGE .....	44
4.6 TRAINING FOR GAS VELOCITY AND GAS VOLUME FRACTION USING STATIC PARAMETERS .....	53
4.7 SEQUENTIAL MODELING.....	55
4.8 SEQUENTIAL MODELING BY CONSIDERING TIER SYSTEM .....	57
<b>5. CONCLUSIONS .....</b>	<b>64</b>
5.1 RECOMMENDATIONS AND FUTURE WORKS.....	64
<b>7. APPENDIX I: GAS PRESSURE USING 7 STATIC PARAMETERS .....</b>	<b>5</b>
<b>8. APPENDIX II: GAS PRESSURE USING 11 STATIC PARAMETERS.....</b>	<b>13</b>
<b>9. APPENDIX III: TIME AVERAGE OF GAS PRESSURE BETWEEN TIME STEP 500 TO 1400) .....</b>	<b>21</b>
<b>10. APPENDIX IV: BLIND TEST RESULTS FOR TIME AVERAGE OF GAS PRESSURE BETWEEN TIME STEP 1500 TO 3400.....</b>	<b>29</b>

**11. APPENDIX V: GAS VELOCITY AND GAS VOLUME FRACTION USING  
STATIC PARAMETERS.....37**

# List of Figures

Figure 2-1	MFiX solution algorithm. ....	6
Figure 2-2	Artificial Neural Network schematic .....	7
Figure 3-1	Geometry and initial condition of the problem in SI units. ....	10
Figure 3-2	Different inlet air velocities (m/s) for MFiX simulations.....	11
Figure 3-3	Conceptual illustration of problem definition.....	12
Figure 3-4	Different flow regime .....	13
Figure 3-5	Three states of ANN training.....	14
Figure 3-6	10,000 sample points used for constructing the ANN .....	14
Figure 3-7	Data used for training the ANN .....	15
Figure 3-8	Data used for calibrating the ANN .....	15
Figure 3-9	Data used for validating the ANN .....	16
Figure 3-10	Learning curve, training error and calibration error .....	17
Figure 3-11	Different inlet air velocities (m/s) for MFiX runs .....	18
Figure 3-12	Training for gas pressure using 7 static parameters.....	19
Figure 3-13	Gas pressure ( $10^5$ Pa) at cross sectional plane $K = 7$ with (a) $V_{inlet} = 0.6$ m/s (b) $V_{inlet} = 1.2$ m/s (c) $V_{inlet} = 0.825$ m/s.....	20
Figure 3-14	Training for gas pressure using 11 static parameters.....	21
Figure 3-15	Time steps span selected for time average.....	22
Figure 3-16	Spatial cross sectional planes used for averaging .....	22
Figure 3-17	Training for gas velocity using 11 static parameters .....	23
Figure 3-18	Training for gas volume fraction using 11 static parameters.....	23
Figure 3-19	Sequential training algorithm.....	24
Figure 3-20	Training for gas velocity using 11 static parameters and gas pressure from ANN <sub>P</sub> (a total of 12 input) .....	24
Figure 3-21	Training for gas volume fraction using 11 static parameters, gas pressure from ANN <sub>P</sub> and gas velocity from ANN <sub>V</sub> .....	25
Figure 3-22	The tier system with the 6 cell in surface contact with the focal cell .....	25
Figure 3-23	Sequential training for gas velocity using tiers of gas pressure.....	26
Figure 3-24	Sequential training for gas volume fraction using tiers of gas pressure and gas velocity.....	26
Figure 4-1	Cross-sectional planes, 3 cm apart, where results are presented .....	27
Figure 4-2	Parity plot of trained ANN and CFD results for gas pressure at inlet velocity of $V_{in}$ of 1.2 m/s and time step of 1400, using 7 static parameters .....	28
Figure 4-3	Error distribution per equation 2-4 for gas pressure at inlet velocity of $V_{in}$ of 1.2 m/s and time step of 1400, using 7 static parameters .....	29
Figure 4-4	CFD and smart proxy results for gas pressure at $K=7$ cross-sectional plane for time step of 1400 and $V_{in} = 1.2$ m/s, using 7 static parameters .....	29
Figure 4-5	Parity plot of trained ANN and CFD results for gas pressure at inlet velocity of 0.9 m/s and time step of 1400, using 7 static parameters .....	30
Figure 4-6	Error distribution per equation 2-4 for gas pressure at inlet velocity of 0.9 m/s and time step of 1400, using 7 static parameters .....	31
Figure 4-7	CFD and smart proxy results for gas pressure at $K=7$ cross-sectional plane, for time step of 1400 and $V_{in}$ of 0.9 m/s, 7 static parameters.....	31

Figure 4-8	Parity plot of ANN and CFD results for gas pressure for blind test condition of inlet velocity of 0.825 m/s and time step of 1400, using 7 static parameters .....	32
Figure 4-9	Error distribution per equation 2-4 for gas pressure for blind test condition of inlet velocity of 0.825 m/s and time step of 1400, using 7 static parameters .....	32
Figure 4-10	CFD and smart proxy results for gas pressure at $K=7$ cross-sectional plane, for time step of 1400 and $V_{in}$ of 0.825 m/s, using 7 static parameters .....	33
Figure 4-11	Parity plot of trained ANN and CFD results for gas pressure at inlet velocity of $V_{in}$ of 1.2 m/s and time step of 1400, using 11 static parameters .....	34
Figure 4-12	Error distribution per equation 2-4 for gas pressure at inlet velocity of $V_{in}$ of 1.2 m/s and time step of 1400, using 11 static parameters .....	35
Figure 4-13	CFD and smart proxy results for gas pressure at $K=7$ cross-sectional plane for time step of 1400 and $V_{in} = 1.2$ m/s, using 11 static parameters .....	35
Figure 4-14	Parity plot of trained ANN and CFD results for gas pressure at inlet velocity of $V_{in}$ of 0.9 m/s and time step of 1400, using 11 static parameters .....	36
Figure 4-15	Error distribution per equation 2-4 for gas pressure at inlet velocity of $V_{in}$ of 0.9 m/s and time step of 1400, using 11 static parameters .....	36
Figure 4-16	CFD and smart proxy results for gas pressure at $K=7$ cross-sectional plane for time step of 1400 and $V_{in} = 0.9$ m/s, using 11 static parameters .....	37
Figure 4-17	Parity plot of ANN and CFD results for gas pressure for blind test condition of inlet velocity of 0.825 m/s and time step of 1400, using 11 static parameters .....	37
Figure 4-18	Error distribution per equation 2-4 for gas pressure for blind test condition of inlet velocity of 0.825 m/s and time step of 1400, using 11 static parameters .....	38
Figure 4-19	CFD and smart proxy results for gas pressure at $K=7$ cross-sectional plane for time step of 1400 and $V_{in} = 0.825$ m/s, using 11 static parameters .....	38
Figure 4-20	Zooming in to the parity plot of trained ANN for gas pressure at inlet velocity of 1.2 m/s and time step of 1400, using 11 static parameters .....	40
Figure 4-21	Zooming in to the parity plot for trained ANN for gas pressure at inlet velocity of 0.9 m/s and time step of 1400, using 11 static parameters .....	40
Figure 4-22	Cells, where the gas pressure is underpredicted by ANN, for time step of 1400, when (a) $V_{in}=1.2$ m/s (b) $V_{in}=0.9$ m/s (c) $V_{in}=0.6$ m/s .....	41
Figure 4-23	Temporal average of CFD and smart proxy results at training for gas pressure, spatially averaged along the fluidized bed at time step=1400 and $V_{in}=0.9$ m/s ...	42
Figure 4-24	Temporal average of CFD and smart proxy results at deployment for gas pressure, spatially averaged along the fluidized bed at time step=1400 and $V_{in}=0.825$ m/s	42
Figure 4-25	Optimized CFD and smart proxy results at deployment for gas pressure, spatially averaged along the fluidized bed at time step=1400 and $V_{in}=0.825$ m/s.....	44
Figure 4-26	Time steps used in time average between time steps 500 to 1400.....	45
Figure 4-27	CFD and smart proxy results for gas pressure averaged over time steps 500 to 1400 at $K=7$ cross-sectional plane with $V_{in}=0.825$ m/s.....	45
Figure 4-28	Time averaged CFD and smart proxy results for gas pressure, spatially averaged along the fluidized bed (time-steps = 500 to 1400 and $V_{in} = 0.825$ m/s).....	46
Figure 4-29	Additional blind tests at $V_{in} = 0.72$ and $V_{in} = 1.02$ m/s .....	46
Figure 4-30	CFD and smart proxy results for gas pressure averaged over time steps 500 to 1400 at $K=7$ cross-sectional plane with $V_{in}=0.72$ m/s.....	47
Figure 4-31	Time averaged CFD and smart proxy results for gas pressure, spatially averaged along the fluidied bed (time-steps = 500 to 1400 and $V_{in} = 0.72$ m/s).....	47

---

Figure 4-32	CFD and smart proxy results for gas pressure averaged over time steps 500 to 1400 at $K=7$ cross-sectional plane with $V_{in}=1.02$ m/s.....	48
Figure 4-33	Time averaged CFD and smart proxy results for gas pressure, spatially averaged along the fluidized bed (time-steps = 500 to 1400 and $V_{in} = 1.02$ m/s).....	49
Figure 4-34	Time steps used for time averaging between time steps 1500 to 3400.....	49
Figure 4-35	Blind test carried out at three different inlet velocities.....	50
Figure 4-36	CFD and smart proxy results for gas pressure averaged over time steps 1500 to 3400 at $K=7$ cross-sectional plane with $V_{in}=0.825$ m/s.....	50
Figure 4-37	Time averaged CFD and smart proxy results for gas pressure, spatially averaged along the fluidized bed (time-steps = 1500 to 3400 and $V_{in} = 0.825$ m/s).....	51
Figure 4-38	CFD and smart proxy results for gas pressure averaged over time steps 1500 to 3400 at $K=7$ cross-sectional plane with $V_{in}=1.02$ m/s.....	51
Figure 4-39	Time averaged CFD and smart proxy results for gas pressure, spatially averaged along the fluidied bed (time-steps = 1500 to 3400 and $V_{in} = 1.02$ m/s).....	52
Figure 4-40	CFD and smart proxy results for gas pressure averaged over time steps 1500 to 3400 at $K=7$ cross-sectional plane with $V_{in}=1.1$ m/s.....	52
Figure 4-41	Time averaged CFD and smart proxy results for gas pressure, spatially averaged along the fluidized bed (time-steps = 1500 to 3400 and $V_{in} = 1.1$ m/s).....	53
Figure 4-42	CFD and smart proxy results for gas velocity at time step=1400, $V_{in}=0.9$ m/s and $K = 7$ cross-sectional plane, using 11 static parameters .....	54
Figure 4-43	CFD and smart proxy results for gas volume fraction at time step=1400, $V_{in}=0.9$ m/s and $K = 7$ cross-sectional plane, using 11 static parameters.....	54
Figure 4-44	Changing the order of sequential training algorithm .....	55
Figure 4-45	Training for gas volume fraction using 11 static parameters and gas pressure ....	56
Figure 4-46	Spatially averaged CFD and smart proxy results for gas volume fraction at time step = 1400 and $V_{in}=0.825$ m/s .....	56
Figure 4-47	Sequential training for gas volume fraction using gas pressure and tier cells .....	57
Figure 4-48	Spatially averaged profile of CFD and smart proxy results for gas volume fraction at time step of 1400 and $V_{in} = 0.825$ m/s, when tier cells are used .....	58
Figure 4-49	Spatial average profile of CFD and smart proxy results for gas volume fraction, averaged over time steps 1500 to 3400 at inlet velocity of 0.6 m/s.....	59
Figure 4-50	Spatial average profile of CFD and smart proxy results for gas volume fraction, averaged over time steps 1500 to 3400 at inlet velocity of 0.69 m/s.....	59
Figure 4-51	Spatial average profile of CFD and smart proxy results for gas volume fraction, averaged over time steps 1500 to 3400 at inlet velocity of 0.75 m/s.....	60
Figure 4-52	Spatial average profile of CFD and smart proxy results for gas volume fraction, averaged over time steps 1500 to 3400 at inlet velocity of 0.9 m/s.....	60
Figure 4-53	Spatial average profile of CFD and smart proxy results for gas volume fraction, averaged over time steps 1500 to 3400 at inlet velocity of 0.94 m/s.....	61
Figure 4-54	Spatial average profile of CFD and smart proxy results for gas volume fraction, averaged over time steps 1500 to 3400 at inlet velocity of 1.05 m/s.....	61
Figure 4-55	Spatial average profile of CFD and smart proxy results for gas volume fraction, averaged over time steps 1500 to 3400 at inlet velocity of 1.2 m/s.....	62
Figure 4-56	Spatial average profile of CFD and smart proxy results for gas volume fraction, averaged over time steps 1500 to 3400 at inlet velocity of 0.825 m/s.....	62

---

Figure 4-57	Spatial average profile of CFD and smart proxy results for gas volume fraction, averaged over time steps 1500 to 3400 at inlet velocity of 1.02 m/s.....	63
Figure 4-58	Spatial average profile of CFD and smart proxy results for gas volume fraction, averaged over time steps 1500 to 3400 at inlet velocity of 1.1 m/s.....	63
Figure 7-1	CFD and smart proxy results for gas pressure at K=1 cross-sectional plane for time step of 1400 and $V_{in}$ of 1.2 m/s, using 7 static parameters .....	5
Figure 7-2	CFD and smart proxy results for gas pressure at K=7 cross-sectional plane for time step of 1400 and $V_{in}$ of 1.2 m/s, using 7 static parameters .....	5
Figure 7-3	CFD and smart proxy results for gas pressure at K=14 cross-sectional plane for time step of 1400 and $V_{in}$ of 1.2 m/s, using 7 static parameters .....	6
Figure 7-4	CFD and smart proxy results for gas pressure at K=21 cross-sectional plane for time step of 1400 and $V_{in}$ of 1.2 m/s, using 7 static parameters .....	6
Figure 7-5	CFD and smart proxy results for gas pressure at K=27 cross-sectional plane for time step of 1400 and $V_{in}$ of 1.2 m/s, using 7 static parameters .....	7
Figure 7-6	CFD and smart proxy results for gas pressure at K=1 cross-sectional plane for time step of 1400 and $V_{in}$ of 0.9 m/s, using 7 static parameters .....	7
Figure 7-7	CFD and smart proxy results for gas pressure at K=7 cross-sectional plane for time step of 1400 and $V_{in}$ of 0.9 m/s, using 7 static parameters .....	8
Figure 7-8	CFD and smart proxy results for gas pressure at K=14 cross-sectional plane for time step of 1400 and $V_{in}$ of 0.9 m/s, using 7 static parameters .....	8
Figure 7-9	CFD and smart proxy results for gas pressure at K=21 cross-sectional plane for time step of 1400 and $V_{in}$ of 0.9 m/s, using 7 static parameters .....	9
Figure 7-10	CFD and smart proxy results for gas pressure at K=27 cross-sectional plane for time step of 1400 and $V_{in}$ of 0.9 m/s, using 7 static parameters .....	9
Figure 7-11	CFD and smart proxy results for gas pressure at K=1 cross-sectional plane for time step of 1400 and $V_{in}$ of 0.825 m/s, using 7 static parameters .....	10
Figure 7-12	CFD and smart proxy results for gas pressure at K=7 cross-sectional plane for time step of 1400 and $V_{in}$ of 0.825 m/s, using 7 static parameters .....	10
Figure 7-13	CFD and smart proxy results for gas pressure at K=14 cross-sectional plane for time step of 1400 and $V_{in}$ of 0.825 m/s, using 7 static parameters .....	11
Figure 7-14	CFD and smart proxy results for gas pressure at K=21 cross-sectional plane for time step of 1400 and $V_{in}$ of 0.825 m/s, using 7 static parameters .....	11
Figure 7-15	CFD and smart proxy results for gas pressure at K=27 cross-sectional plane for time step of 1400 and $V_{in}$ of 0.825 m/s, using 7 static parameters .....	12
Figure 8-1	CFD and smart proxy results for gas pressure at K=1 cross-sectional plane for time step of 1400 and $V_{in}$ of 1.2 m/s, using 11 static parameters .....	13
Figure 8-2	CFD and smart proxy results for gas pressure at K=7 cross-sectional plane for time step of 1400 and $V_{in}$ of 1.2 m/s, using 11 static parameters .....	13
Figure 8-3	CFD and smart proxy results for gas pressure at K=14 cross-sectional plane for time step of 1400 and $V_{in}$ of 1.2 m/s, using 11 static parameters .....	14
Figure 8-4	CFD and smart proxy results for gas pressure at K=21 cross-sectional plane for time step of 1400 and $V_{in}$ of 1.2 m/s, using 11 static parameters .....	14
Figure 8-5	CFD and smart proxy results for gas pressure at K=27 cross-sectional plane for time step of 1400 and $V_{in}$ of 1.2 m/s, using 11 static parameters .....	15
Figure 8-6	CFD and smart proxy results for gas pressure at K=1 cross-sectional plane for time step of 1400 and $V_{in}$ of 0.9 m/s, using 11 static parameters .....	15

Figure 8-7	CFD and smart proxy results for gas pressure at K=7 cross-sectional plane for time step of 1400 and $V_{in}$ of 0.9 m/s, using 11 static parameters .....	16
Figure 8-8	CFD and smart proxy results for gas pressure at K=14 cross-sectional plane for time step of 1400 and $V_{in}$ of 0.9 m/s, using 11 static parameters .....	16
Figure 8-9	CFD and smart proxy results for gas pressure at K=21 cross-sectional plane for time step of 1400 and $V_{in}$ of 0.9 m/s, using 11 static parameters .....	17
Figure 8-10	CFD and smart proxy results for gas pressure at K=27 cross-sectional plane for time step of 1400 and $V_{in}$ of 0.9 m/s, using 11 static parameters .....	17
Figure 8-11	CFD and smart proxy results for gas pressure at K=1 cross-sectional plane for time step of 1400 and $V_{in}$ of 0.825 m/s, using 11 static parameters .....	18
Figure 8-12	CFD and smart proxy results for gas pressure at K=7 cross-sectional plane for time step of 1400 and $V_{in}$ of 0.825 m/s, using 11 static parameters .....	18
Figure 8-13	CFD and smart proxy results for gas pressure at K=14 cross-sectional plane for time step of 1400 and $V_{in}$ of 0.825 m/s, using 11 static parameters .....	19
Figure 8-14	CFD and smart proxy results for gas pressure at K=21 cross-sectional plane for time step of 1400 and $V_{in}$ of 0.825 m/s, using 11 static parameters .....	19
Figure 8-15	CFD and smart proxy results for gas pressure at K=27 cross-sectional plane for time step of 1400 and $V_{in}$ of 0.825 m/s, using 11 static parameters .....	20
Figure 9-1	CFD and smart proxy results for gas pressure averaged over time steps 500 to 1400 at K=1 cross-sectional plane and $V_{in}=0.825$ m/s .....	21
Figure 9-2	CFD and smart proxy results for gas pressure avergaed over time steps 500 to 1400 at K=7 cross-sectional plane and $V_{in}=0.825$ m/s .....	21
Figure 9-3	CFD and smart proxy results for gas pressure avergaed over time steps 500 to 1400 at K=14 cross-sectional plane and $V_{in}=0.825$ m/s .....	22
Figure 9-4	CFD and smart proxy results for gas pressure avergaed over time steps 500 to 1400 at K=21 cross-sectional plane and $V_{in}=0.825$ m/s .....	22
Figure 9-5	CFD and smart proxy results for gas pressure avergaed over time steps 500 to 1400 at K=27 cross-sectional plane and $V_{in}=0.825$ m/s .....	23
Figure 9-6	CFD and smart proxy results for gas pressure avergaed over time steps 500 to 1400 at K=1 cross-sectional plane and $V_{in}=0.72$ m/s .....	23
Figure 9-7	CFD and smart proxy results for gas pressure avergaed over time steps 500 to 1400 at K=7 cross-sectional plane and $V_{in}=0.72$ m/s .....	24
Figure 9-8	CFD and smart proxy results for gas pressure avergaed over time steps 500 to 1400 at K=17 cross-sectional plane and $V_{in}=0.72$ m/s .....	24
Figure 9-9	CFD and smart proxy results for gas pressure avergaed over time steps 500 to 1400 at K=21 cross-sectional plane and $V_{in}=0.72$ m/s .....	25
Figure 9-10	CFD and smart proxy results for gas pressure avergaed over time steps 500 to 1400 at K=27 cross-sectional plane and $V_{in}=0.72$ m/s .....	25
Figure 9-11	CFD and smart proxy results for gas pressure avergaed over time steps 500 to 1400 at K=1 cross-sectional plane and $V_{in}=1.02$ m/s .....	26
Figure 9-12	CFD and smart proxy results for gas pressure avergaed over time steps 500 to 1400 at K=7 cross-sectional plane and $V_{in}=1.02$ m/s .....	26
Figure 9-13	CFD and smart proxy results for gas pressure avergaed over time steps 500 to 1400 at K=14 cross-sectional plane and $V_{in}=1.02$ m/s .....	27
Figure 9-14	CFD and smart proxy results for gas pressure avergaed over time steps 500 to 1400 at K=21 cross-sectional plane and $V_{in}=1.02$ m/s .....	27

Figure 9-15	CFD and smart proxy results for gas pressure avergaed over time steps 500 to 1400 at K=27 cross-sectional plane and $V_{in}=1.02$ m/s .....	28
Figure 10-1	CFD and smart proxy results for gas pressure avergaed over time steps 1500 to 3400 at K=1 cross-sectional plane and $V_{in}=0.825$ m/s .....	29
Figure 10-2	CFD and smart proxy results for gas pressure avergaed over time steps 1500 to 3400 at K=7 cross-sectional plane and $V_{in}=0.825$ m/s .....	29
Figure 10-3	CFD and smart proxy results for gas pressure avergaed over time steps 1500 to 3400 at K=14 cross-sectional plane and $V_{in}=0.825$ m/s .....	30
Figure 10-4	CFD and smart proxy results for gas pressure avergaed over time steps 1500 to 3400 at K=21 cross-sectional plane and $V_{in}=0.825$ m/s .....	30
Figure 10-5	CFD and smart proxy results for gas pressure avergaed over time steps 1500 to 3400 at K=27 cross-sectional plane and $V_{in}=0.825$ m/s .....	31
Figure 10-6	CFD and smart proxy results for gas pressure avergaed over time steps 1500 to 3400 at K=1 cross-sectional plane and $V_{in}=1.02$ m/s .....	31
Figure 10-7	CFD and smart proxy results for gas pressure avergaed over time steps 1500 to 3400 at K=7 cross-sectional plane and $V_{in}=1.02$ m/s .....	32
Figure 10-8	CFD and smart proxy results for gas pressure avergaed over time steps 1500 to 3400 at K=7 cross-sectional plane and $V_{in}=1.02$ m/s .....	32
Figure 10-9	CFD and smart proxy results for gas pressure avergaed over time steps 1500 to 3400 at K=21 cross-sectional plane and $V_{in}=1.02$ m/s .....	33
Figure 10-10	CFD and smart proxy results for gas pressure avergaed over time steps 1500 to 3400 at K=27 cross-sectional plane and $V_{in}=1.02$ m/s .....	33
Figure 10-11	CFD and smart proxy results for gas pressure avergaed over time steps 1500 to 3400 at K=1 cross-sectional plane and $V_{in}=1.1$ m/s .....	34
Figure 10-12	CFD and smart proxy results for gas pressure avergaed over time steps 1500 to 3400 at K=7 cross-sectional plane and $V_{in}=1.1$ m/s .....	35
Figure 10-13	CFD and smart proxy results for gas pressure avergaed over time steps 1500 to 3400 at K=14 cross-sectional plane and $V_{in}=1.1$ m/s .....	35
Figure 10-14	CFD and smart proxy results for gas pressure avergaed over time steps 1500 to 3400 at K=21 cross-sectional plane and $V_{in}=1.1$ m/s .....	36
Figure 10-15	CFD and smart proxy results for gas pressure avergaed over time steps 1500 to 3400 at K=27 cross-sectional plane and $V_{in}=1.1$ m/s .....	36
Figure 11-1	CFD and smart proxy results for gas velocity at time step=1400, $V_{in}=0.9$ m/s and K=1 cross-sectional plane, using 11 static parameters .....	37
Figure 11-2	CFD and smart proxy results for gas velocity at time step=1400, $V_{in}=0.9$ m/s and K=7 cross-sectional plane, using 11 static parameters .....	37
Figure 11-3	CFD and smart proxy results for gas velocity at time step=1400, $V_{in}=0.9$ m/s and K=4 cross-sectional plane, using 11 static parameters .....	38
Figure 11-4	CFD and smart proxy results for gas velocity at time step=1400, $V_{in}=0.9$ m/s and K=21 cross-sectional plane, using 11 static parameters .....	38
Figure 11-5	CFD and smart proxy results for gas velocity at time step=1400, $V_{in}=0.9$ m/s and K=27 cross-sectional plane, using 11 static parameters .....	39
Figure 11-6	CFD and smart proxy results for gas volume fraction at time step=1400, $V_{in}=0.9$ m/s and K=1 cross-sectional plane, using 11 static parameters.....	39
Figure 11-7	CFD and smart proxy results for gas volume fraction at time step=1400, $V_{in}=0.9$ m/s and K=7 cross-sectional plane, using 11 static parameters.....	40

Figure 11-8 CFD and smart proxy results for gas volume fraction at time step=1400,  $V_{in}=0.9$  m/s and  $K=14$  cross-sectional plane, using 11 static parameters..... 40

Figure 11-9 CFD and smart proxy results for gas volume fraction at time step=1400,  $V_{in}=0.9$  m/s and  $K=21$  cross-sectional plane, using 11 static parameters..... 41

Figure 11-10 CFD and smart proxy results for gas volume fraction at time step=1400,  $V_{in}=0.9$  m/s and  $K=27$  cross-sectional plane, using 11 static parameters..... 41

## List of Tables

Table 2-1	Multiphase Flow Modeling Approaches [11].....	5
Table 3-1	Original data partitioning.....	17
Table 3-2	Important numbers in Neural Network Model.....	19
Table 3-3	ANN model parameters .....	21
Table 4-1	$R^2$ of different training scenarios .....	39
Table 4-2	Some of the ANN internal parameters before and after optimization .....	43
Table 4-3	Quality of training $R^2$ with and without using gas pressure .....	55
Table 5-1	Execution time for CFD and smart proxy.....	64

# Acronyms, Abbreviations, and Symbols

Term	Description
<b>AI</b>	Artificial Intelligence
<b>ANN</b>	Artificial Neural Network
<b>CFD</b>	Computational Fluid Dynamics
<b>CSV</b>	Comma Separated Value
<b>DM</b>	Data Mining
<b>EIA</b>	Energy Information Administration
<b>IGCC</b>	Integrated Coal Gasification Combined Cycle
<b>KPI</b>	Key Performance Indicator
<b>MFIX</b>	Multiphase Flow with Interphase eXchange
<b>MSE</b>	Mean Square Error
<b>NETL</b>	National Energy Technology Laboratory
<b>PDE</b>	Partial Differential Equation
<b>RMSE</b>	Root Square of Mean Square Error
<b>VTU</b>	Visualization Toolkit Unstructured points data
<b>UQ</b>	Uncertainty Quantification

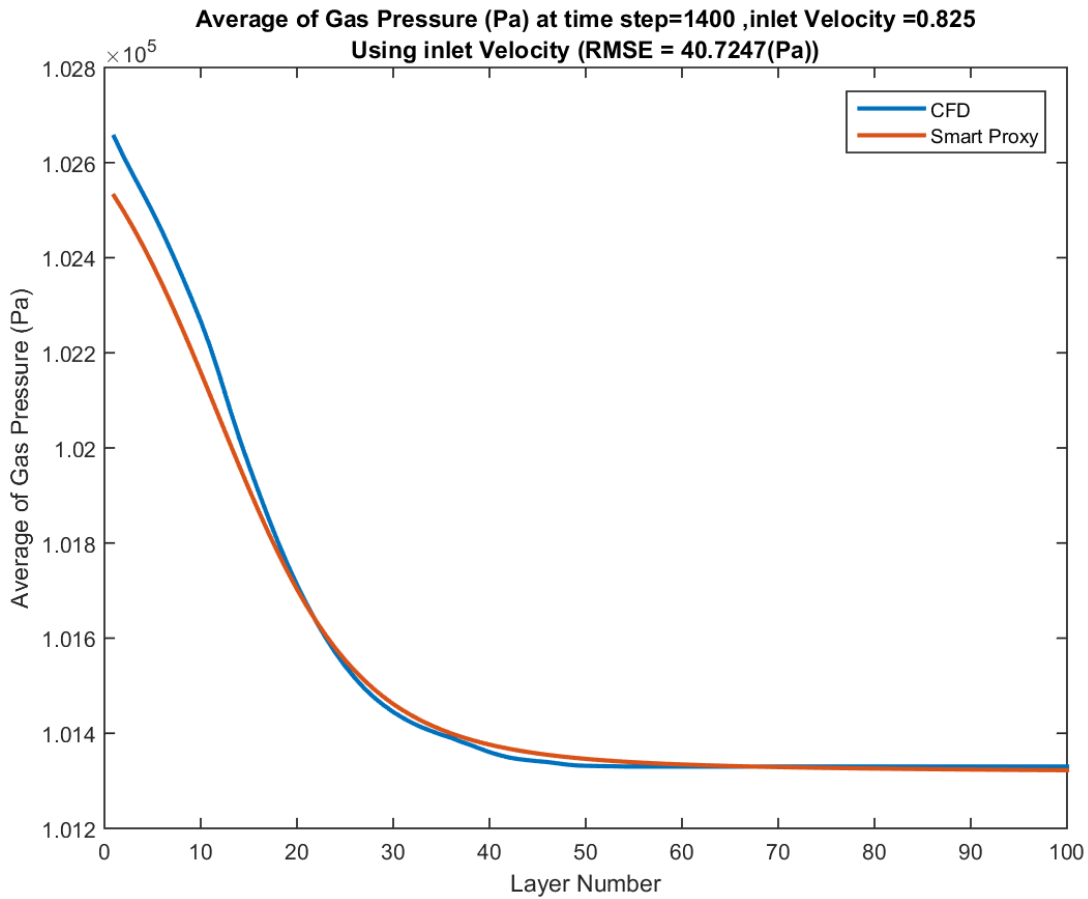
# Acknowledgments

Professor Mohaghegh acknowledges the support provided by an appointment to the National Energy Technology Laboratory (NETL) Faculty Research Participation Program, sponsored by the U.S. Department of Energy and administered by the Oak Ridge Institute for Science and Education. The authors would like to express their appreciation to Dr. Aytekin Gel from ALPEMI Consulting, LLC for his valuable comments. This work is performed as part of NETL research for the U.S. Department of Energy's Cross Cutting Program.

**EXECUTIVE SUMMARY**

To ensure the usefulness of simulation technologies in practice, their credibility needs to be established with Uncertainty Quantification (UQ) methods. In this project, smart proxy is introduced to significantly reduce the computational cost of conducting large number of multiphase CFD simulations, which is typically required for non-intrusive UQ analysis. Smart proxy for CFD models are developed using pattern recognition capabilities of Artificial Intelligence (AI) and Data Mining (DM) technologies.

Several CFD simulation runs with different inlet air velocities for a rectangular fluidized bed are used to create a smart CFD proxy that is capable of replicating the CFD results for the entire geometry and inlet velocity range. The smart CFD proxy is validated with blind CFD runs (CFD runs that have not played any role during the development of the smart CFD proxy). The developed and validated smart CFD proxy generates its results in seconds with reasonable error (less than 10%). Upon completion of this project, UQ studies that rely on hundreds or thousands of smart CFD proxy runs can be accomplished in minutes. Following figure demonstrates a validation example (blind CFD run) showing the results from the MFiX simulation and the smart CFD proxy for pressure distribution across a fluidized bed at a given time-step (the layer number corresponds to the vertical location in the bed).



## 1. INTRODUCTION

Fossil fuel continues to be a reliable source of energy for power generation in the United States and worldwide. Technologies, such as chemical looping and gasification, aim to reduce the carbon emission of fossil fuel based power plants. Simulation technologies can reduce the time and cost of the development and deployment of such advanced technologies and allow rapid scale-up of these technologies. Simulation can be used to test new designs to ensure reliable operation under a variety of operating conditions. However, to ensure their usefulness in practice, the credibility of the simulations needs to be established with Uncertainty Quantification (UQ) methods. To this end, National Energy Technology Laboratory (NETL) has been applying non-intrusive UQ methodologies to categorize and quantify uncertainties in CFD simulations of gas-solid multiphase flows, which are encountered in fossil fuel based energy systems [1, 2, 3, 4]. Gas-solid flows are inherently highly unsteady and chaotic flows, where sharp discontinuity can exist at the interface between phases. The challenge in CFD simulation of gas-solid flows is to adequately resolve the structures that exist at different spatial and temporal scales in an inherently transient flow. Additionally, in reacting gas-solid flow simulations, small time steps are needed in order to not only resolve the temporal scales of the flow, but also ensure numerical stability of the solution. A rule of thumb for adequate spatial resolution is for the grid spacing to be about 10 times the particle diameter [5]. The grid requirement for maintaining such a ratio of grid size to particle diameter for smaller size particles makes such simulations computationally costly and impractical [4]. Recent work at NETL [4] has shown the number of simulations, which is required for non-intrusive uncertainty quantification, can easily exceed many tens of simulations. The spatial and temporal resolution requirements for multiphase flows make CFD simulations computationally expensive and potentially beyond the reach of many design analysts.

It is clear that a paradigm shift in simulation technology is needed in order to make reacting gas-solid flow CFD simulations with appropriate grid resolution more practical for design and optimization purposes during design scale up. To accelerate the design and analysis process, high fidelity surrogate models that can capture the flow behavior of the design under consideration can be utilized. Surrogate models are increasingly used in design exploration, optimization and sensitivity analysis. Advances in big data analytics and machine learning has enabled the possibility of construction of data fitted metamodels (aka surrogate models), which can adequately duplicate the behavior of the CFD model results that was used for their construction. This new technology has been successfully applied in the upstream petroleum industry [6] [7] [8] [9]. Smart Proxy modeling takes advantage of pattern recognition capabilities of artificial intelligence and machine learning to build powerful tools to predict the behavior of a system with far less computational cost compared to traditional CFD simulators.

The goal of this research project is to build a smart proxy model at the cell level, which is constructed from simulation data generated by high fidelity CFD models to, in effect, replace the use of computationally expensive CFD for the design space under study for further analysis and optimization. When compared to traditional proxy modeling techniques such as Reduced Order Models (ROM), the advantage of smart proxy is associated with its unique characteristics of (a) not simplifying the physics of the original CFD model, and (b) not reducing the resolution (in time and space) of the original CFD model. The smart proxy can be used to perform non-intrusive uncertainty quantification analysis in order to quantify errors and uncertainties that are inherent in any simulation and to quantify uncertainties in the model predictions that result from the

---

uncertainties in the input variables. The smart proxy could potentially allow the user to explore the performance of the design, well beyond the CFD simulation time window. In other words, few hundred seconds of CFD simulation time can be used to construct a smart proxy, which can be used to explore the design performance of the unit after many hours of performance. The uniqueness of this approach is in:

1. Developing a unique engineering-based data preparation technology that optimizes the training of the neural networks. This innovative technique incorporates supervised fuzzy cluster analysis to:
  - a. Identify the most influential parameters for the training process, and
  - b. Identify the optimum partitioning of the data for training, calibration and validation.
2. Unique, innovative, and optimum preparation of the raw data extracted from the CFD for the training, calibration, and validation of a series of neural networks that together will form the final CFD smart proxy.
3. Using an “ensemble-based” approach to building the smart proxy, taking advantage of multiple neural networks and intelligent agents to accomplish the objectives of the project.

## **1.1 STRUCTURE OF THE WORK**

The research and development concentrating on the CFD smart proxy modeling will be presented in multiple reports. Each report will concentrate on a major portion of the research work and accomplishments that are useful to the general research community. The report presented in this document summarizes the building of the data driven predictive models at the cell level for replicating the CFD simulation for the UQ purpose. This report includes five chapters. In chapter one (this chapter), the problem was defined, and the final objective of the research was articulated.

In chapter two, a brief definition of multiphase flow and its governing equations are provided to lay the groundwork for understanding the engineering and scientific details associate with the CFD model being studied. Also, the literature about the use of AI and Machine Learning related to fluid dynamics problems, is reviewed (this chapter is repeated in all four reports associated with this project in order to make each report to serve as a standalone document).

Chapter three discusses the methodology and the machine learning method, which is used in this research. The artificial neural network with all the required information is introduced in this chapter. The network architecture with all input and output system are presented and discussed. Results and discussions are presented in chapter four, and finally, the conclusions and recommendations for the next phase of the research are presented in chapter five

## 2. BACKGROUND

This section of the report is dedicated to providing some basic, but necessary background on three major components of this research work.

### 2.1 MFiX

Multiphase flows, both reacting and non-reacting, are part of many processes in power generation and chemical processing industries. As expressed earlier, CFD is a valuable tool in design and optimization of processes and reactors used in these industries. NETL has been in the forefront of developing CFD modeling tools that can help engineers and designers in improving the performance of processes such as gasification, chemical looping. The MFiX (Multiphase Flow with Interphase eXchanges) suite of CFD software [10] is an open-source, general purpose multiphase CFD software suitable for modeling the hydrodynamics, along with heat transfer and chemical reaction for a wide spectrum of flow conditions (dilute to dense). Multiphase flows can be modeled either in a continuum (Eulerian) framework, a Lagrangian framework or a hybrid Eulerian-Lagrangian framework. The two frameworks can be summarized as follow:

- Continuum (Eulerian): Both solid phase and gas phase are treated as interpenetrating continuum (Two Fluid Model, TFM). Multiple solid phases can be used to describe multiple solid particles of different sizes and properties (Multi Fluid Model, MFM). Continuum approach is computationally less intensive but it cannot easily capture particle scale details such as particle size distribution, particle shape and many others [11].
- Discrete Particle (Lagrangian): Track each particle in the fluid by using Newton's Law of motion. This method is more straightforward to apply, even in multiphase flow, but the computational cost is high [11].

There are several approaches to modeling multiphase gas-solid flows. Depending on the application, either the gas phase or the solid phase or both phases can be modeled in Eulerian or Lagrangian framework [11] [12] [13]. Table 2-1 shows the different modeling approaches to gas-solid multiphase flow modeling. In the present work, the MFiX-TFM is used to model a rectangular 3D fluidized bed. MFiX-TFM treats both the gas phase and particulate phase as interpenetrating continuous phases. The governing equations employed for the conservation of mass and momentum for each phase ( $m, n = g$  for gas phase and  $m, n = s$  for solid phase) are

$$\frac{\partial}{\partial t}(\epsilon_m \rho_m) + \nabla \cdot (\epsilon_m \rho_m \vec{v}_m) = \sum_{\substack{n=1 \\ n \neq m}}^{N_m} R_{mn}$$

2-1

$$\frac{\partial}{\partial t}(\varepsilon_m \rho_m \vec{v}_m) + \nabla \cdot (\varepsilon_m \rho_m \vec{v}_m \vec{v}_m) = \nabla \cdot (\bar{\bar{S}}_m) + \varepsilon_m \rho_m \vec{g} - \sum_{\substack{n=1 \\ n \neq m}}^M I_{mn}$$

2-2

Where

$\varepsilon_m$  is the phase volume fraction

$\rho_m$  is the phase density

$\vec{v}_m$  is the phase velocity vector

$R_{mn}$  is mass transfer between phases

$\bar{\bar{S}}_g$  is the phase stress tensor

$I_{mn}$  is the interaction force representing the momentum transfer between the phases

The closure terms for the solid phases are obtained through kinetic theory of granular flow. Detailed information on the constitutive relationships used to model momentum exchange between the phases along with the solid stress model incorporated in MFiX-TFM can be obtained from MFiX online documentations [14] [15].

Equations 2-1 and 2-2 form a system of nonlinear partial differential equations. An iterative algorithm is used in MFiX to solve this system of PDEs. Figure 2-1 illustrates the solution sequences used in MFiX for solving the equations 2-1 and 2-2. As it is discussed in the next section, it is crucial to follow the same sequence in constructing the smart proxy.

**Table 2-1 Multiphase Flow Modeling Approaches [11]**

	<i>Name</i>	<i>Gas Phase</i>	<i>Solid Phase</i>	<i>Coupling</i>	<i>Scale</i>
1	<i>Discrete bubble model</i>	<i>Lagrangian</i>	<i>Eulerian</i>	<i>Drag Closure for bubbles</i>	<i>10 m</i>
2	<i>Two Fluid Model</i>	<i>Eulerian</i>	<i>Eulerian</i>	<i>Gas-Solid drag closure</i>	<i>1 m</i>
3	<i>Unresolved Discrete particle model</i>	<i>Eulerian</i>	<i>Lagrangian</i>	<i>Gas-particle drag closure</i>	<i>0.1 m</i>
4	<i>Resolved Discrete particle model</i>	<i>Eulerian</i>	<i>Lagrangian</i>	<i>Boundary condition at particle surface</i>	<i>0.01 m</i>
5	<i>Molecular Dynamics</i>	<i>Lagrangian</i>	<i>Lagrangian</i>	<i>Elastic collisions at particle surface</i>	<i>&lt;0.001 m</i>

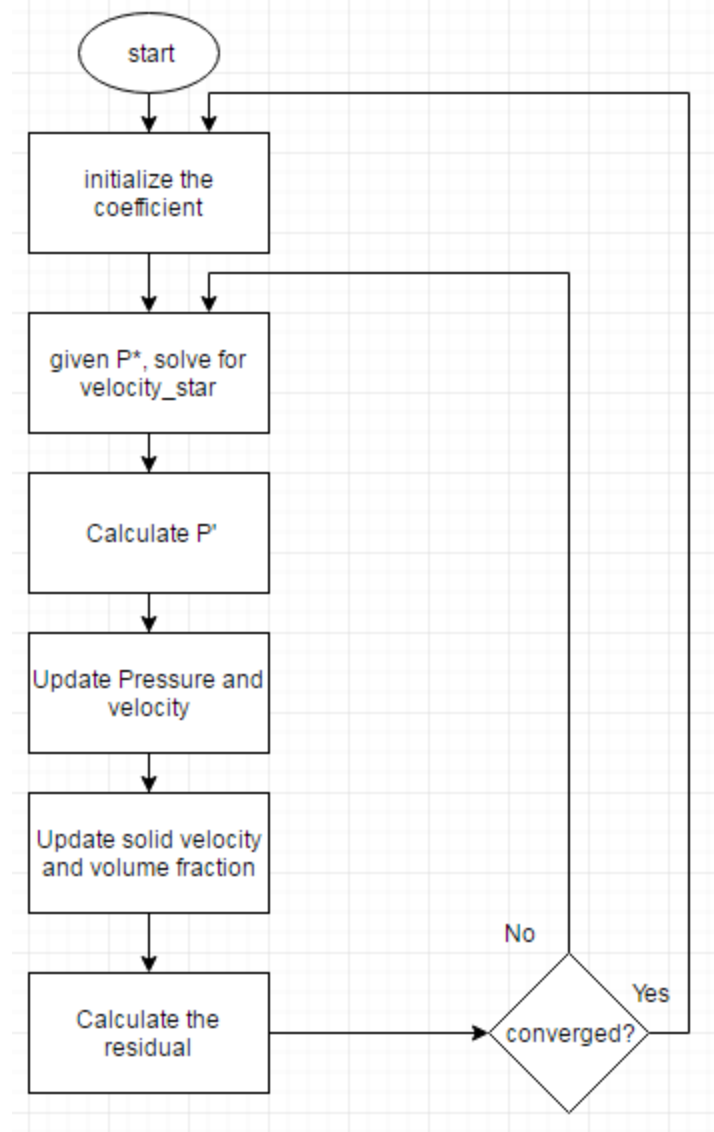


**Figure 2-1 MFiX solution algorithm.**

## 2.2 MACHINE LEARNING

Based on the definition presented by Arthur Samuel [16], “*Machine learning is a field of study that gives computers the ability to learn without being explicitly programmed.*”

Machine learning is a process through which computer will learn from data to find a possible pattern in the data set. This process encompasses three main components:

- Learning algorithm
- Data
- Patterns in the data

If these three components are present, a successful learning process can be achieved based on the capability of the learning algorithm. There are two major types of Machine Learning: supervised learning and unsupervised learning [17].

In supervised learning, the training data consists of both input and output values and the learning algorithm finds a functional relationship between the two. Examples for supervised learning are approximating the shoe size by knowing the person's height and weight or classifying the type of cancer (malignant, benign) based on the patient's age and tumor size. In the first example, the output of the supervised learning process has a continuous form and it is called Regression. In the second example, the output of the learning process has a discrete form and it is called classification.

In unsupervised learning, no information about the output is included in the learning data. The learning algorithm objective is to find a pattern among the input data. For instance, grouping the vehicles to good or bad cars. This process is sometimes called clustering.

### 2.2.1 Artificial Neural Network

One of the popular machine learning processes is Artificial Neural Network (ANN). The idea of ANN came from the neurons of the brain and the way they are communicating with each other to solve a problem. Each artificial neural network consists of an input layer, one or more hidden layers, and an output layer. The number of neurons (processing elements) in the output and the input layers are chosen based on the nature of the problem being solved and the properties which are going to be predicted. Figure 2-2 shows a typical ANN with three input neurons and two output neurons. ANN has one or more hidden layers and each layer has a specific number of neurons [18]. In order to have a well-trained network, proper parameters should be introduced to the network. If improper data are used to train the network there is no guarantee to have a well-trained network that leads to correct predictions, in other words, *"Garbage in, Garbage out."* In the upcoming sections of this report, a smart way of selecting parameters will be introduced.

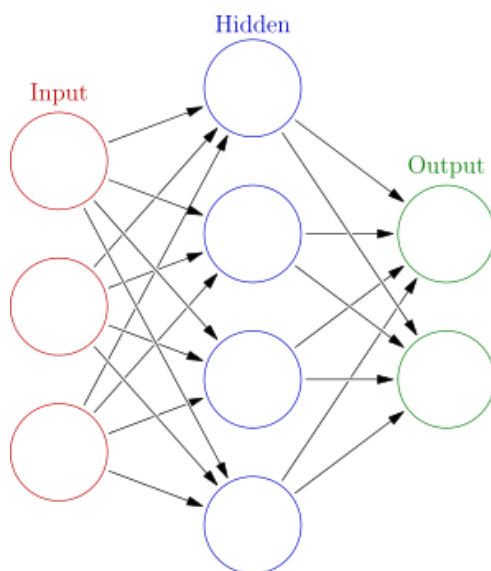


**Figure 2-2 Artificial Neural Network schematic**

The number of hidden layers and the number of neurons in each hidden layer depends on the complexity of the problem, number of parameters, and number of records. Experience also plays an important role in this decision making. Hence, there is no universally acceptable recipe for them but as a rule of thumb, the number of neurons in the first hidden layer shouldn't be less than the number of input parameters.

### 2.2.1.1 Objective function

Regardless of the learning method, each machine learning process needs an optimization procedure that helps the process reduce the error as much as possible. The very common and simple objective function in supervised learning is the summation of all the differences between predicted values by the learning method and the actual values of the output. Since summation of positive and negative errors can reduce the size of the overall error, the objective function is defined as the square of the difference between actual and predicted values [18], as shown by equation 2-3.

$$J(w_j) = \frac{1}{2m} \sum_{i=1}^m (y_{actual} - y_{predicted})^2$$

2-3

Where  $w_j$  is the weighting vector. During the learning process, the learning algorithm tries to assign different weights to each of the connection between neurons in Figure 2-2, in a way that the global error of the objective function becomes minimum. Also, a blind calibration is done simultaneously to stop the learning process, which we will discuss the validation and test in more depth in the next sections of this report.

In machine learning, the dataset used for training of ANN has to be normalized, before the data is introduced for training. Therefore, the quality of ANN is characterized by error (discrepancy) distribution between mean normalized CFD data (used for training) and mean normalized ANN output as shown by equation 2-4.

$$\% Error = \frac{CFD_{value} - CFD_{mean\ value}}{MAX(CFD_{value}) - MIN(CFD_{value})} - \frac{Smart\ Proxy_{value} - CFD_{mean\ value}}{MAX(CFD_{value}) - MIN(CFD_{value})}$$

2-4

## 2.3 PREVIOUS WORK

The idea of using Artificial Intelligence in petroleum engineering was first introduced by Mohaghegh and Ameri [19]. They took advantage of ANN for predicting the permeability of the formation based on geological well logs. Mohaghegh and Ameri [19] showed that neural network

is capable of making the task of permeability determination automated rather than doing it over and over by log analyst. They also stated that neural network can handle far more complex tasks. Mohaghegh et al. [20] used ANN for predicting gas storage well performance after hydraulic fracture in their later investigations.

Alizadehdakhel et al. [21] successfully used ANN to predict the pressure loss of a two-phase flow in the 2-cm diameter tube. Gas and liquid velocities and the pressure drop along the pipe were the three input parameters to ANN, with average pressure drop being the output of ANN. They utilized 8 different networks with different number of neurons to find out the optimum number of neurons. Mean Squared Error and R-square were used as a criterion to pick the best network design. They also obtained the most efficient transfer function between Log-Sigmoid, Hyperbolic-Tangent Sigmoid, and linear.

Shahkarami et al. [9] used ANN to model the pressure and saturation distribution in a reservoir which was used for CO<sub>2</sub> sequestration. This problem required a large number of time steps for simulation of CO<sub>2</sub> injection and storage using a commercial software. They ran 10 different cases in CMG (commercial reservoir simulator) and then the results were used as input for ANN. The output of the ANN was pressure distribution, water saturation, and CO<sub>2</sub> mole fraction. 80% of the data coming from the CMG simulation runs were used to train the network while 10% were used for the calibration. The remaining 10% of data was used for validation process. They have shown that ANN can be used as a powerful tool for multiphase flow simulation in oil and gas industry.

Esmaili et al. [22] incorporated a newly developed machine learning based reservoir modeling technology known as Data-Driven Reservoir Modeling [23] in order to model fluid flow in shale reservoirs using detail well logs, completion, and production data. By understanding the behavior of the shale reservoir, conducting the hydraulic fracture could be much easier. Moreover, this method has the ability to perform the history matching on the production data. Kalantari-Dehghani et al. [24] coupled numerical reservoir simulator with AI methods to develop a shale proxy model that is able to regenerate numerical simulation results in just a few seconds. They introduced three different well-based tier systems to achieve a comprehensive input data for the ANN. In another work, Kalantari-Dehghani et al. [25] showed that data-driven proxy models at the hydraulic fracture cluster level could be used separately as a reservoir simulator especially in low permeability reservoir such as shale which has a nonlinear behavior.

### 3. METHODS

In this section, the solution methodology and the required steps for constructing the neural network are discussed.

#### 3.1 CFD SIMULATION SETUP

A schematic of the rectangular fluidized bed, used in this study is shown in Figure 3-1. The fluidized bed, which is 0.12 x 0.72 x 0.12 m in X, Y and Z directions has an initial bed height of 0.12 m, and initial bed voidage of 0.42. The bed material has a density of 2000 kg/m<sup>3</sup> and a diameter of 400 μm. Based on a grid resolution study, which has been discussed in part one report [26], the grid size 27x162x27 in X, Y and Z directions is selected, hence, the grid spacing to particle diameter of 11 is obtained. Details of the CFD simulation set up was covered in the part one report of this project, [26], and will not be repeated here.

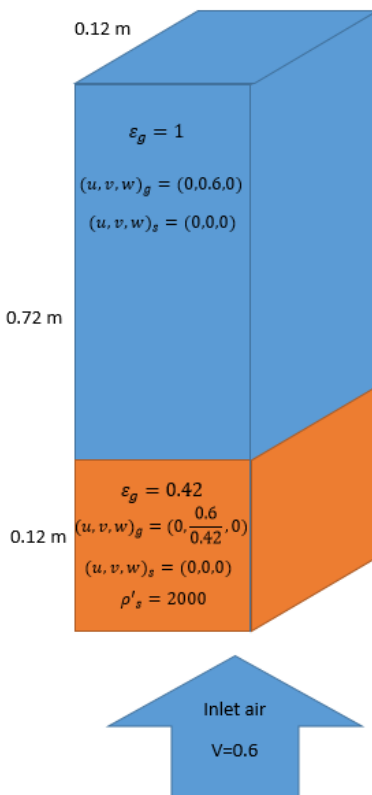


Figure 3-1 Geometry and initial condition of the problem in SI units.

#### 3.2 PROBLEM DEFINITION

The MFiX model has been created and executed successfully for multiple inlet velocities. The data generated by the CFD runs with a variety of inlet velocities is used for the training, calibration, and validation process of the neural network model. Furthermore, additional CFD simulations with different inlet velocities are performed and are excluded from the neural network training

process. The additional CFD simulations are used to test the predictive capabilities of the smart CFD proxy, in what is referred to as a blind test.

### 3.2.1 Interpolating the inlet air velocity

In this project, the inlet air velocity varies from a minimum value of 0.6 m/s to a maximum value of 1.2 m/s (Figure 3-2). The inlet air velocity is assumed to be uniform across the fluidized bed inlet (Figure 3-1) with air discharging into atmospheric pressure at the outlet.

The goal of this project is to predict the behavior of a fluidized bed with any given inlet air velocity (within the velocity range used for training) at any specific time within a very short period of time (in seconds). Total of 11 CFD simulations have been carried out, when only the inlet velocity has been changed. Figure 3-2 shows the 11 inlet velocities used in this study. The neural network is trained with only 7 of the 11 velocities shown in Figure 3-2. The predictive capability of the trained neural network is evaluated with the remaining 4 inlet velocities, which have not been used during the training process of ANN. This blind test process is discussed further in section 3.3.4. Figure 3-3 shows the concept of this project.

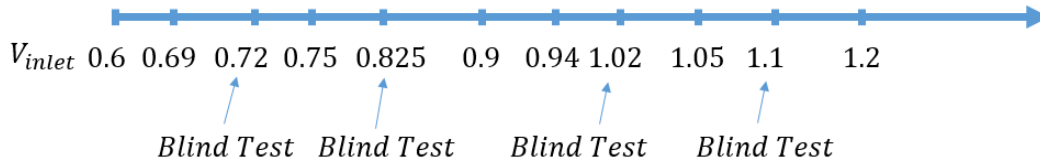


**Figure 3-2** Different inlet air velocities (m/s) for MFIX simulations

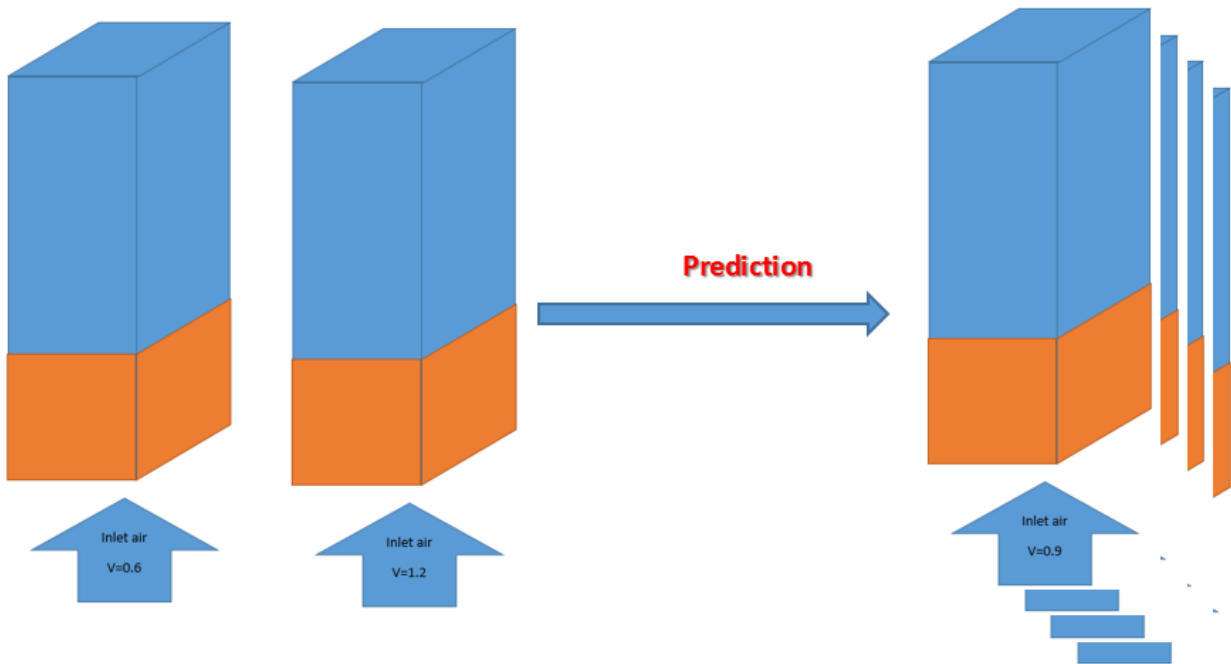


**Figure 3-3 Conceptual illustration of problem definition**

### 3.3 ARTIFICIAL NEURAL NETWORK SETUP

Once the output files of MFiX are converted to \*.csv file they are ready to be reorganized to serve as the input to the Artificial Neural Network (ANN). Every time-step and every inlet velocity has one \*.csv file containing 9 columns and 118,098 rows (size of the modeled fluidized bed,  $27 \times 162 \times 27 = 118,098$  computational cells). Each column represents one property such as pressure and each row corresponds to one cell. Depending on the solution scenario, which will be discussed later, some of these columns and rows will be used as input or output.

#### 3.3.1 Neural Network architecture

Each artificial neural network consists of an input layer, one or more hidden layers, and an output layer. The input and output parameters are chosen based on the nature of the problem and the property which is going to be predicted.

The number of inputs and outputs are chosen based on the problem and the solution scenario which will be discussed in detail in the next section. There is no clear guideline on how many hidden layers and neurons are required at each layer. The type of problem and user experience, along with few rules of thumb are the primary factors in determining the number of hidden layers and neurons. One such rule is that the number of neurons in the first hidden layer shouldn't be less than the number of input parameters. For the first try, only one hidden layer with 15 neurons is considered. The network characteristics and the activation function were described in the part one report of this series, [26], and will not be repeated here.

### 3.3.2 Input and output

In the previous report of this series, [26], it was shown that non-cascading scenario had a downside which was the need for the MFIX results at each time-step. In order to train the ANN at time step (t), the CFD results at time step (t-1) were used as input to ANN, along with static parameters, such as location of each cell or distance between each cell to the walls. The output for the non-cascading training process was one dynamic parameter, such as pressure or velocities or volume fraction at time step (t). In the present report, static parameters, CFD results and other model input parameters such as gas inlet velocity are used at time step (t) to train the ANN for the same time step (t). The output of the neural network is either gas pressure, gas volume fraction or gas velocity. Some important details regarding the use of neighboring cells and the tier system associated with them were described in detail in the part one report, [26], and will not be repeated here.

The process of fluidization, as shown in Figure 3-4, starts with the bed material moving upward like a slug flow, Figure 3-4a, until the maximum bed expansion is reached, Figure 3-4b, and the bed starts to collapse. In Figure 3-4 color red indicates high voidage (low solid volume fraction) and color blue indicates low voidage (high solid volume fraction). Up to now, the solid flow is symmetrical. Once the bed collapses, smaller bubbles are formed, and the bed behaves more chaotically, Figure 3-4c. And ultimately, the bed becomes fully fluidized and chaotic, Figure 3-4d.

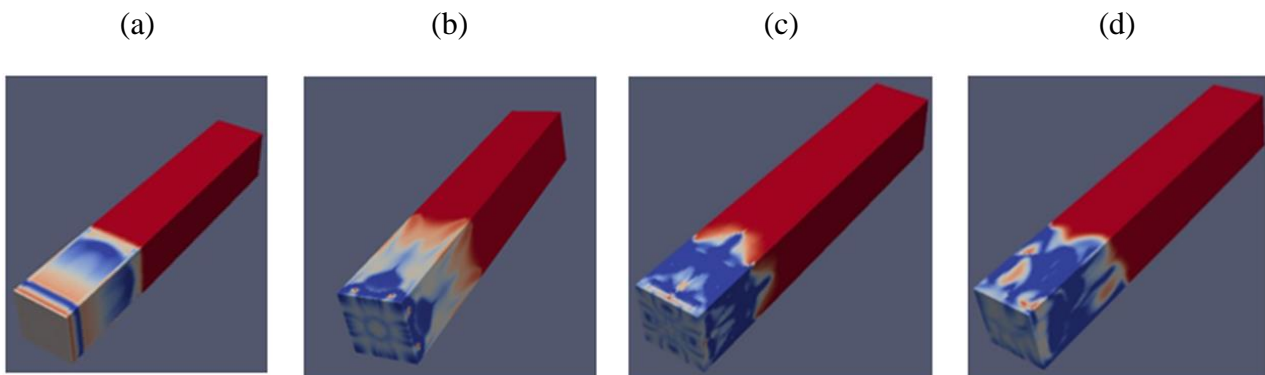


**Figure 3-4 Different flow regime**

CFD data at time step 1400 is chosen for ANN training, since this time step represents the initial chaotic stage, when smaller bubbles are formed, and the bed starts to fluidize, Figure 3-4c. Other time-steps will be studied later in different scenarios for different purposes.

### 3.3.3 Data partitioning

A good ANN is a model that learns the pattern in the given data-set while it is able to predict the behavior of a new unseen dataset, this model is called “Just Right”. If the ANN does not learn the pattern in the data very well the model is called “Under-fit”. If the ANN learns the pattern of the

data very well with a very small error but it is not able to predict the behavior of a new unseen dataset the model is called “Over-fit”. Under-fitting occurs for so many reasons such as lack of information (the model should have more parameters and more examples). Overfitting occurs when the network learns to mimic almost all the data points exactly but when it comes to the prediction, the model performs poorly for a new unseen data, in other words the model memorizes all the data points. Figure 3-5 shows these 3 states of training.

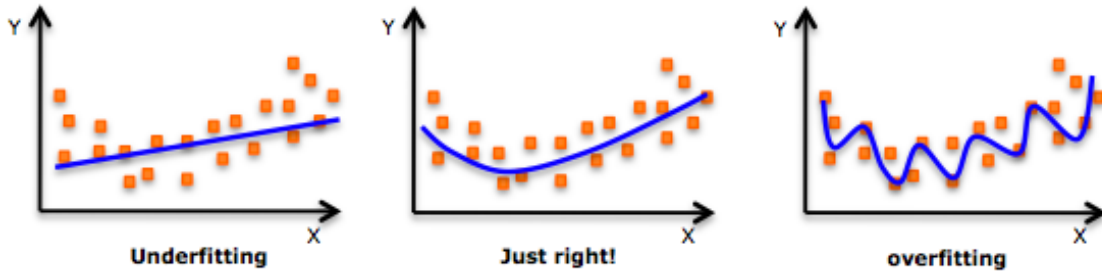


Figure 3-5 Three states of ANN training

To overcome the overfitting problem, the data is partitioned into three subsets. Each subset is used for training, calibrating and validating the ANN. The process of data partitioning can best be explained by considering the sample dataset shown in Figure 3-6. This figure shows 10,000 data points that can be used to construct an ANN. The dataset is partitioned into a training subset (Figure 3-7, 70% of the original data points, selected randomly), calibration subset (Figure 3-8, 15% of the original data points, selected randomly), and validation subset (Figure 3-9, the remaining 15% of the original dataset).

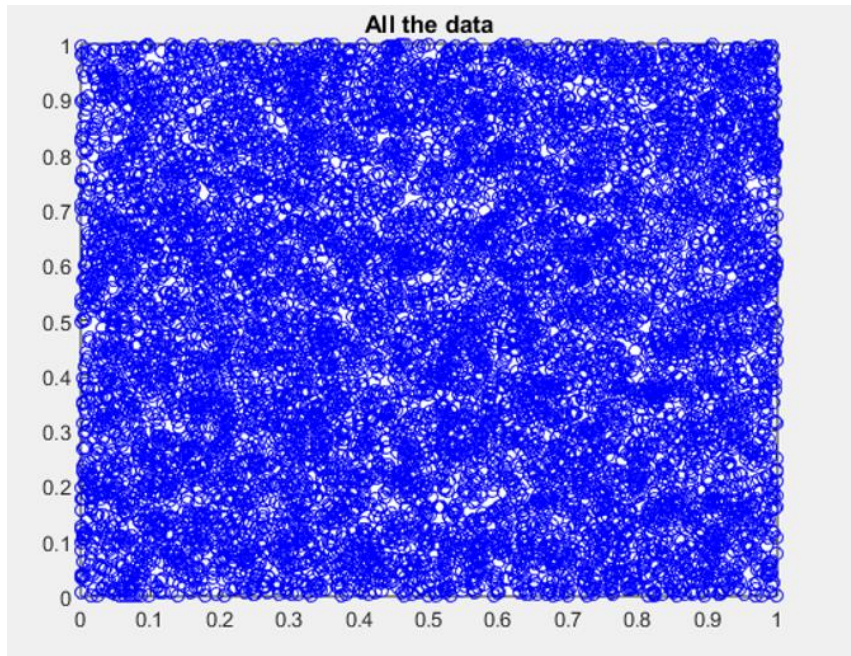
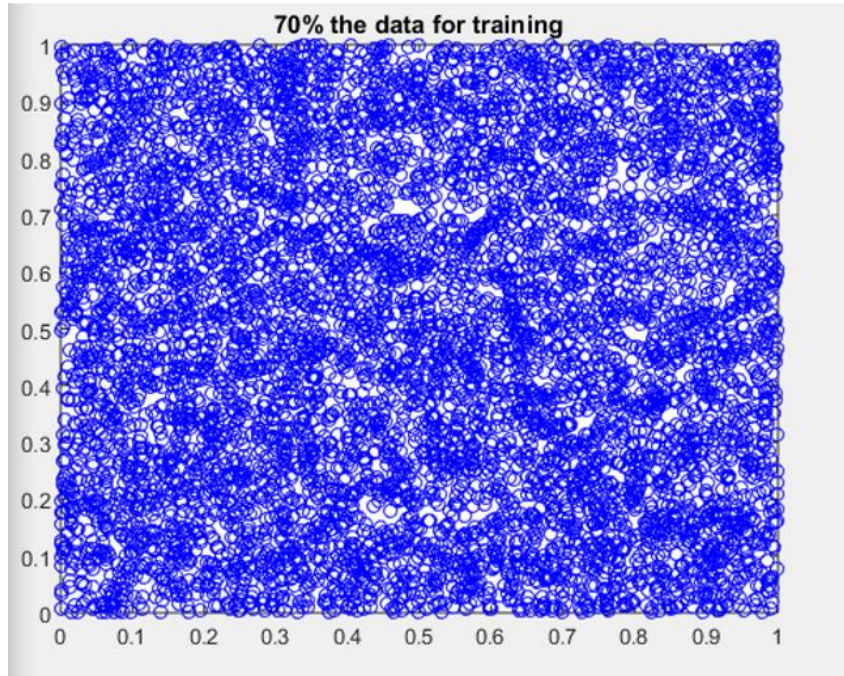
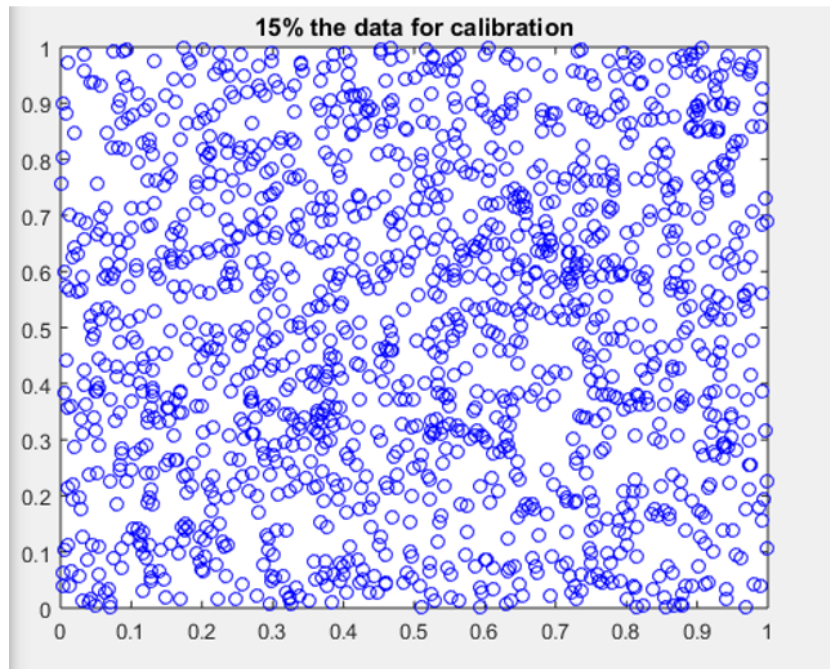


Figure 3-6 10,000 sample points used for constructing the ANN



**Figure 3-7** Data used for training the ANN



**Figure 3-8** Data used for calibrating the ANN



**Figure 3-9** Data used for validating the ANN

Training is an iterative process where in each iteration the optimization algorithm aims to reduce the error. An iteration is defined as the process through which all the records in the training data set are introduced to the ANN once and the error between the actual (target) output and those predicted by the ANN are calculated and the impact of the calculated error is back-propagated throughout the ANN in order to modify the weights associated with all the connections between neurons in the ANN. In this example, the training dataset, shown in Figure 3-7 is used to train the ANN. The training process stops based on some user defined criteria. This criterion could be the total number of iterations, or the total time of training, or lowest possible error, or the number of validation failure or a combination of those. In this project, the combination of all the mentioned criteria are used to terminate the training process. The learning algorithm is such that the network learns more with increasing number of iterations, but in order to avoid overfitting or memorization, the calibration dataset, shown in Figure 3-8, is used concurrently with the training ANN and training is terminated once enough learning is achieved. Training is stopped once the calibration error reaches a minimum. Error during both training and calibration initially decreases, as shown in Figure 3-10. However, if ANN overfits or memorizes the data, the calibration error increases, while the training error continues to decrease. If the calibration error increases for a predefined number of iterations, the training stops. Most of the time, number of failure in calibration is the criterion which makes the training stop. The model at this point is usually the best trained ANN model because it has provided the lowest possible error for the calibration data set (used in a blind test fashion), while it has an acceptable error for the training data set.

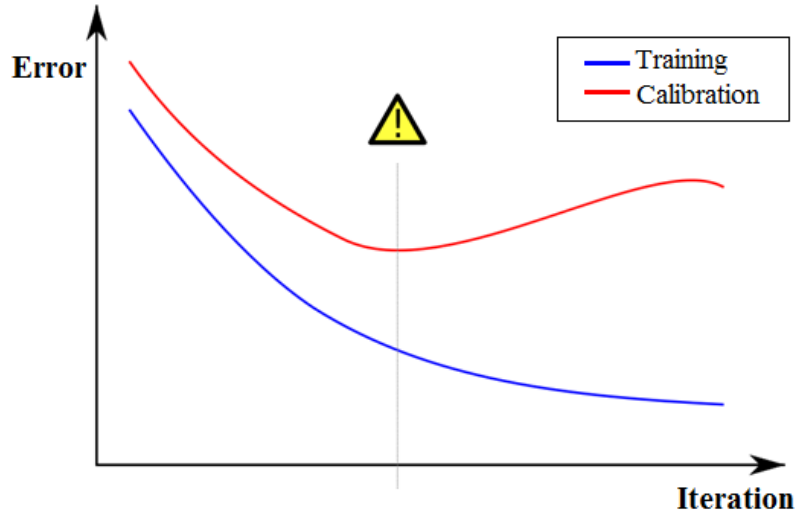


**Figure 3-10 Learning curve, training error and calibration error**

The validation data set, shown in Figure 3-9, is used upon the completion of the training process when the best ANN is achieved. Having an ANN model with a low calibration error does not mean that the ANN is a good predictor. The ANN is deemed properly trained, when the error from the validation process, which like the calibration process is being performed in a blind test manner, is also acceptable. The percentage of the data partitioning used for the preliminary study of this project is shown in Table 3-1. It is important to mention that this partitioning is the preliminary one and a deeper study will be conducted on the percentage of the data as it will be described in the upcoming sections of this report.

It is noteworthy to reiterate that the input datasets used for training have to be different enough, such that there is variability in the flow field. This variability will provide a greater opportunity for ANN to learn.

**Table 3-1 Original data partitioning**

<i>Data</i>	<i>Training</i>	<i>Calibration</i>	<i>Validation</i>
<i>Percentage of data (%)</i>	70	15	15

### **3.3.4Blind test**

As mentioned earlier, total of 11 CFD simulations have been carried out, when only the inlet velocity has been changed. Of the 11 CFD simulations, 4 have been set aside and used for blind testing, Figure 3-11. A blind test is when some of the data that was not used during the training of ANN, is used to further validate the predictive capability of the trained ANN, Figure 3-11. The difference between calibration and validation during the training process and the complete blind

test is that the records (data) in the calibration and validation process during the training are a subset of the original data that are chosen randomly from the original dataset, as explained earlier. However, the entire records (data) are used during the blind test.

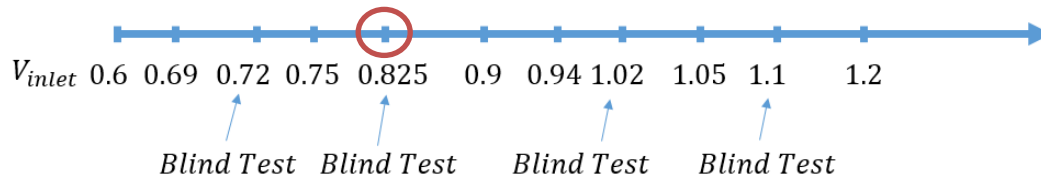


**Figure 3-11** Different inlet air velocities (m/s) for MFIX runs

### 3.4 SOLUTION SCENARIOS

Different scenarios are considered to reach the final goal of this project. The term “*Different scenarios*” refers to having different input and output structures and also using different time-steps for the training, while the training technique is the same in all the scenarios. Depending on what time-step(s) and what inlet velocity(s) and how they are used for the training, different scenarios will be designed which is the main discussion of the following section. Each scenario has two parts, first is the training process and second is the deployment process.

As it was stated earlier, the goal of this research project is to build a smart proxy model at the cell level, which is constructed from CFD based data. The smart proxy can reduce the use of computationally expensive CFD for the design space under study. This is particularly beneficial, when conducting uncertainty quantification analysis, using CFD. The scenarios outlined below show the systematic steps taken, from least number of input parameters used during the training to the when the most number of input parameters are used during the ANN training. The scenarios followed in order of complexity are:

- Training an ANN for gas pressure using 7 static parameters at a single time step, as discussed in section 3.4.1
- Training an ANN for gas pressure using 11 static parameters at a single time step, as discussed in section 3.4.2
- Optimization of ANN, discussed in section 3.4.3
- Temporal and spatial averaging of ANN data from time steps 500 to 1400 and time steps 1500 to 3400 are discussed in section 3.4.4
- Training an ANN for velocity and gas volume fraction using 11 static parameters at a single time step, as discussed in section 3.4.5
- Sequential modeling, where an ANN for velocity uses the trained ANN for pressure as the input and the ANN for gas volume fraction uses the trained ANN for velocity and pressure as inputs. More details are provided in section 3.4.6
- Sequential training, when the tier system is used and information from the surrounding cells are used in the training of ANN, as discussed in section 3.4.7

### 3.4.1 Training for gas pressure using 7 static parameters

A neural network is trained with 7 static parameters (6 distances to the boundaries and 1 inlet velocity) at time step 1400. Seven inlet velocities are used to build this scenario. According to Figure 3-12, the 7 static parameters, including 6 distances to the walls plus the inlet velocity form the inputs and the gas pressure of time-step 1400 of different inlet velocities set as the output. For this preliminary run, one time-step from the breakdown flow regime (time-step 1400) is used for the training. The other time-steps will be used in following sections.

Figure 3-12 shows the input and the output of the ANN for this step. Each inlet velocity at each time-step has  $27 \times 27 \times 162$  (=118,098) records, so total  $7 \times 118,098$  (=826,686) records are used in this scenario. It's important to reiterate that in the training stage, CFD output results for the variable that ANN is being trained for, are input to ANN, along with the static parameters.

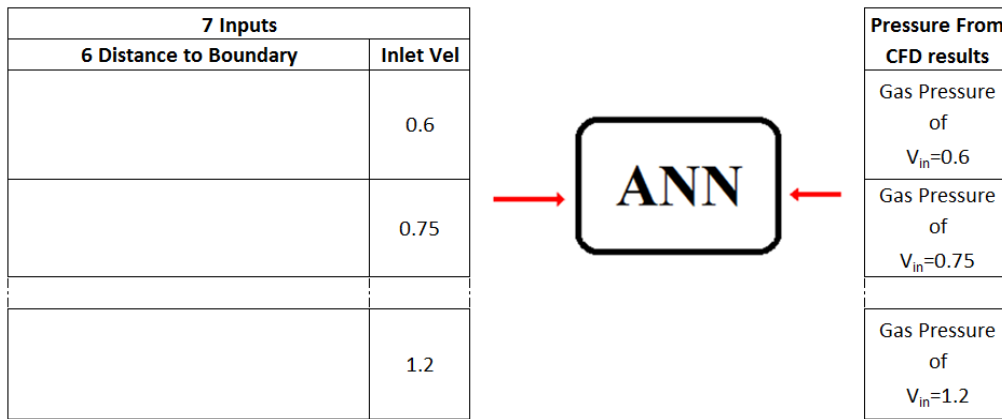


**Figure 3-12 Training for gas pressure using 7 static parameters**

Table 3-2 summarizes the ANN numerical values, when 7 input parameters are used. The same ANN numerical values are used through this work, with the exception of number of input parameters and hence number of records changing going from one scenario to the next. Figure 3-13 shows the distribution of gas pressure in the fluidized bed for different inlet velocities of 0.6 and 1.2 m/s and blind test condition of 0.825 m/s. This figure shows that there is enough spatial variation in the bed for the neural network to learn from. The results of training ANN with 7 static parameters are presented in section 4.2.

**Table 3-2 Important numbers in Neural Network Model**

<i>Number of Inputs</i>	7
<i>Number of hidden layers</i>	1
<i>Number of Hidden Neurons</i>	15
<i>Number of records</i>	826,686
<i>Number of Output</i>	1

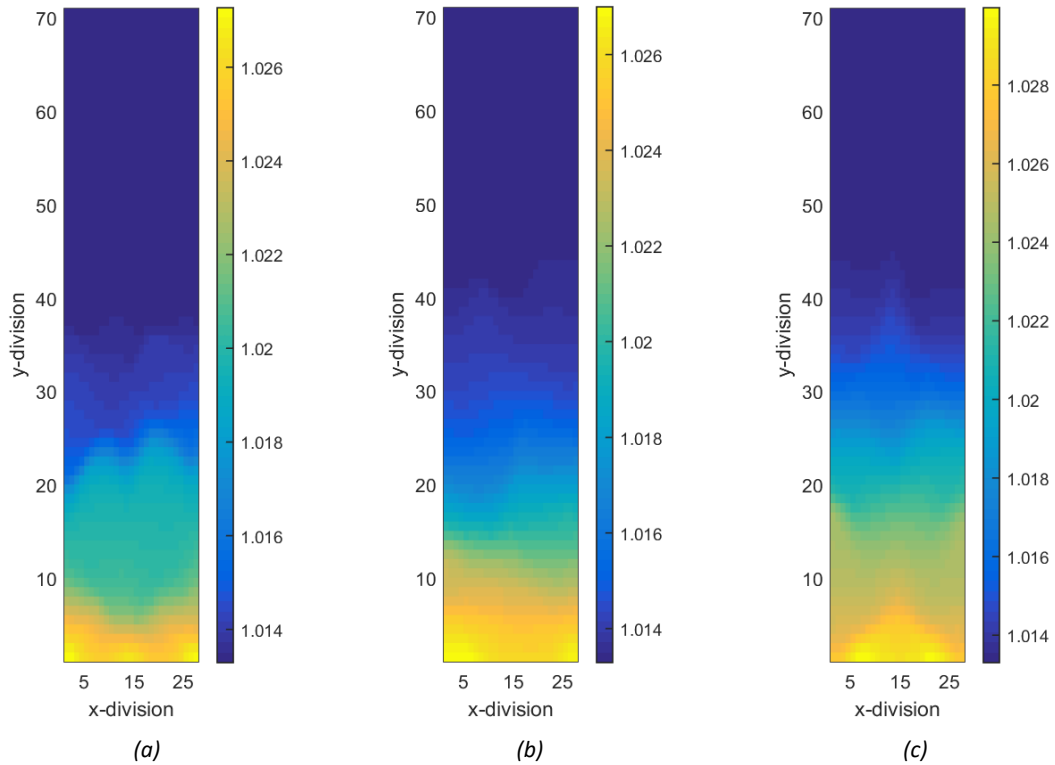


**Figure 3-13 Gas pressure ( $10^5$  Pa) at cross sectional plane  $K = 7$  with (a)  $V_{inlet} = 0.6$  m/s (b)  $V_{inlet} = 1.2$  m/s (c)  $V_{inlet} = 0.825$  m/s**

### **3.4.2 Training for gas pressure using 11 static parameters**

In the previous scenario, 7 attributes were used in the training process which might not have been enough for the training. Our effort is to find the static attributes to give network more flexibility to find the patterns in gas pressure and at the same time we want these attributes to be available all the time and that is why static parameters are chosen. Data scientists usually try to remove all the redundant attributes from the training set, but sometimes redundancy could help ANN to find out the hidden pattern in the data. Since there are no more static attributes available it is decided to use the indices of the cells. Adding I, J, K and the index of each cell will add the location of each data point, in the physical domain, to the training process and worth exploring. The results of training with 11 static parameters are presented in section 4.3.

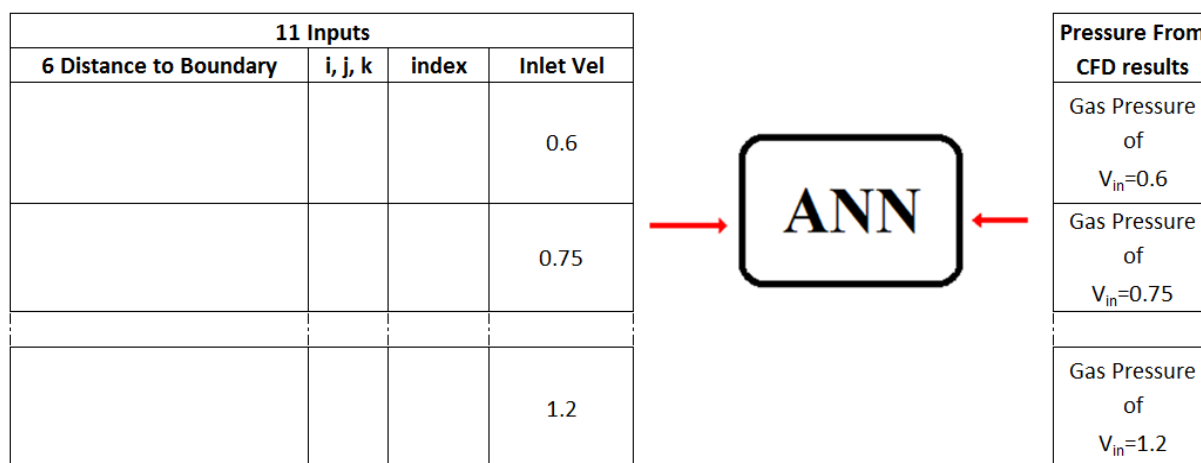


**Figure 3-14 Training for gas pressure using 11 static parameters**

### 3.4.3 Optimizing the ANN

Some of the model parameters, which can affect the quality of ANN are listed in Table 3-3. These parameters undergo an optimization process, in order to improve the quality of ANN. The results of ANN optimization are presented in section 4.4.

**Table 3-3 ANN model parameters**

<i>ANN Parameters</i>	<i>Current Status</i>
<i>Number of hidden layers</i>	<i>1</i>
<i>Number of Hidden Neurons</i>	<i>15</i>
<i>Training Algorithm</i>	<i>Levenberg-Marquardt</i>
<i>Transfer Function</i>	<i>TANSIG</i>

### 3.4.4 Time and space average

Flow in a fluidized bed is highly transient and chaotic. As such, even multiple CFD simulations of the same flow conditions yield different instantaneous flow fields, although the time averaged flow fields should be the same. For this reason, the performance of a fluidized bed is typically assessed based on the time and/or space averaged behavior of the various variables such as pressure, velocities and volume fraction of gas and solid particles.

More than one ANN is needed in order to perform time average analysis of the smart proxy results. This is achieved by constructing 10 ANNs for time steps 500 to 1400, at an increment of 100-time steps and 20 ANNs for time steps 1500 to 3400 at an increment of 100 time steps, using the training approach outlined in Figure 3-14. Each time step is 0.001 seconds of simulation time. Figure 3-15 shows the two-time periods used for time averaging, for time steps 500 to 1400, and for time steps 1500 to 3400, representing flow conditions depicted in Figure 3-4(a) to (b) and Figure 3-4(c) to

(d) respectively. In this fluidized bed, since the predominated flow direction is in the Y-direction, the output results of ANN is averaged across the cross-sectional area, perpendicular to the flow direction, as seen in Figure 3-16. Section 4.5 shows the results of time averaging step.

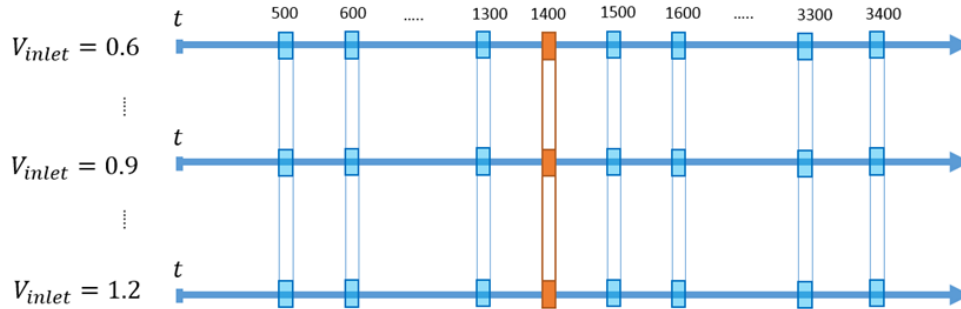


**Figure 3-15 Time steps span selected for time average**

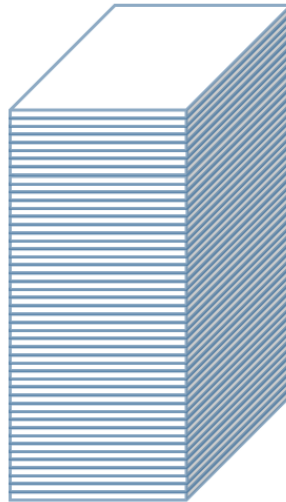
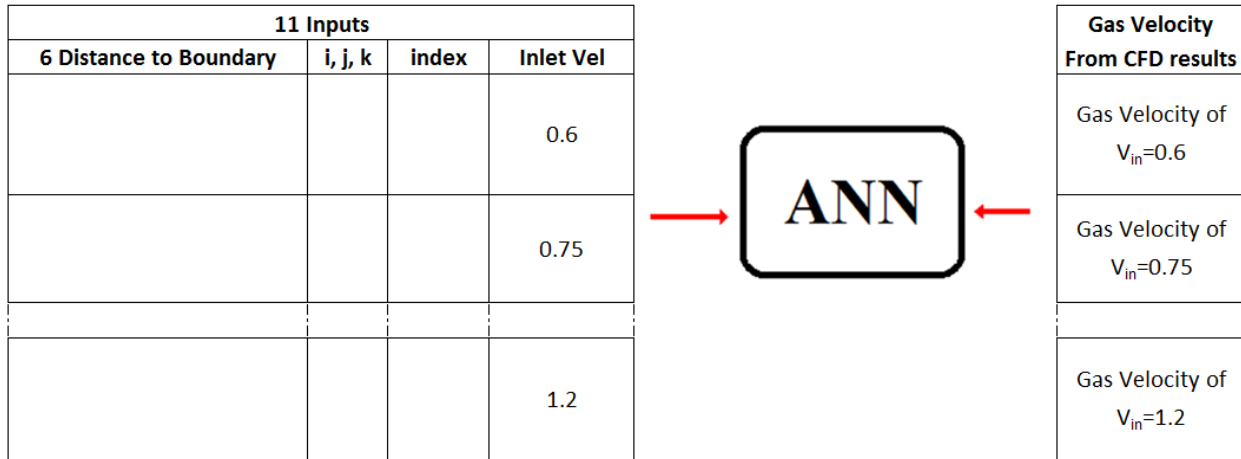


**Figure 3-16 Spatial cross sectional planes used for averaging**

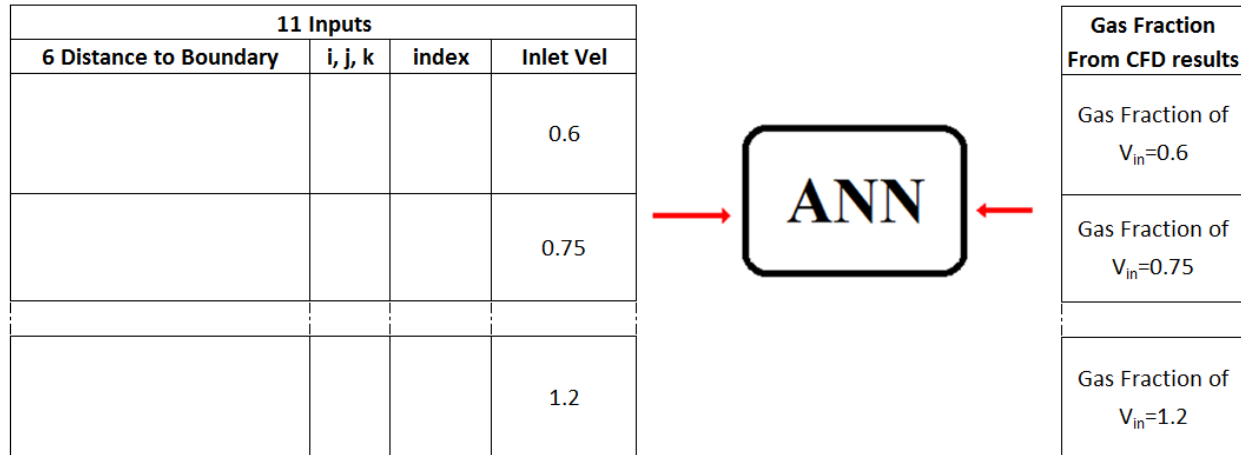
### **3.4.5 Training for gas velocity and gas volume fraction using static parameters**

Figure 3-17 and Figure 3-18 show the training approach for gas velocity and volume fraction, when 11 static parameters are used. However, at the deployment stage, only the static parameters are used as inputs to ANN. The gas velocity used for training of ANN is the magnitude of the velocity vector from CFD calculated by equation 3-1. Section 4.6 shows the results of approach outlined here.

$$V_g = \sqrt{V_{g_x}^2 + V_{g_y}^2 + V_{g_z}^2}$$



**Figure 3-17 Training for gas velocity using 11 static parameters**



**Figure 3-18 Training for gas volume fraction using 11 static parameters**

### 3.4.6 Sequential modeling

The sequential modeling approach is outlined in Figure 3-19. In this training approach, the output of trained ANN for gas pressure field is used as input parameter for the training of ANN for the velocity field, as seen in Figure 3-20. And the output of trained ANN for pressure field and velocity field are used as input parameters for training of ANN for gas volume fraction, as seen in Figure 3-21. The approach used in this step of development of the smart proxy has been inspired by the approach commonly used in the numerical solution of PDEs, which increases the converging speed. This approach is expected to have a lower error. The results of sequential training of ANN are provided in section 4.7.

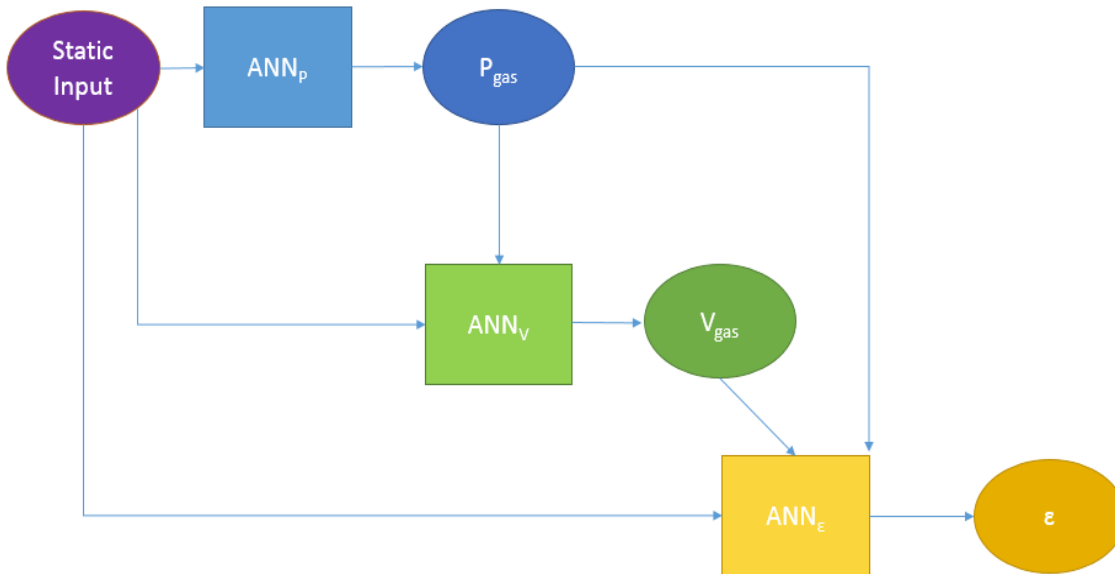


**Figure 3-19** Sequential training algorithm

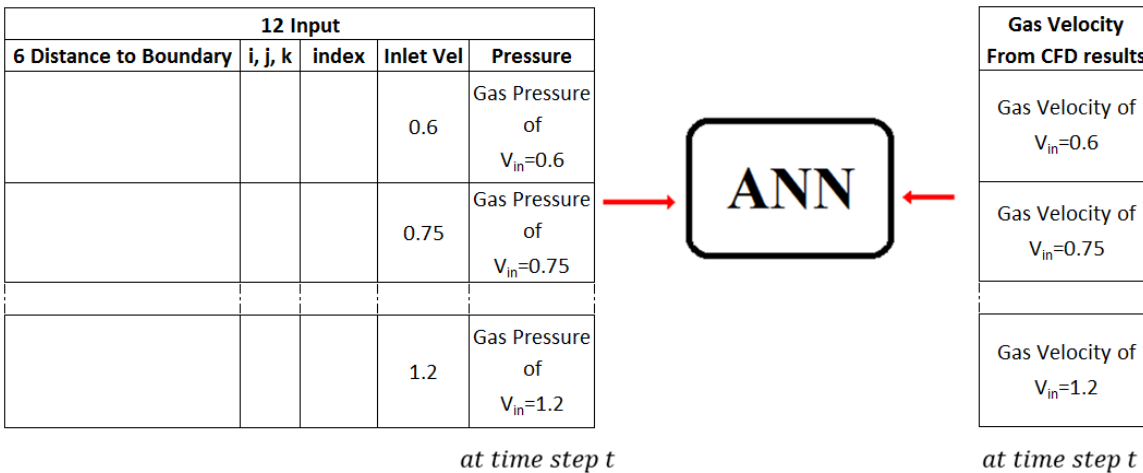


**Figure 3-20** Training for gas velocity using 11 static parameters and gas pressure from ANN<sub>p</sub> (a total of 12 input)

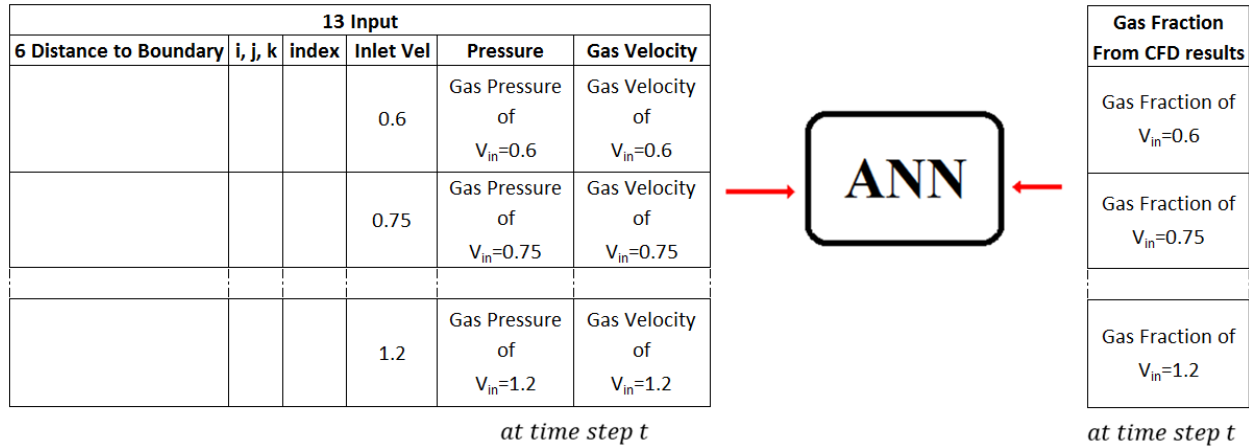


**Figure 3-21 Training for gas volume fraction using 11 static parameters, gas pressure from ANN<sub>p</sub> and gas velocity from ANN<sub>v</sub>**

**3.4.7 Sequential modeling by considering tier system**

As it was discussed in our first report, [26], using a tier system is an effective way of communicating relevant information from the surrounding cells. A cell is in contact with 26 of its surrounding cells (6 having surface contact with the original cell, 12 having line contact with the original cell, and 8 having point contact with the original cell), providing information associated with these connected cells can be helpful to the learning of the physics of the fluidized bed by the smart proxy.

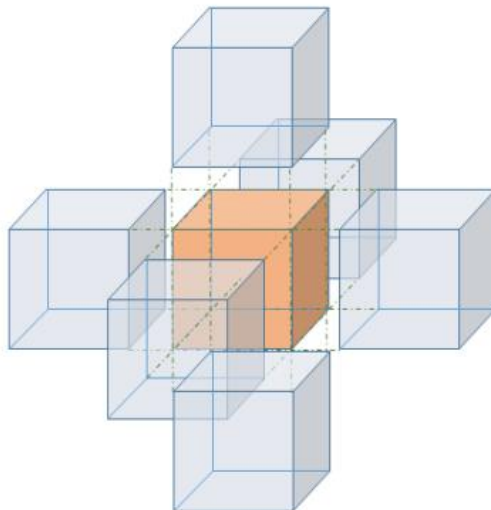


**Figure 3-22 The tier system with the 6 cell in surface contact with the focal cell**

Like any numerical method, the values of each cell have a relation with the value of the surrounding blocks. With that idea in mind, the ANN will not only learn from the static parameters and the value(s) of the parameters of the cell, it will also learn from the surrounding cells which are called “Tier” cells. There are several tiers at the neighbor of each cell and depending on the

complexity of the problem, one can use tier 1 (surface contact), tier 2 (line contact), and tier 3 (point contact) cells as input to the ANN.

Figure 3-22 shows a tier 1 structure, where the main (focal) cell is surrounded by its 6 neighboring cells. For this case, only tier 1 will be used. Depending on the complexity of the problem and spatial and temporal correlations between different tiers and the center cell more or less input parameters might be required (tier 2 or 3). By adding the tier 1 system to the input attributes, the number of inputs becomes 18 for gas velocity which is shown in Figure 3-23. The number of inputs becomes 25 for gas volume fraction as it is depicted in Figure 3-24.

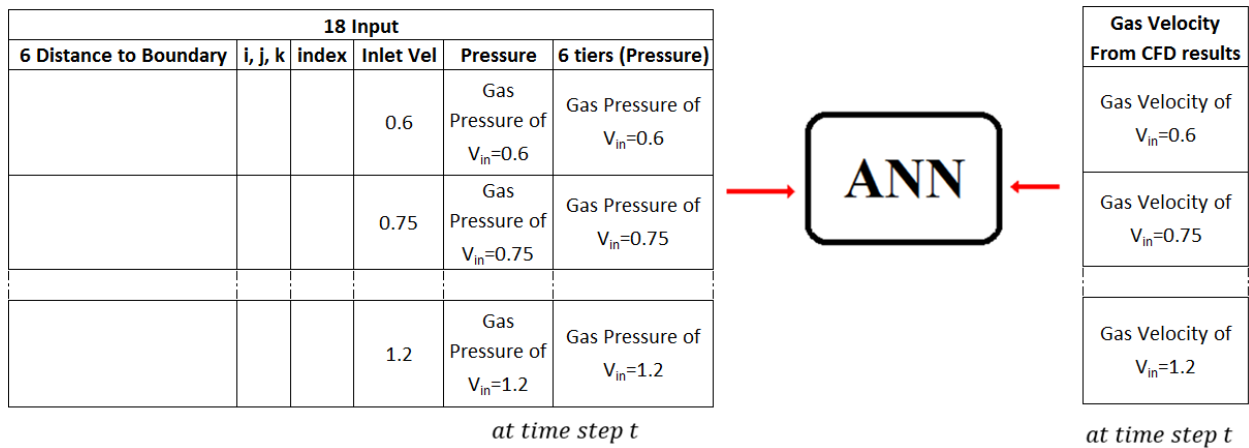


**Figure 3-23 Sequential training for gas velocity using tiers of gas pressure**

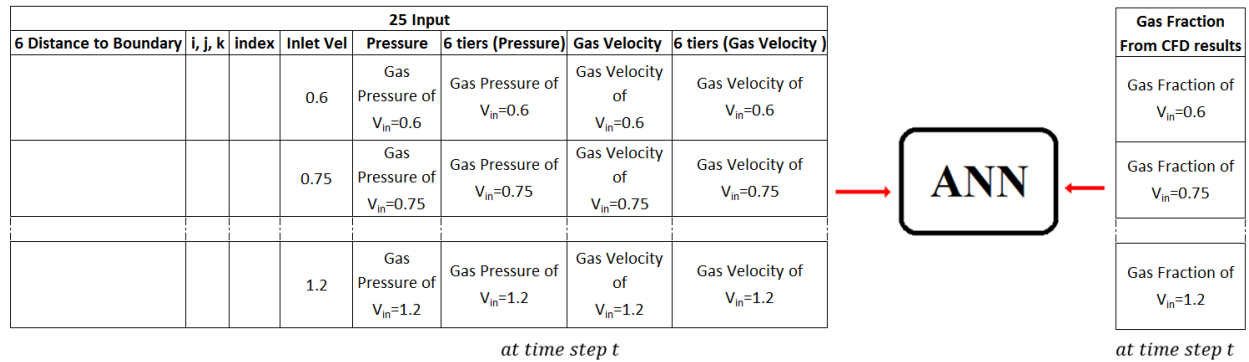


**Figure 3-24 Sequential training for gas volume fraction using tiers of gas pressure and gas velocity**

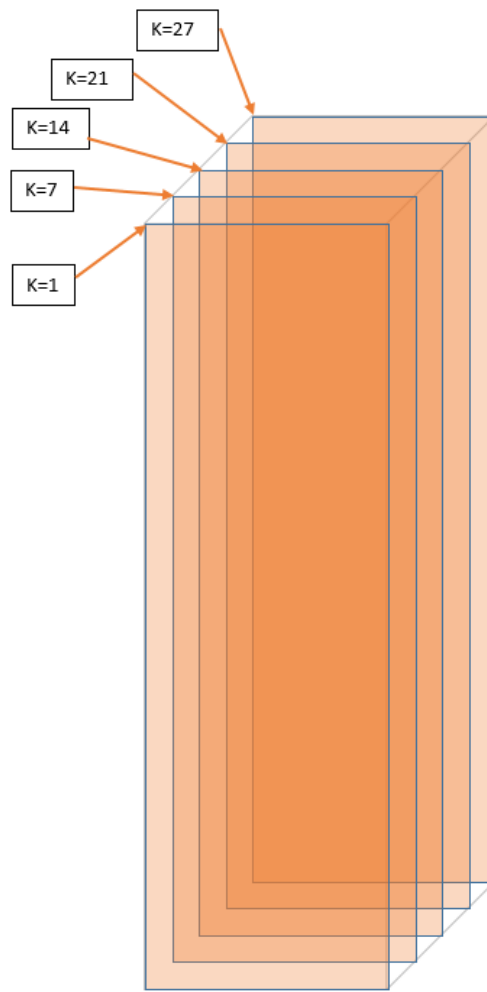
## 4. RESULTS AND DISCUSSIONS

The results of the various scenarios outlined in the previous section are discussed in this section.

### 4.1 PRESENTATION OF THE RESULT

To compare the CFD results with the smart proxy results, 5 vertical cross-sectional planes, 3 cm apart, are selected, where the contour plots for the various output parameters are presented. The locations of these vertical planes are shown in Figure 4-1.

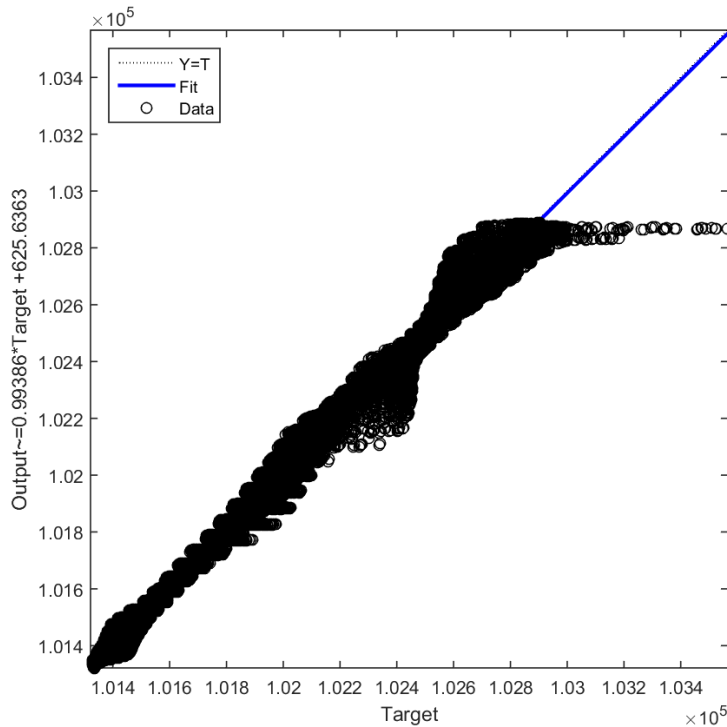
Detailed comparison will be shown in the following sections for different solution scenarios at cross-sectional plane of  $K = 7$ . Results for the other planes are shown in the appendices. Each figure has three subplots, the left plot is the result of MFiX CFD simulation model, the middle plot is the result of the smart proxy which is the output of ANN, and the right plot is the error distribution which is the difference between CFD and the smart proxy.



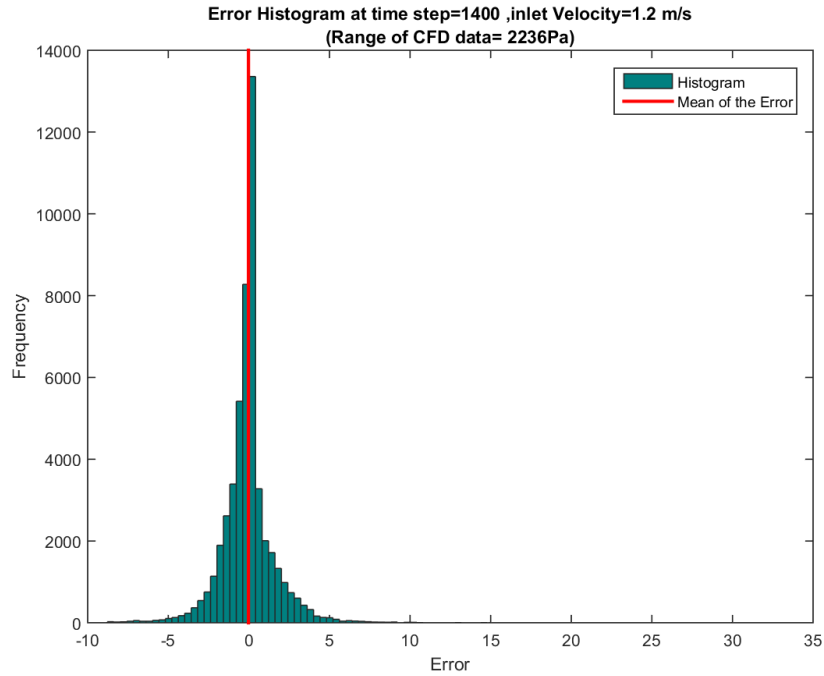
**Figure 4-1** Cross-sectional planes, 3 cm apart, where results are presented

## 4.2 TRAINING FOR GAS PRESSURE USING 7 STATIC PARAMETERS AT A SINGLE TIME STEP

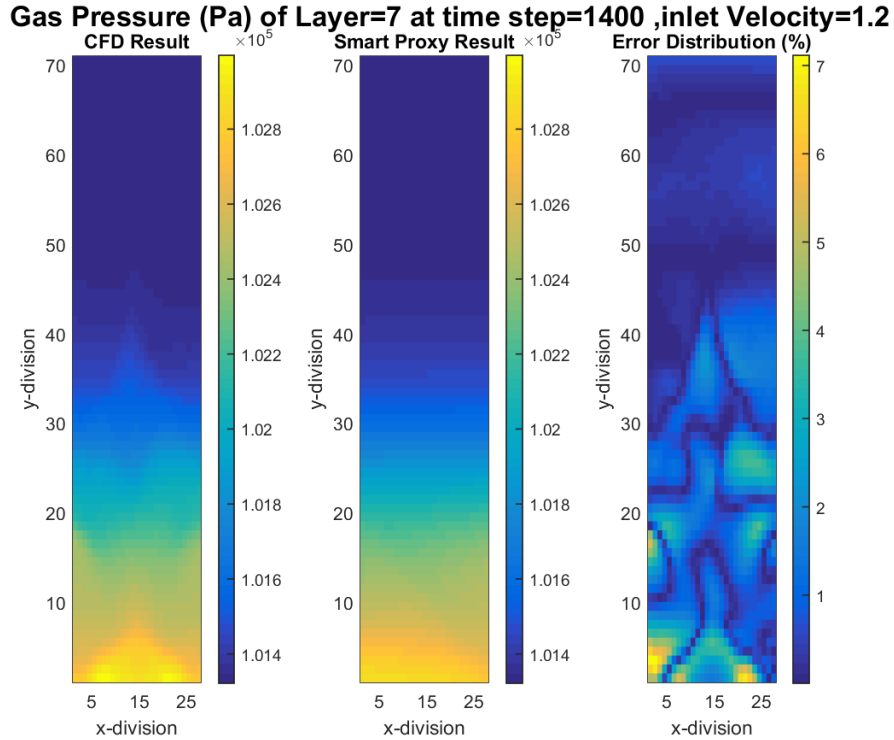
Figure 3-11 shows the 7 different inlet velocity conditions used in the current study, along with the velocity condition used for blind test of the trained ANN. Seven static parameters, as shown in Figure 3-12 are used for the training of the ANN. Figure 4-2 shows the quality of the trained ANN, when inlet velocity of  $V_{in} = 1.2$  (m/s) is used. The blue line is the linear fit to the data. It is clear from Figure 4-2 that the ANN required more training in the lower region of the fluidized bed, where pressure is the highest. The  $R^2$ , which is a measure of how well the regression model can explain the variability observed in the dataset that is used for constructing the model (trained ANN output) is 0.99432. To better access the quality of the trained ANN, the histogram for the discrepancy between the ANN results and the CFD data used for training for data shown in Figure 4-2 is constructed. The percent error or discrepancy is defined by equation 2-4 and is shown in Figure 4-3. It is clear from Figure 4-3 that there is no systematic bias in the data shown in Figure 4-2. The mean value in Figure 4-3 is nearly zero, which indicates there are as many cells underpredicted by ANN than cells that are overpredicted. Figure 4-4 shows the gas pressure distribution in CFD and smart proxy in the 2<sup>nd</sup> cross-sectional plane at time step of 1400. The maximum error of less than 7%, based on equation 2-4, is observed in the gas pressure at the lower portion of the fluidized bed. To get the actual discrepancy between actual CFD data and ANN output, contour scales in Figure 4-4 has to be multiplied by 22.36 Pa, which is the difference between maximum and minimum pressure values in the CFD data set used for training divided by 100.



**Figure 4-2 Parity plot of trained ANN and CFD results for gas pressure at inlet velocity of  $V_{in}$  of 1.2 m/s and time step of 1400, using 7 static parameters**



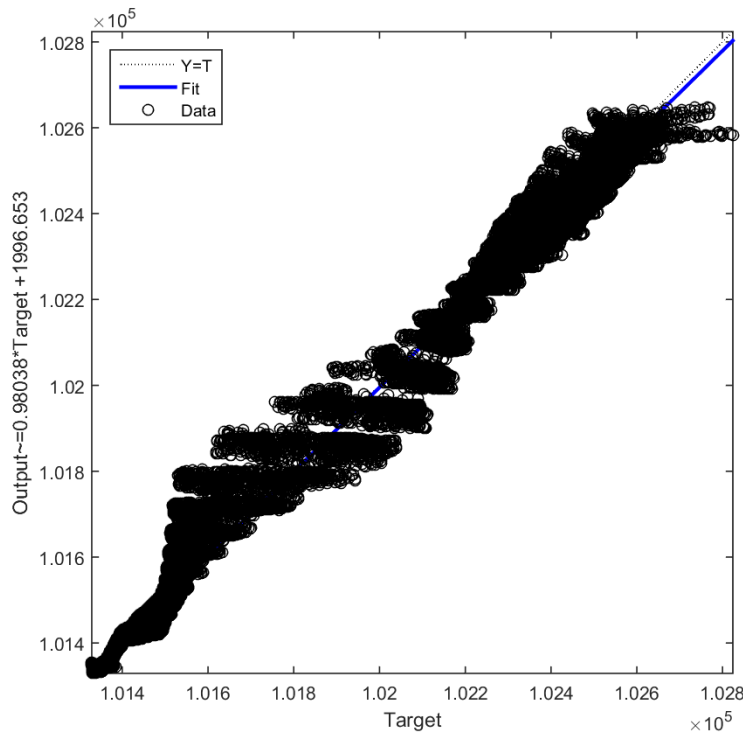
**Figure 4-3** Error distribution per equation 2-4 for gas pressure at inlet velocity of  $V_{in}$  of 1.2 m/s and time step of 1400, using 7 static parameters



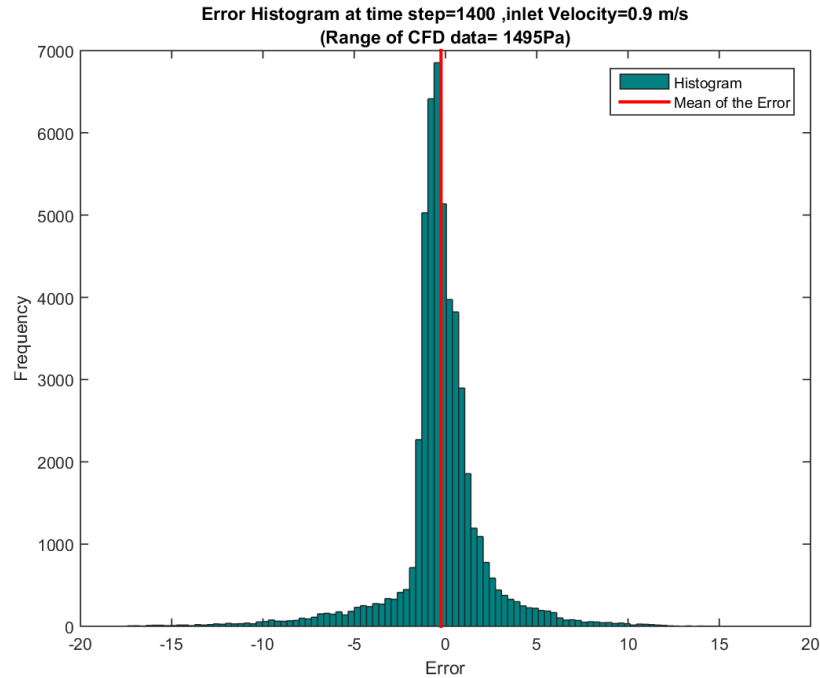
**Figure 4-4** CFD and smart proxy results for gas pressure at  $K=7$  cross-sectional plane for time step of 1400 and  $V_{in} = 1.2$  m/s, using 7 static parameters

Figure 4-5 shows the training quality of the ANN, when the inlet velocity of  $V_{in} = 0.9$  (m/s) is used. The  $R^2$  for the trained ANN output is 0.98845. The distribution of percent error, as defined by equation 2-4, is shown in Figure 4-6. It is clear from Figure 4-6 that there is no systematic bias in the data shown in Figure 4-5. The mean value in Figure 4-6 is -0.05, which indicates there are as many cells underpredicted by ANN than cells that are overpredicted. Figure 4-7 shows the gas pressure distribution in CFD and smart proxy in the 2<sup>nd</sup> cross-sectional plane at time-step of 1400.

At lower inlet gas velocity, the discrepancy between the trained ANN and the CFD results is primarily around the bed and freeboard interface. The maximum error of about 16%, based on equation 2-4, is observed in the gas pressure at the lower portion of the fluidized bed. To get the actual discrepancy between actual CFD data and ANN output, contour scales in Figure 4-7 has to be multiplied by 14.95 Pa, which is the difference between maximum and minimum pressure values in the CFD data set used for training divided by 100.



**Figure 4-5 Parity plot of trained ANN and CFD results for gas pressure at inlet velocity of 0.9 m/s and time step of 1400, using 7 static parameters**



**Figure 4-6 Error distribution per equation 2-4 for gas pressure at inlet velocity of 0.9 m/s and time step of 1400, using 7 static parameters**

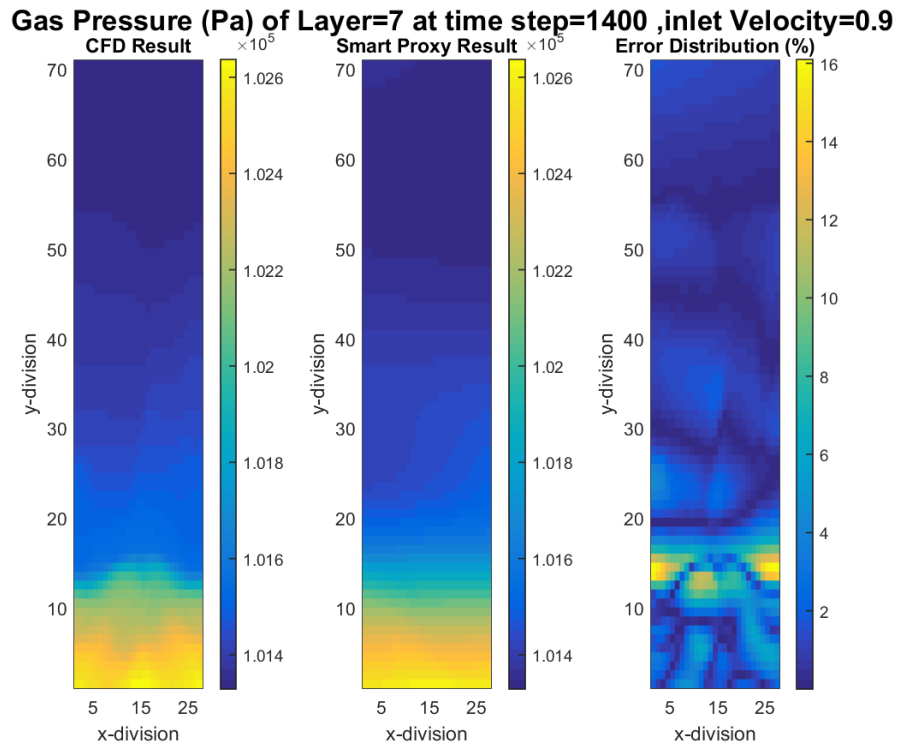


**Figure 4-7 CFD and smart proxy results for gas pressure at K=7 cross-sectional plane, for time step of 1400 and  $V_{in}$  of 0.9 m/s, 7 static parameters**

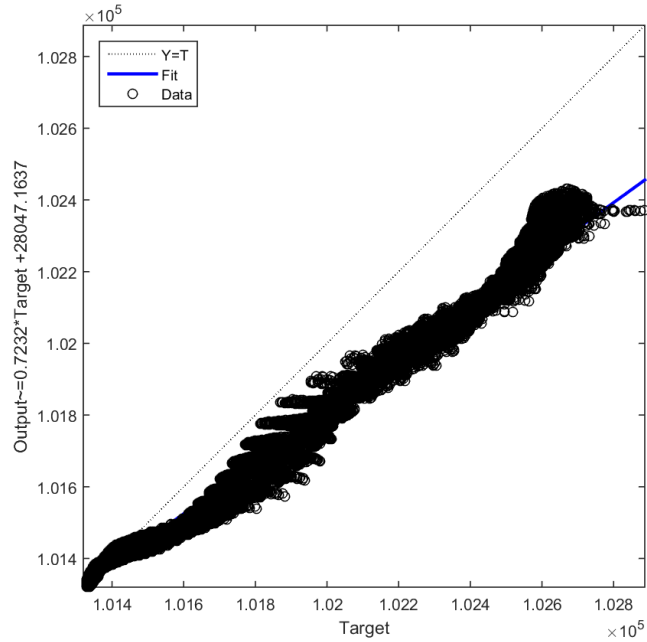


**Figure 4-8 Parity plot of ANN and CFD results for gas pressure for blind test condition of inlet velocity of 0.825 m/s and time step of 1400, using 7 static parameters**

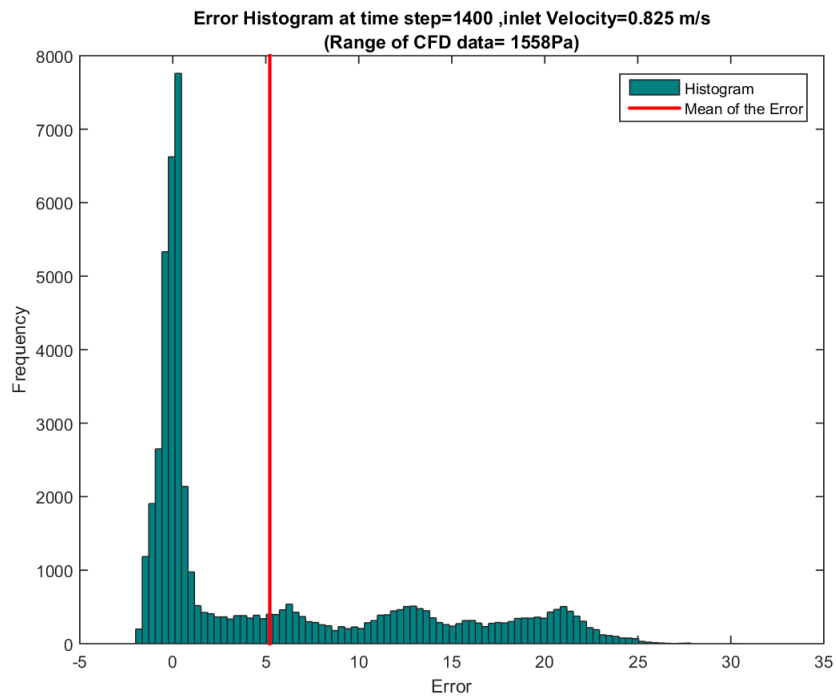


**Figure 4-9 Error distribution per equation 2-4 for gas pressure for blind test condition of inlet velocity of 0.825 m/s and time step of 1400, using 7 static parameters**

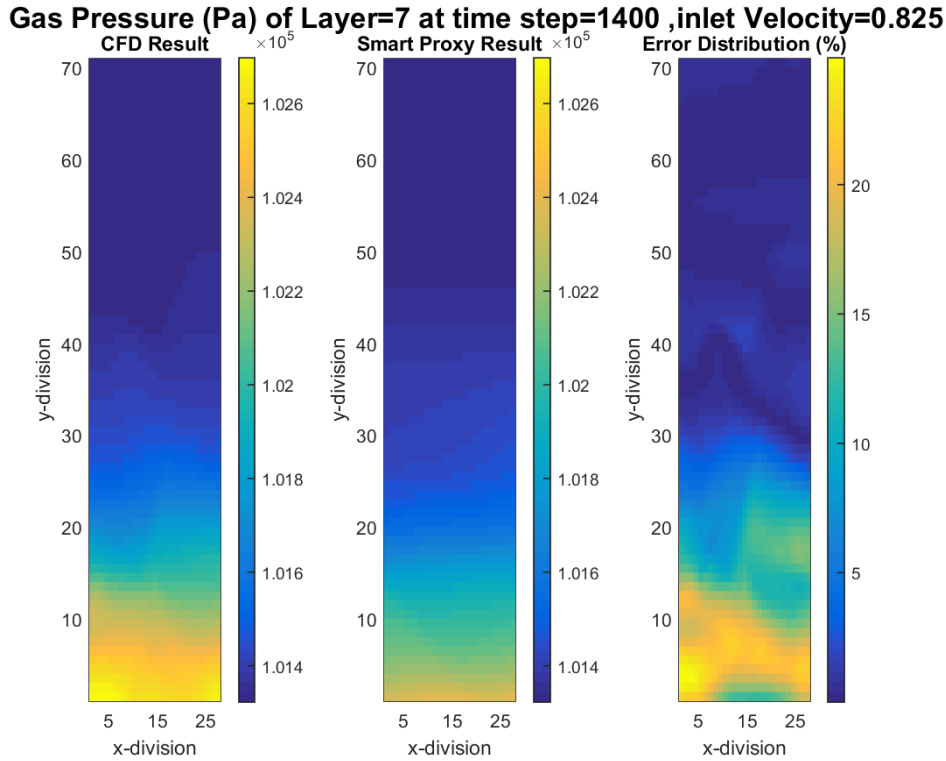


**Figure 4-10 CFD and smart proxy results for gas pressure at K=7 cross-sectional plane, for time step of 1400 and  $V_{in}$  of 0.825 m/s, using 7 static parameters**

A blind test at inlet velocity of  $V_{in}=0.825$  (m/s) is carried out to test the quality of the ANN during deployment. Figure 4-8 shows the comparison between the CFD results (target) with ANN prediction at the inlet velocity value, which was not used as part of training. It is clear that the ANN under predicts the gas pressure field in the entire bed, as also evident from the  $R^2$  value of 0.87822. The error distribution, as defined by equation 2-4, is shown in Figure 4-9. It is clear from Figure 4-9 that the error distribution is skewed towards positive error values, with a mean value of 5%. This skewedness indicates that there is systematic bias in the data shown in Figure 4-8. The trained ANN in a blind test, systematically underpredicts the gas pressure. Figure 4-10 shows the pressure distribution at  $K = 7$  cross-sectional plane for both CFD and ANN for the blind test. The maximum error of about 25%, based on equation 2-4, is observed in the gas pressure in the fluidized bed. To get the actual discrepancy between actual CFD data and ANN output, contour scales in Figure 4-8 has to be multiplied by 15.58 Pa, which is the difference between maximum and minimum pressure values in the CFD data set used for training divided by 100. A closer look at the  $R^2$  values shown in Figure 4-2, Figure 4-5, and Figure 4-8 points to  $R^2$  standalone, not being a reliable measure of the quality of the ANN output. The use of 7 static parameters at a single time step clearly leads to prediction of a more dilute flow by ANN during deployment and hence is not acceptable. The gas pressure distribution at other cross-sectional planes for this case are provided in Appendix I.

### 4.3 TRAINING FOR GAS PRESSURE USING 11 STATIC PARAMETERS AT A SINGLE TIME STEP

To improve the quality of training, the 11 static parameters shown in Figure 3-14, are used for training of the ANN. Figure 4-11 shows that the output of the trained ANN under-predicts gas pressure at the lower part of the bed, at time step 1400. The  $R^2$  for data in Figure 4-11 is 0.99712. As in previous section, the quality of the trained ANN is further accessed by constructing the error distribution, as defined by equation 2-4, for data in Figure 4-11. The percent error (discrepancy) is shown in Figure 4-12. It is clear from Figure 4-12 that there is no systematic bias in the data shown in Figure 4-11. The mean value in Figure 4-12 is nearly zero, which indicates there are as many cells underpredicted by ANN than cells that are overpredicted. The gas pressure distribution in CFD and smart proxy in the 2<sup>nd</sup> cross-sectional plane at time step of 1400 is shown in Figure 4-13. Although the maximum error in Figure 4-13 is about 5% and is lower than the previous case, when 7 static parameters were used for training, the trained ANN still under-predicts the pressure field and hence predicates a more dilute flow field. The same general trends are observed, when the inlet velocity of  $V_{in} = 0.9$  m/s is used for training ANN, Figure 4-14 and Figure 4-16. As in the previous section, the percent error shown in Figure 4-13, Figure 4-16, and Figure 4-19 are the error defined by equation 2-4. To get the actual discrepancy between actual CFD data and ANN output, error contour scales has to be multiplied by 22.36, 14.95, and 15.58 Pa for Figure 4-13, Figure 4-16, and Figure 4-19 respectively. The multiplier factor is the difference between maximum and minimum pressure values in the CFD data set used for training divided by 100 for each case.

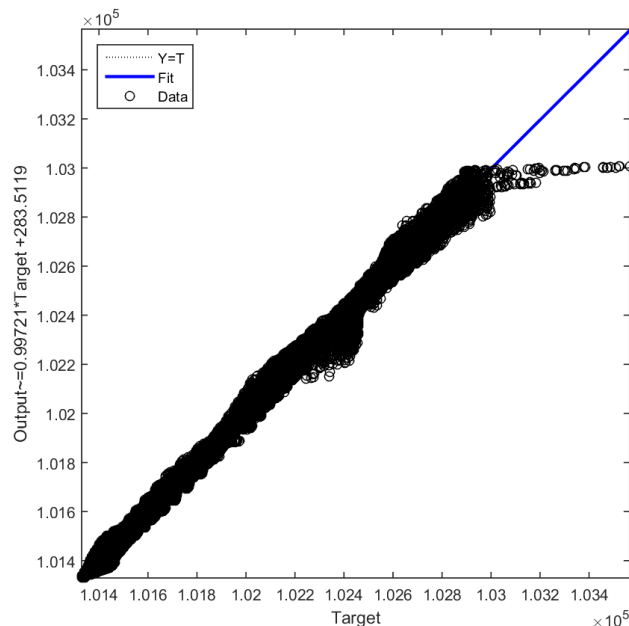


**Figure 4-11 Parity plot of trained ANN and CFD results for gas pressure at inlet velocity of  $V_{in}$  of 1.2 m/s and time step of 1400, using 11 static parameters**

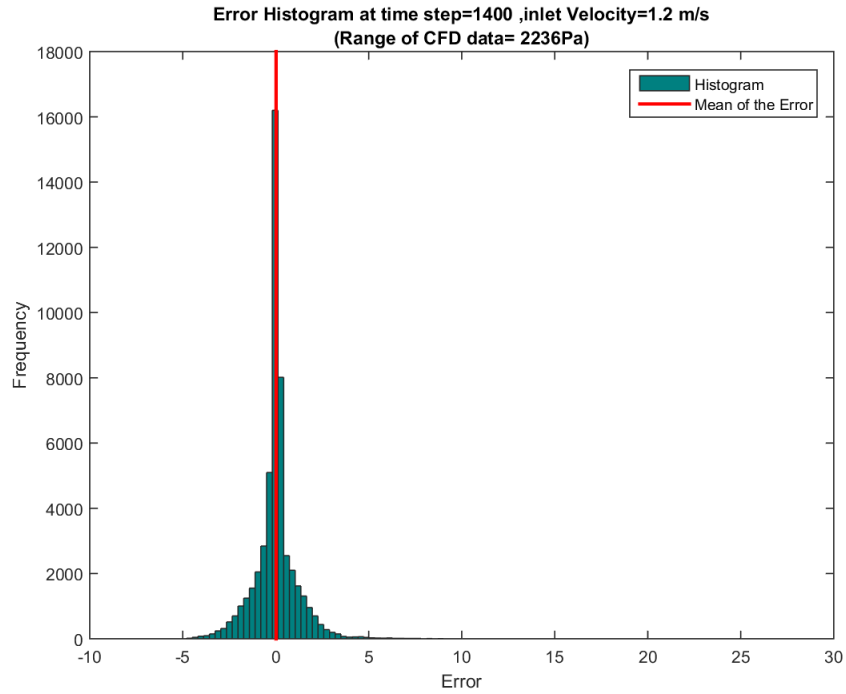


**Figure 4-12** Error distribution per equation 2-4 for gas pressure at inlet velocity of  $V_{in}$  of 1.2 m/s and time step of 1400, using 11 static parameters

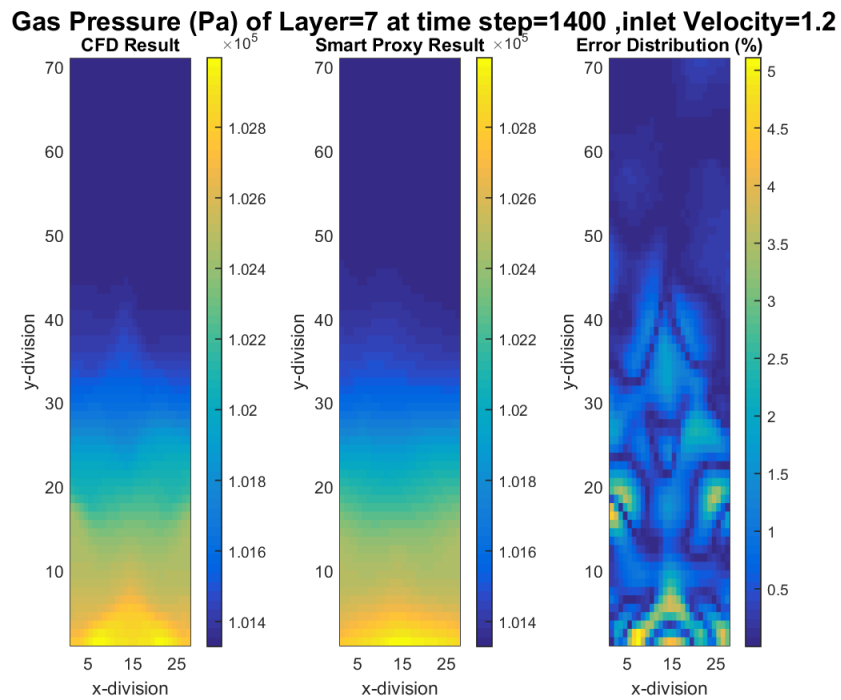


**Figure 4-13** CFD and smart proxy results for gas pressure at  $K=7$  cross-sectional plane for time step of 1400 and  $V_{in} = 1.2$  m/s, using 11 static parameters

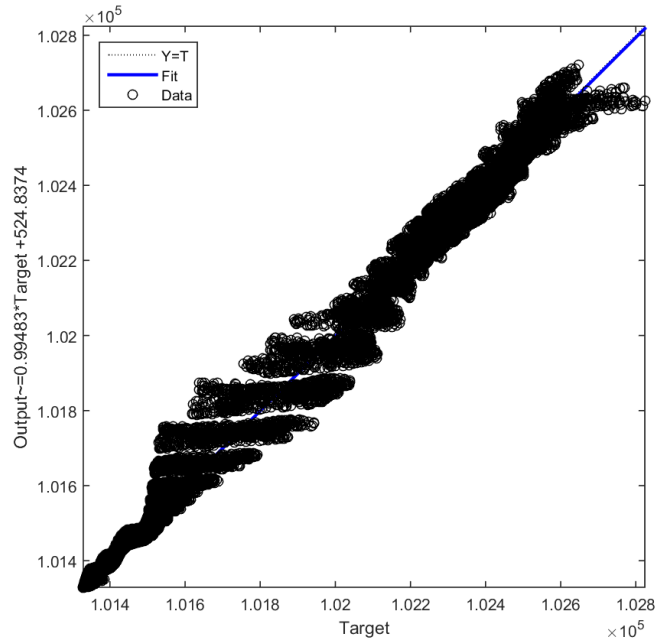


**Figure 4-14 Parity plot of trained ANN and CFD results for gas pressure at inlet velocity of  $V_{in}$  of 0.9 m/s and time step of 1400, using 11 static parameters**

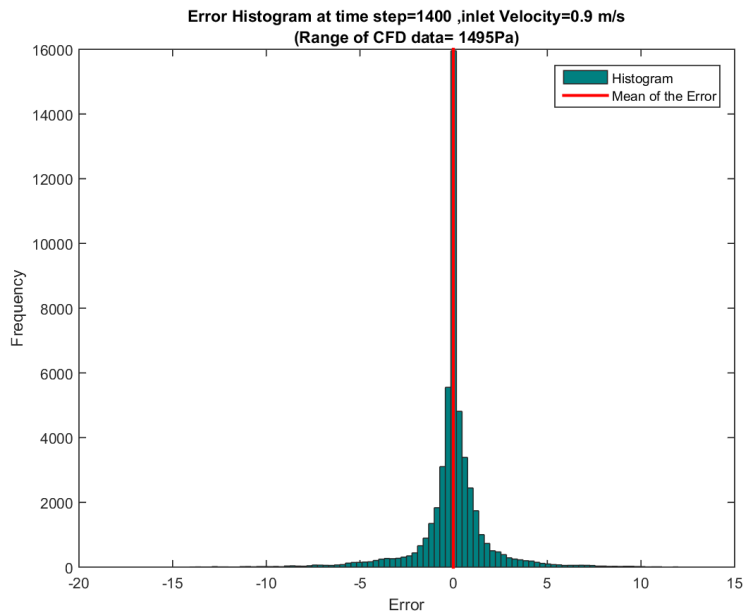


**Figure 4-15 Error distribution per equation 2-4 for gas pressure at inlet velocity of  $V_{in}$  of 0.9 m/s and time step of 1400, using 11 static parameters**

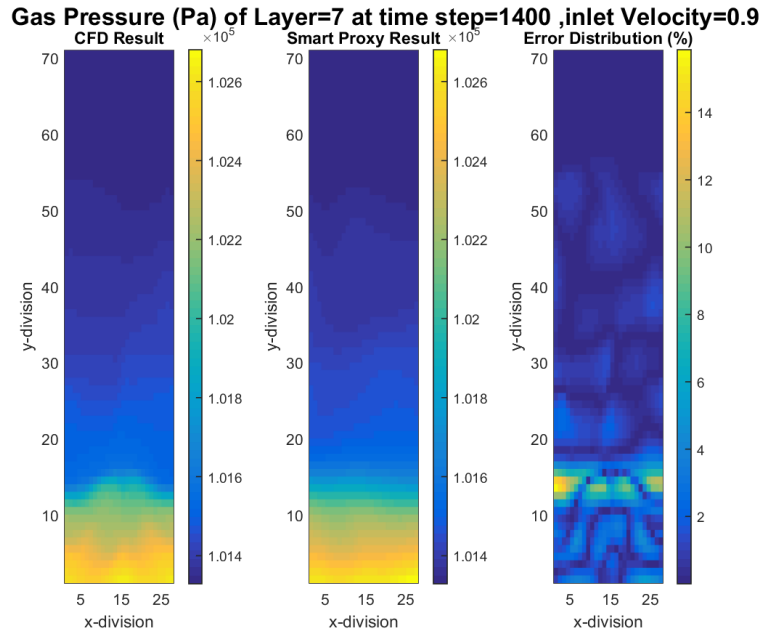


Figure 4-16 CFD and smart proxy results for gas pressure at K=7 cross-sectional plane for time step of 1400 and  $V_{in} = 0.9$  m/s, using 11 static parameters

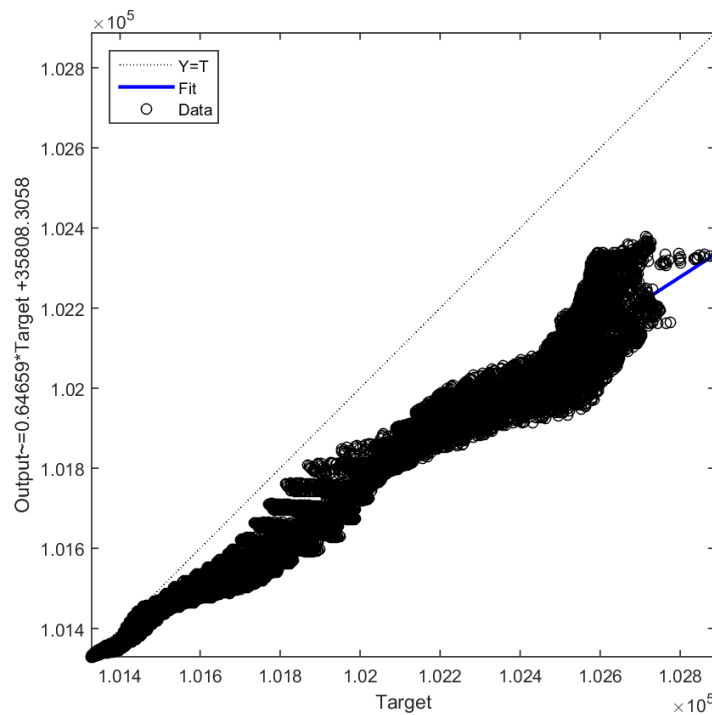
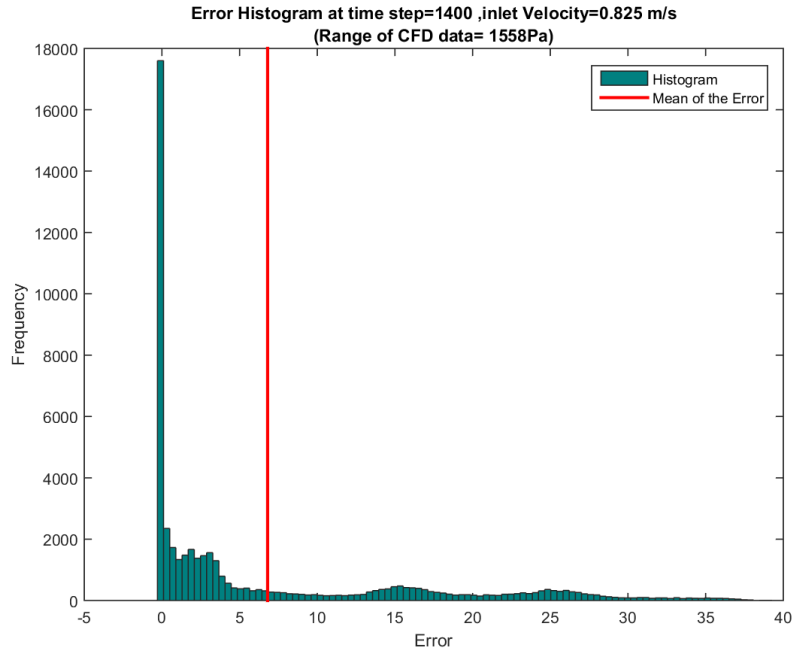
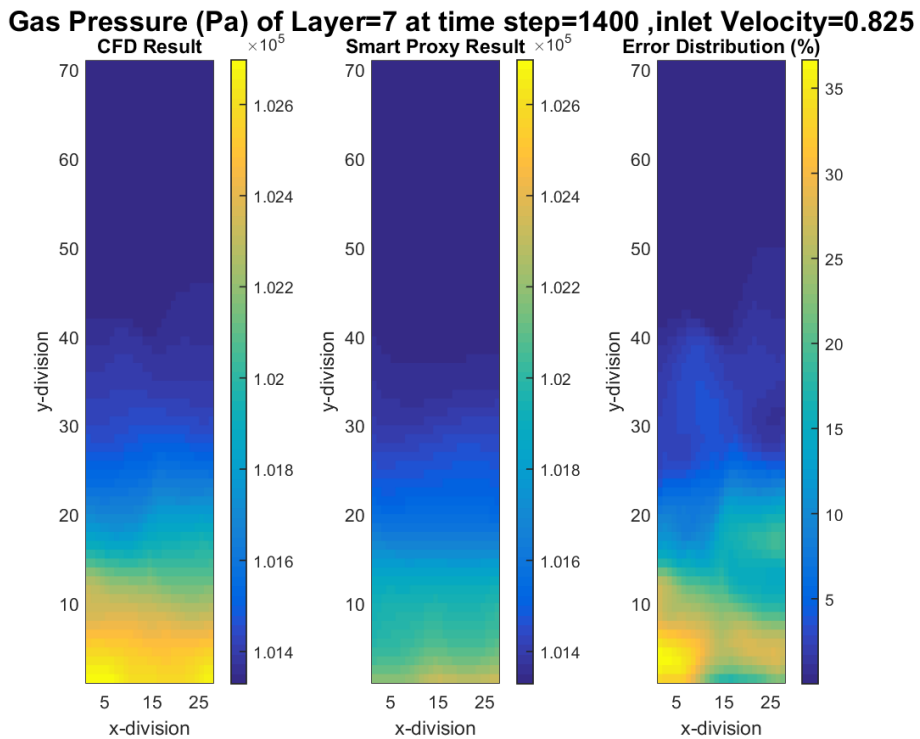


Figure 4-17 Parity plot of ANN and CFD results for gas pressure for blind test condition of inlet velocity of 0.825 m/s and time step of 1400, using 11 static parameters



**Figure 4-18 Error distribution per equation 2-4 for gas pressure for blind test condition of inlet velocity of 0.825 m/s and time step of 1400, using 11 static parameters**



**Figure 4-19 CFD and smart proxy results for gas pressure at K=7 cross-sectional plane for time step of 1400 and  $V_{in} = 0.825$  m/s, using 11 static parameters**

The result of the blind test of ANN at inlet velocity of  $V_{in}=0.825$  m/s are shown in Figure 4-17 through Figure 4-19. The error distribution, as defined by equation 2-4, is shown in Figure 4-18. It is clear from Figure 4-18 that the error distribution is skewed towards positive error values, with a mean value of 7%. This skewedness indicates that there is systematic bias in the data shown in Figure 4-17. The trained ANN in a blind test, systematically underpredicts the gas pressure. As it was the case in the previous section, the ANN predicts a more dilute flow, when it is used at an inlet velocity, which was not part of the training data set. The outcome of the tests with 7 and 11 static parameters at time step of 1400 is summarized in Table 4-1 in terms of the calculated  $R^2$ . Marginal improvement in the training process of ANN is achieved, when 11 static parameters are used instead of 7 static parameters during the training. However, regardless of the number of parameters used, the quality of the trained ANN is not acceptable, when used in a blind test case, with inlet velocity of 0.825 m/s.

**Table 4-1  $R^2$  of different training scenarios**

<i>Scenario</i>	$V_{in}=1.2$	$V_{in}=0.9$	$V_{in}=0.825$
<i>Using 7 static parameters</i>	0.99432	0.98845	0.77128
<i>Using 11 static parameters</i>	0.99712	0.99366	0.53532

An expanded view of areas in Figure 4-11 and Figure 4-14, where ANN under-predicts gas pressure are shown in Figure 4-20 and Figure 4-21. To better isolate these areas, local cells with pressure value greater than 103 kPa in Figure 4-20 and cells with pressure values greater than 102.6 kPa in Figure 4-21 are shown in Figure 4-22. It is clear from Figure 4-22 that there are handful of cells in the vicinity of inlet that gas pressure is under-predicted by ANN. To investigate further gas pressure under-prediction in the lower part of the fluidized bed, average gas pressure across planes perpendicular to the flow, as shown in Figure 3-16, is compared to that of CFD results and shown in Figure 4-23, for the training case with inlet velocity of 0.9 m/s. The agreement for the spatially averaged gas phase pressure between ANN and CFD is very favorable, even though the cell based comparison of the same two data sets points to larger discrepancies in the lower part of the bed. In fact, this discrepancy is far more evident, when ANN is used in the deployment mode as shown in Figure 4-24, which is the spatially averaged gas pressure along the bed for the case of inlet velocity of 0.825 m/s (blind test). The gas pressure at other cross-sectional planes are provided in appendix II. To improve the quality of ANN training process, particularly in the lower portion of the fluidized bed, where gas pressure is under-predicted, various techniques are employed and outlined in the next section.

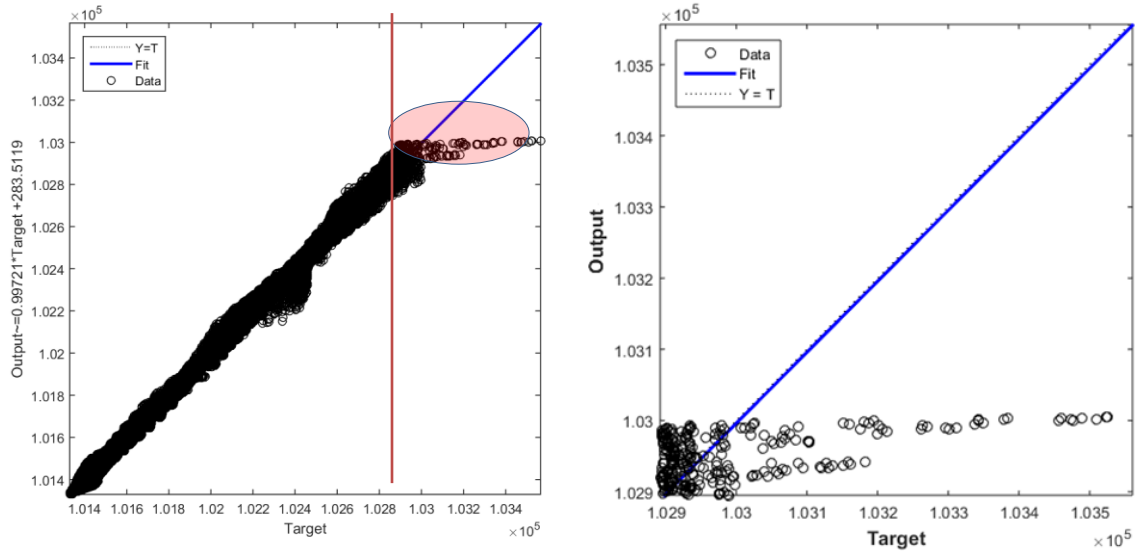


**Figure 4-20** Zooming in to the parity plot of trained ANN for gas pressure at inlet velocity of 1.2 m/s and time step of 1400, using 11 static parameters

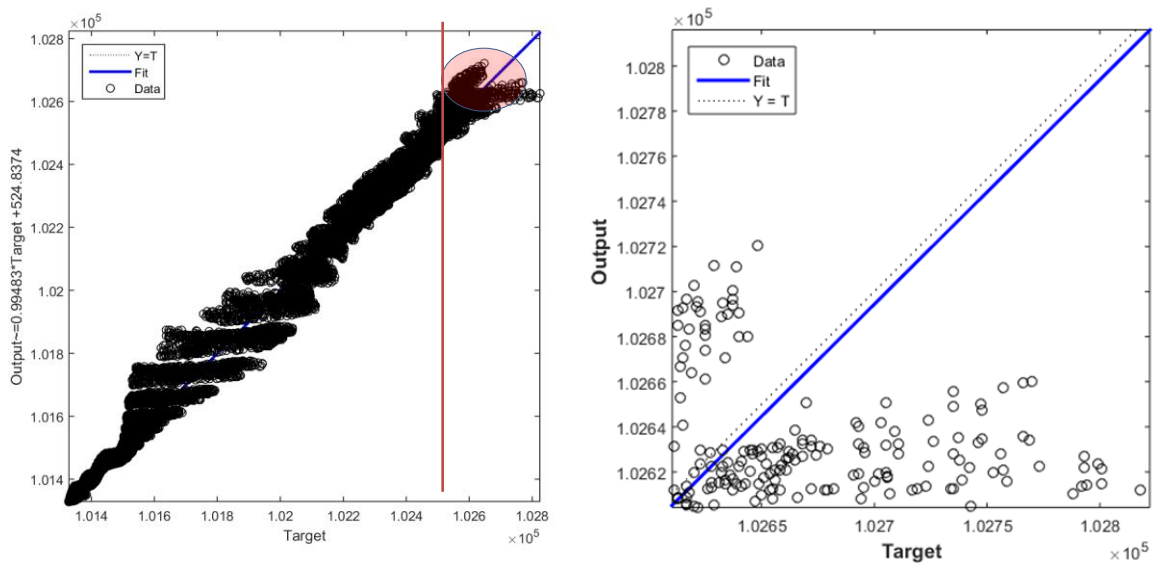


**Figure 4-21** Zooming in to the parity plot for trained ANN for gas pressure at inlet velocity of 0.9 m/s and time step of 1400, using 11 static parameters

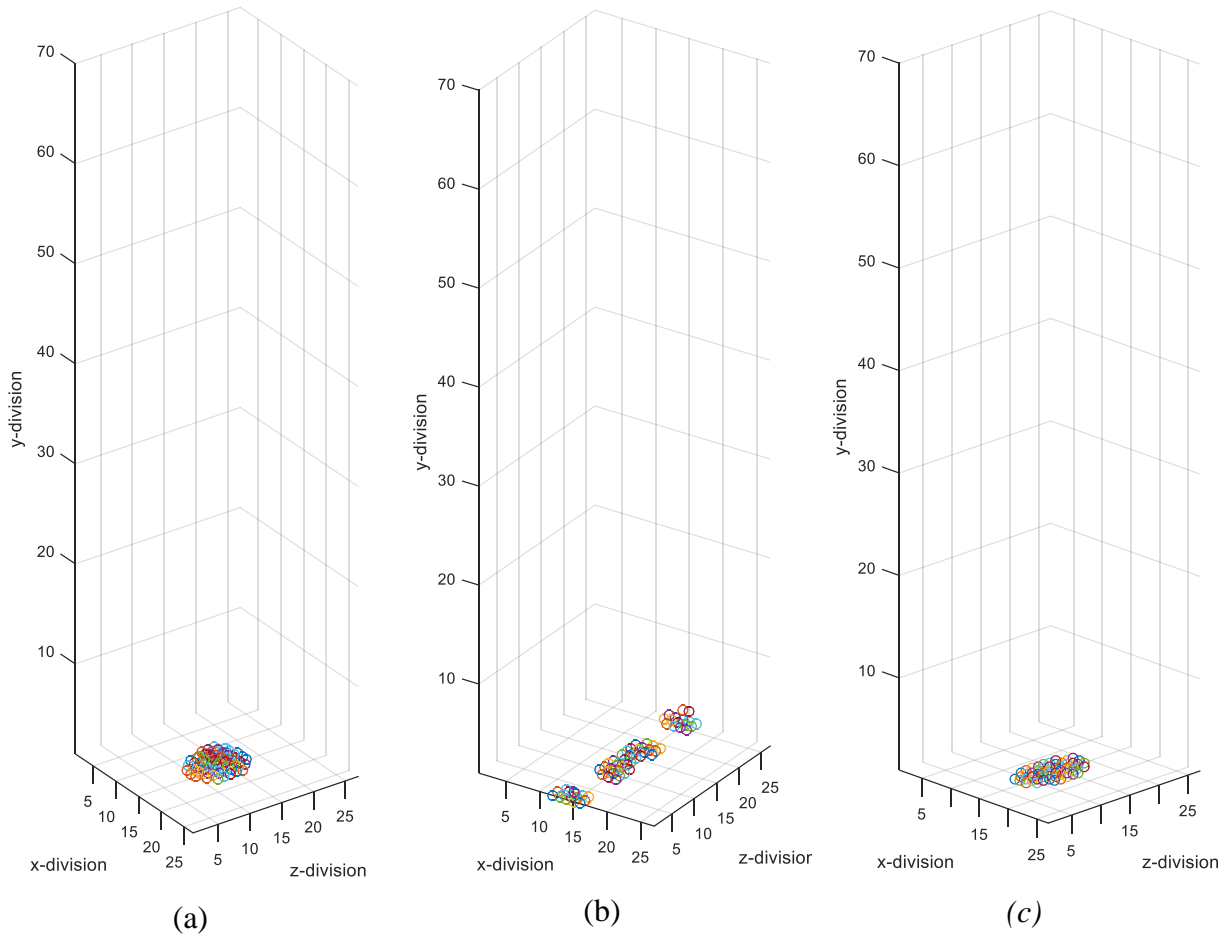


**Figure 4-22** Cells, where the gas pressure is underpredicted by ANN, for time step of 1400, when (a)  $V_{in}=1.2$  m/s (b)  $V_{in}=0.9$  m/s (c)  $V_{in}=0.6$  m/s

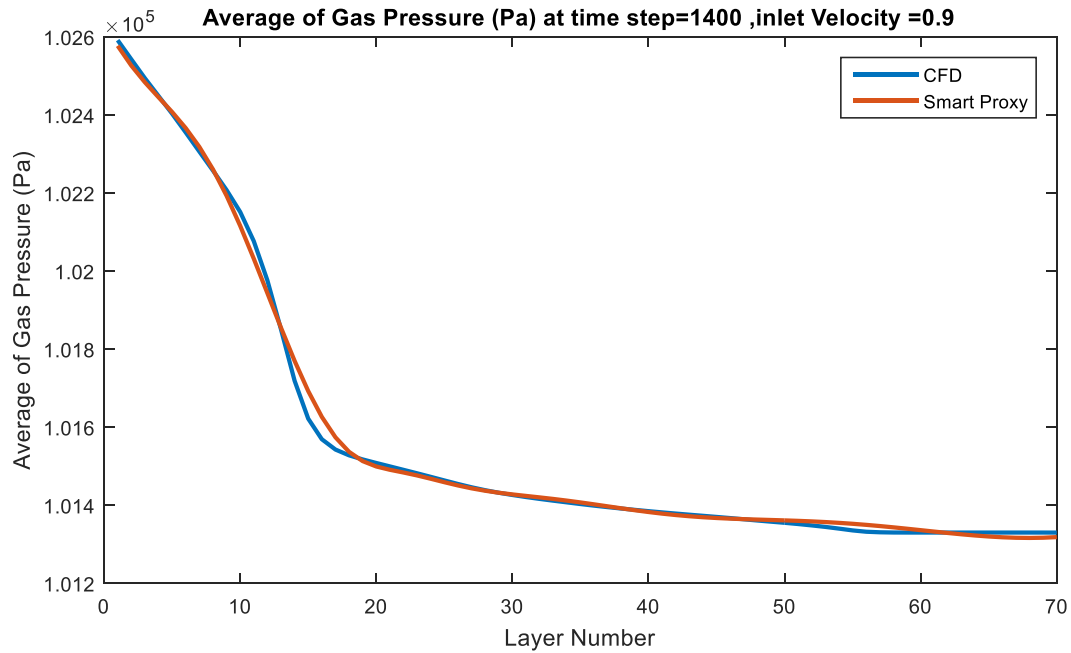


**Figure 4-23** Temporal average of CFD and smart proxy results at training for gas pressure, spatially averaged along the fluidized bed at time step=1400 and  $V_{in}=0.9$  m/s

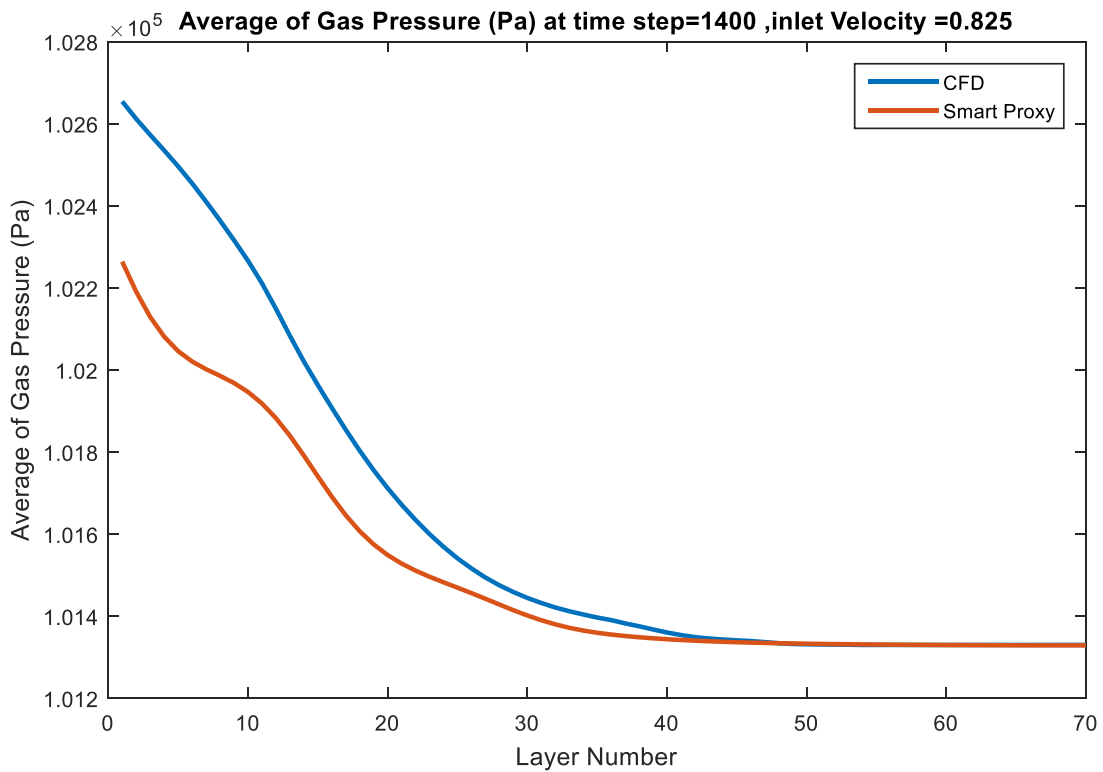


**Figure 4-24** Temporal average of CFD and smart proxy results at deployment for gas pressure, spatially averaged along the fluidized bed at time step=1400 and  $V_{in}=0.825$  m/s

#### 4.4 OPTIMIZING THE ANN

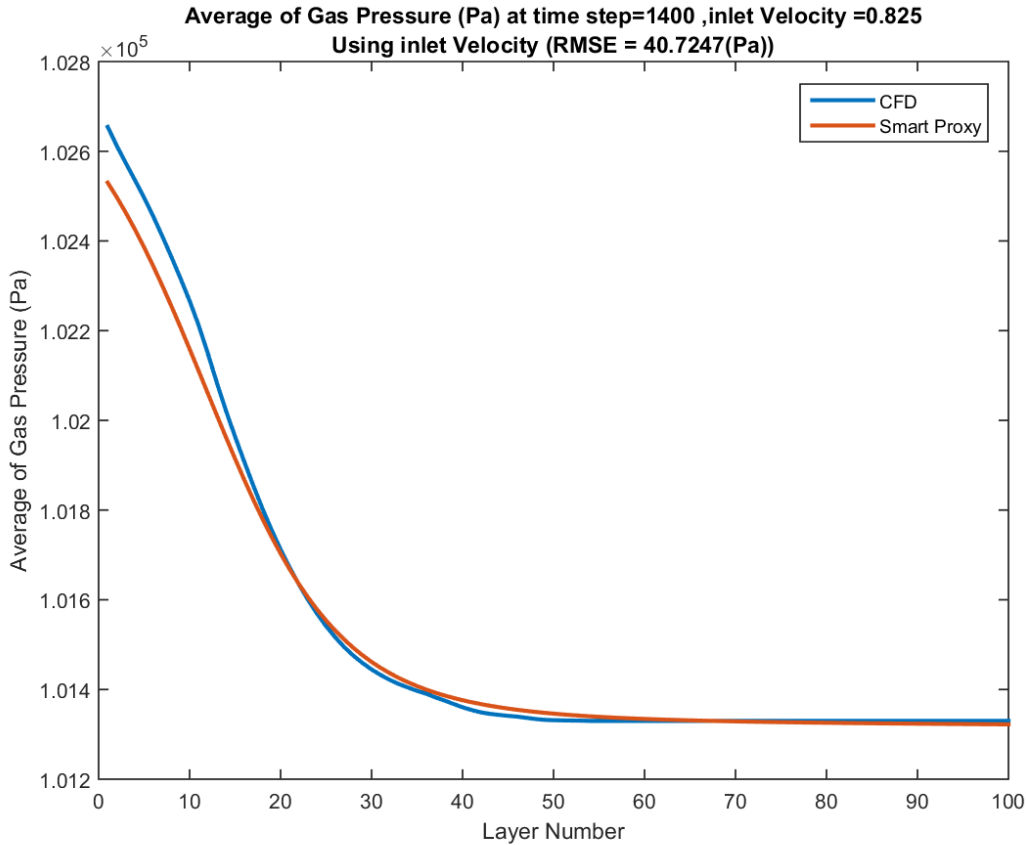
The techniques outlined below are some of the techniques employed during the training process in order to improve the quality of the trained ANN.

1. Training one ANN for the lower bed are and one ANN for the rest of the fluidized bed,
2. Training different ANNs for each X-Z layer (cross sectional areas perpendicular to the flow) in the lower portion of the bed and 2 ANNs for the rest of the fluidized bed,
3. Training different ANNs for each X-Z layer while using the values of the (Y-I) layers as input to predict the values for the Y layer,
4. Tuning the ANN internal parameters by training hundreds of ANNs,
5. Training the ANN by introducing dimensionless inlet velocity values and different forms of inlet velocities ( $\sqrt{V_{in}}, V_{in}^2, V_{in}^3, \log V_{in}, \dots$ ),

Not all the optimization techniques used led to improvement in better training of ANN. Of the 5-improvement technique listed above, item 4 exhibited the most improvement in the quality of the trained ANN. Table 4-2 outlines some of the improvements, which were achieved by applying item 4 of the list above. All of these techniques share the same basic neural network architecture.

**Table 4-2 Some of the ANN internal parameters before and after optimization**

	<i>Originally (before optimization)</i>	<i>After Optimization</i>
<b><i>Number of hidden layers</i></b>	<i>1</i>	<i>2</i>
<b><i>Number of Hidden Neurons</i></b>	<i>15</i>	<i>1<sup>st</sup> layer: 6 2<sup>nd</sup> layer 3</i>
<b><i>Training Algorithm</i></b>	<i>Levenberg-Marquardt</i>	<i>Gradient Descent with adaptive LR</i>
<b><i>Transfer Function</i></b>	<i>TANSIG</i>	<i>Hidden layers: LOGSIG Output layer: PURELIN</i>



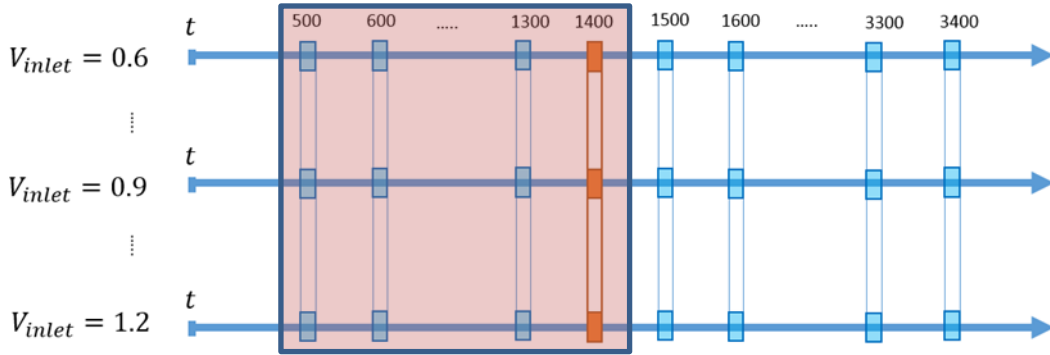
**Figure 4-25 Optimized CFD and smart proxy results at deployment for gas pressure, spatially averaged along the fluidized bed at time step=1400 and  $V_{in}=0.825$  m/s**

Figure 4-25 shows the spatially averaged gas pressure along the fluidized bed, after optimization, for the same conditions depicted in Figure 4-24. Clearly, the ANN prediction in the deployment mode (blind test) has drastically improved after the various optimization techniques that were applied.

The process of optimizing the predictive quality of the ANN was only briefly mentioned in this section. Details of how such optimizations are accomplished are of major importance to construction of an ANN, with high degree of fidelity. As such, this topic will be discussed in greater details in the next report.

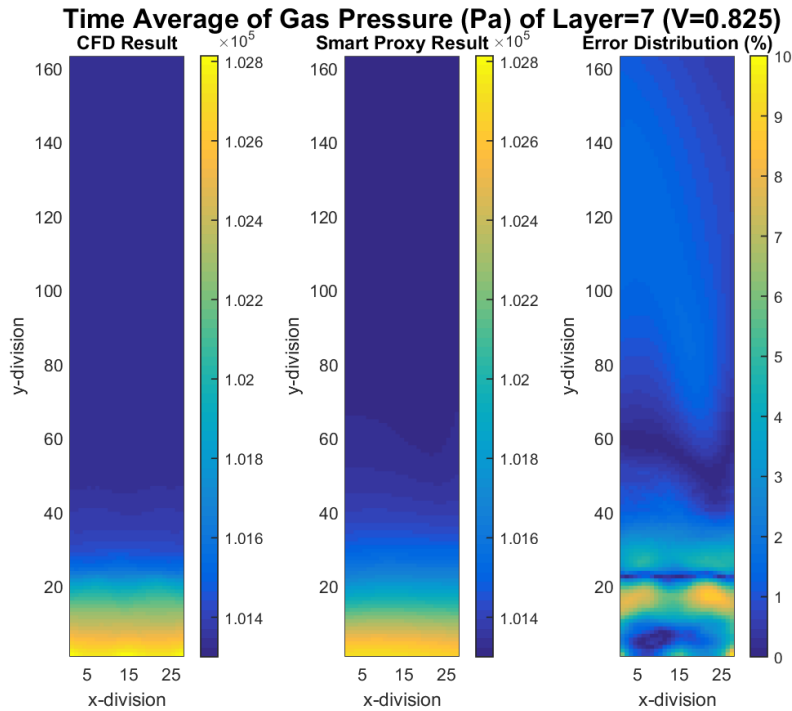
#### 4.5 TIME AVERAGE

The approach developed in sections 4.3 and 4.4 is used to develop series of ANNs at time steps 500 to 1400 at an increment of 100, as shown in Figure 4-26. The ANN results are time averaged and the temporally averaged values are compared to temporally averaged CFD results for the same time interval of time step 500 through time step 1400.

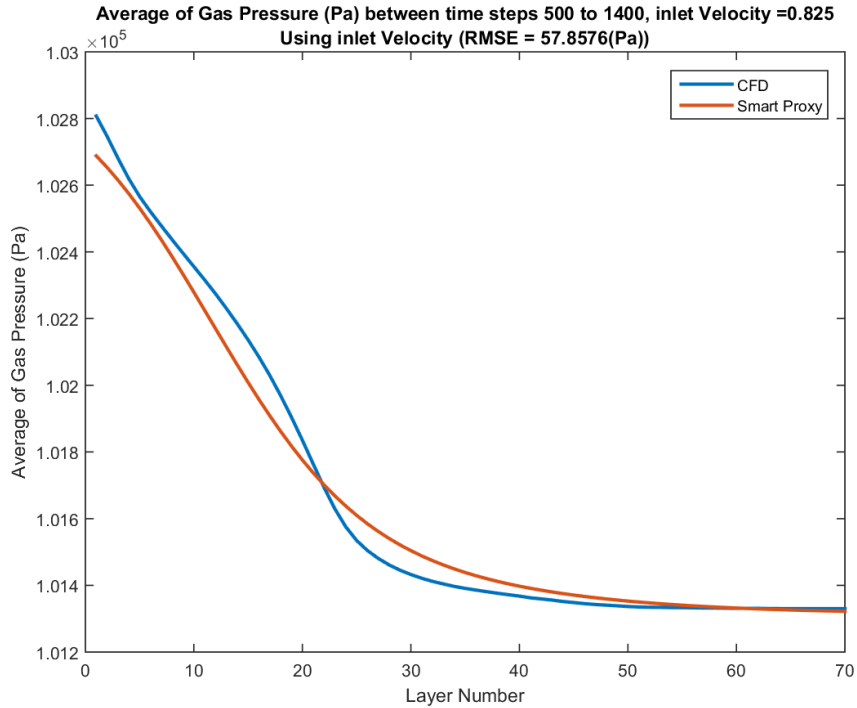


**Figure 4-26** Time steps used in time average between time steps 500 to 1400

Figure 4-27 shows the comparison of time averaged gas pressure between ANN in deployment mode and CFD results at  $K = 7$  plane for time-steps 500 to 1400 and inlet velocity of  $V_{in}=0.825$  m/s. This inlet velocity is part of the blind test. Figure 4-27 shows a favorable agreement between the time averaged ANN prediction and CFD results. The maximum error is about 10% in the bed. Additional figures at other cross sectional planes for this flow condition are provided in Appendix III. Figure 4-28 shows the time average of spatially averaged gas pressure. The RMSE in Figure 4-28 is 58 Pa, which is less than 4% of the pressure drop across the fluidized bed.

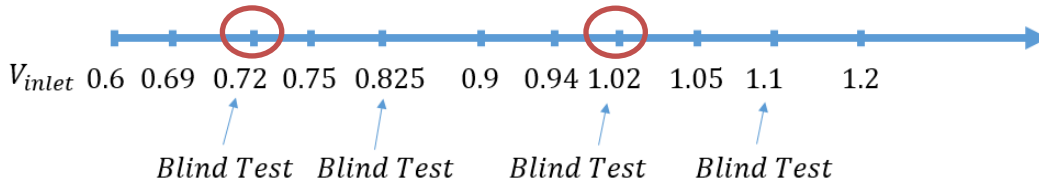


**Figure 4-27** CFD and smart proxy results for gas pressure averaged over time steps 500 to 1400 at  $K=7$  cross-sectional plane with  $V_{in}=0.825$  m/s



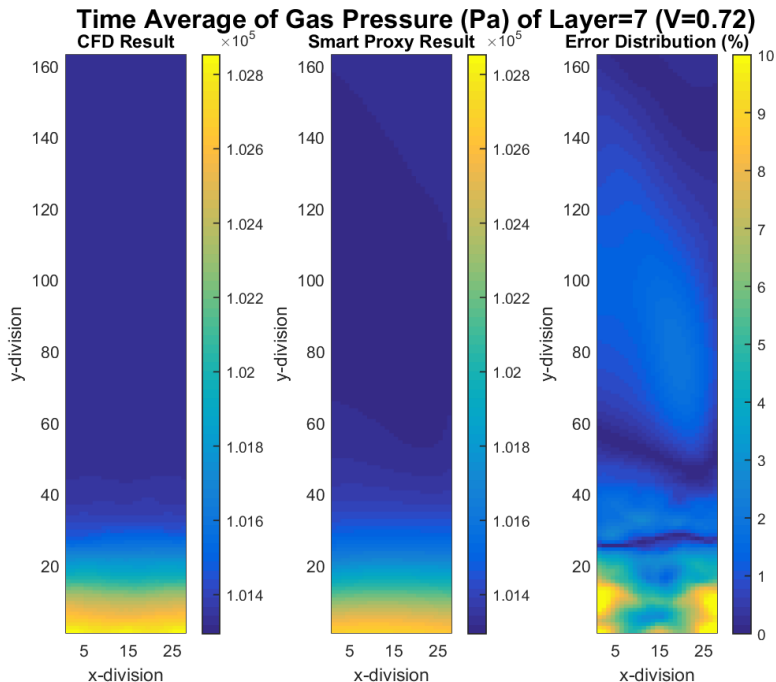
**Figure 4-28 Time averaged CFD and smart proxy results for gas pressure, spatially averaged along the fluidized bed (time-steps = 500 to 1400 and  $V_{in} = 0.825$  m/s)**

To examine the robustness of this technique and its predictive capability the same process is repeated for two other blind tests (inlet velocity value that were not included in the training sets). The new blind tests had the inlet velocities of  $V_{in} = 0.72$  m/s and  $V_{in} = 1.02$  m/s, as shown in Figure 4-29.

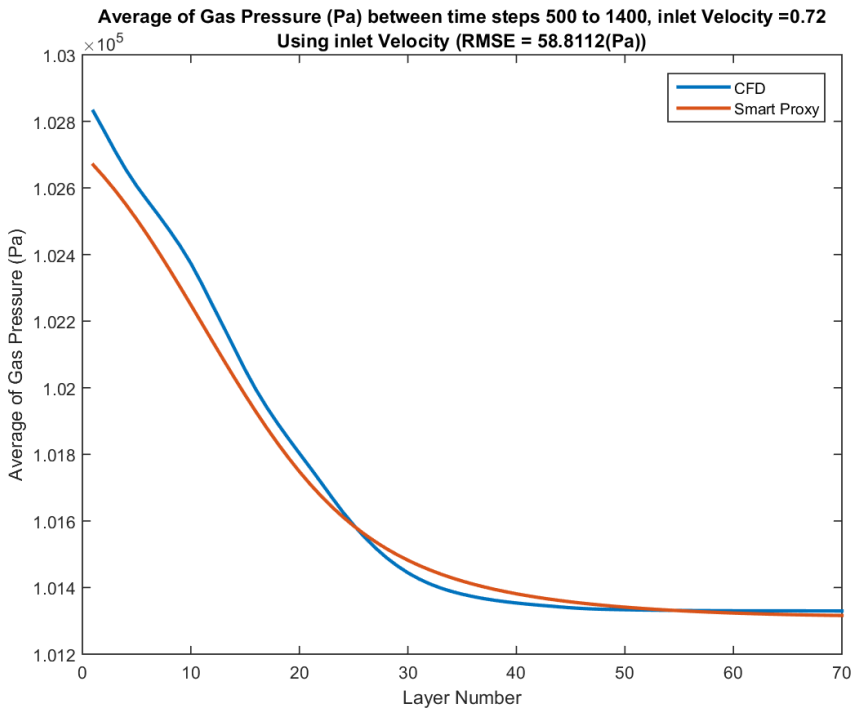


**Figure 4-29 Additional blind tests at  $V_{in} = 0.72$  and  $V_{in} = 1.02$  m/s**

Figure 4-30 shows the time average gas pressure from CFD and the smart proxy at  $K = 7$  plane using time-steps 500 through 1400 with inlet gas velocity of  $V_{in} = 0.72$  m/s. Reasonable agreement is observed in Figure 4-30 between CFD result and ANN prediction, with the maximum error of 10% along the walls in the bed. Additional figures showing the average gas pressure at different cross sectional planes for this blind test are provided in Appendix III. Figure 4-31 shows the time average of the spatially averaged gas pressure values along the fluidized bed. The RMSE in Figure 4-31 is 59 Pa, which is less than 4% of the pressure drop across the fluidized bed.



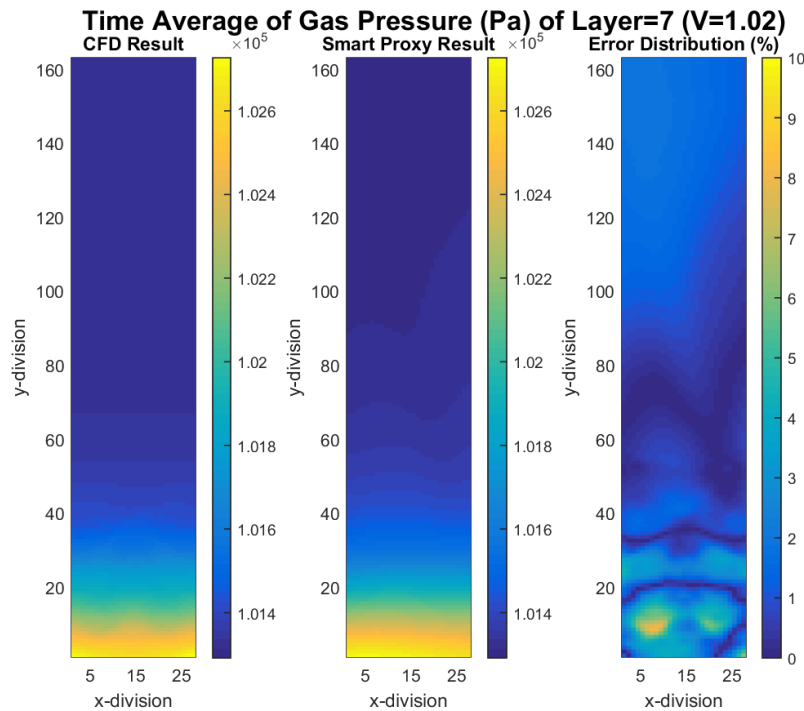
**Figure 4-30** CFD and smart proxy results for gas pressure averaged over time steps 500 to 1400 at K=7 cross-sectional plane with  $V_{in}=0.72$  m/s



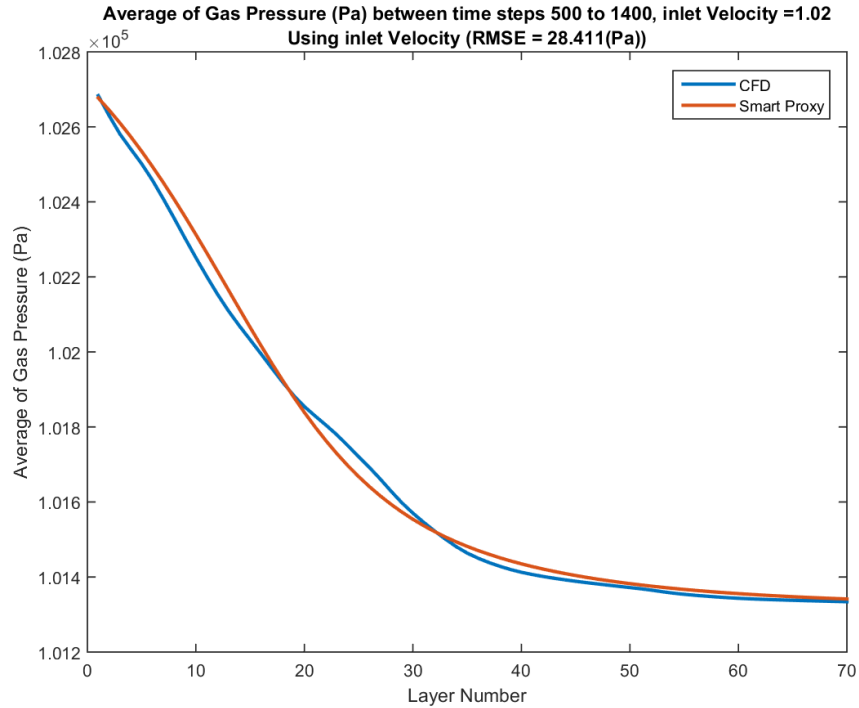
**Figure 4-31** Time averaged CFD and smart proxy results for gas pressure, spatially averaged along the fluidized bed (time-steps = 500 to 1400 and  $V_{in} = 0.72$  m/s)

Figure 4-32 shows the time average gas pressure from CFD and the smart proxy at  $K = 7$  cross sectional plane using time-steps 500 through 1400 for  $V_{in}=1.02$  m/s. The agreement between CFD results and ANN prediction is favorable, with the maximum error of about 10% in the bed. Additional figures at other cross sectional planes are provided in Appendix III.

Figure 4-33 shows the time average of spatially averaged gas pressure along the fluidized bed. The RMSE for this blind test is 28.411 Pa, which is about 2% of the pressure drop across the fluidized bed.

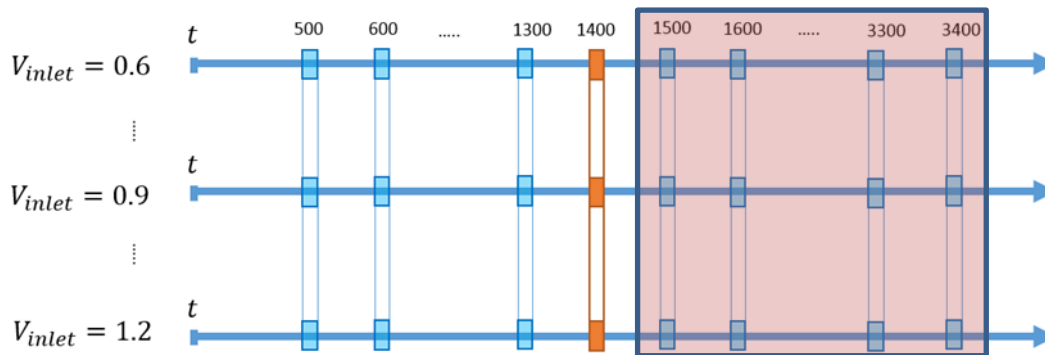


**Figure 4-32** CFD and smart proxy results for gas pressure averaged over time steps 500 to 1400 at  $K=7$  cross-sectional plane with  $V_{in}=1.02$  m/s

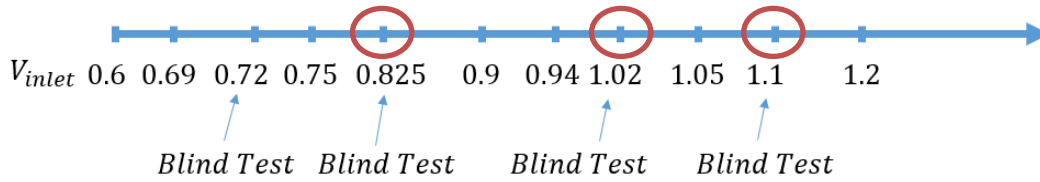


**Figure 4-33 Time averaged CFD and smart proxy results for gas pressure, spatially averaged along the fluidized bed (time-steps = 500 to 1400 and  $V_{in} = 1.02$  m/s)**

The smart proxy model is able to capture the behavior of the time-steps 500 through 1400 reasonably well, when flow is more of a slugging flow. The following figures illustrate the performance of the ANN, over time steps 1500 to 3400, when flow becomes fluidized. Series of ANNs are constructed at time steps 1500 to 3400 at an increment of 100, as shown in Figure 4-34. Once the ANNs are trained, three blind tests, as outlined in Figure 4-35 are carried out.



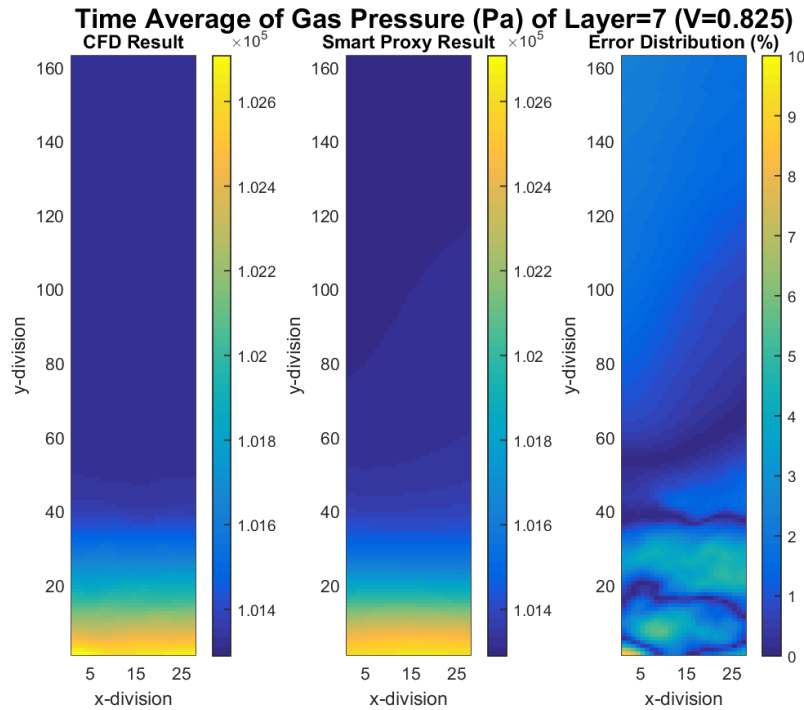
**Figure 4-34 Time steps used for time averaging between time steps 1500 to 3400**



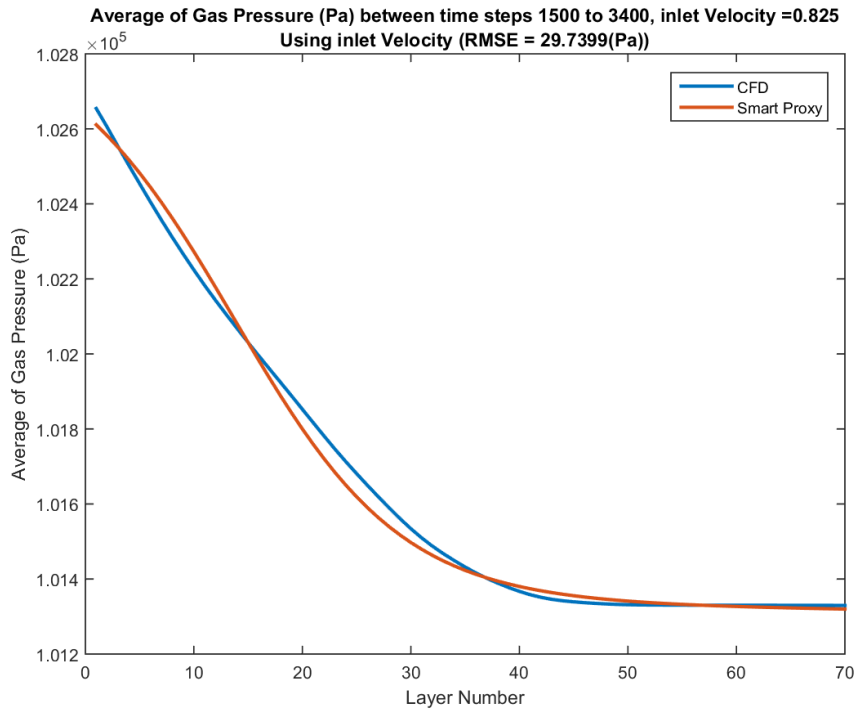
**Figure 4-35** Blind test carried out at three different inlet velocities

Figure 4-36, Figure 4-38, and Figure 4-40 show the time average of gas pressure for the CFD and the smart proxy for the 2<sup>nd</sup> cross-sectional plane using time average for the time-steps 1500 through 3400 for  $V_{in}=0.825$  m/s,  $V_{in}=1.02$  m/s, and  $V_{in}=1.1$  m/s, respectively. These figures display good agreements between pressure distributions calculated by the CFD and those predicted by the smart proxy. Additional figures for these three blind tests are provided in Appendix IV.

Figure 4-37, Figure 4-39, and Figure 4-41 show the time average of spatially averaged gas pressure along the fluidized bed. The RMSE of ANN prediction for  $V_{in}=0.825$  m/s,  $V_{in}=1.02$  m/s, and  $V_{in}=1.1$  m/s, is 30 Pa, 38 Pa and 76 Pa respectively.



**Figure 4-36** CFD and smart proxy results for gas pressure averaged over time steps 1500 to 3400 at K=7 cross-sectional plane with  $V_{in}=0.825$  m/s



**Figure 4-37** Time averaged CFD and smart proxy results for gas pressure, spatially averaged along the fluidized bed (time-steps = 1500 to 3400 and  $V_{in} = 0.825$  m/s)

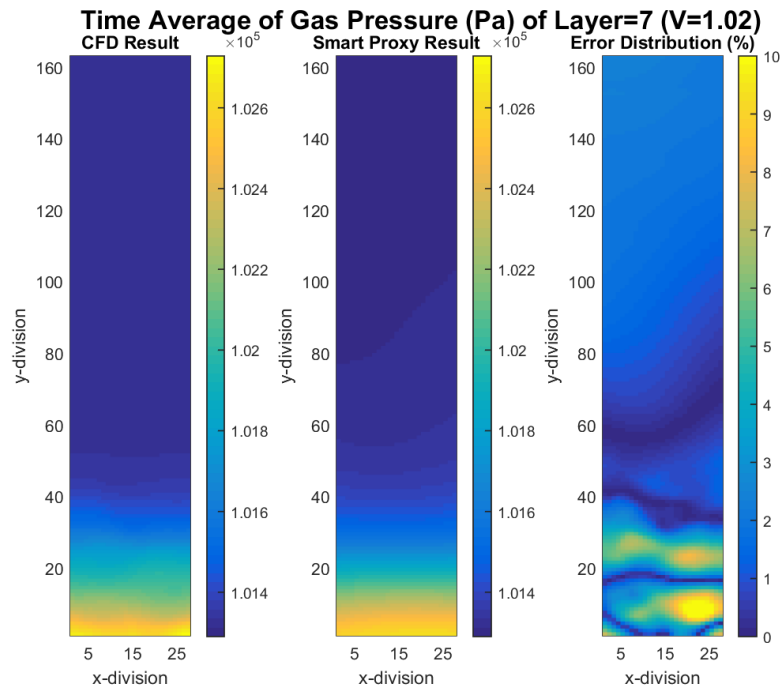


**Figure 4-38** CFD and smart proxy results for gas pressure averaged over time steps 1500 to 3400 at K=7 cross-sectional plane with  $V_{in}=1.02$  m/s

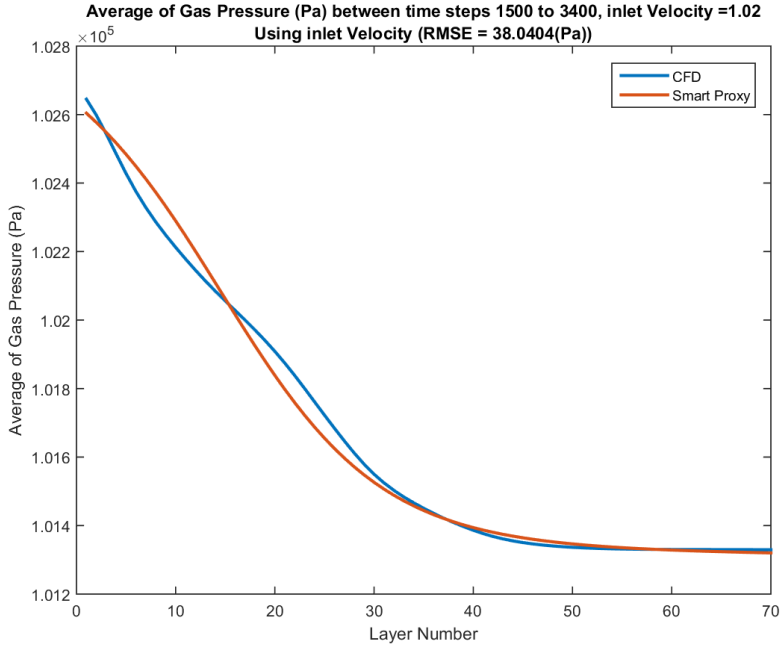


**Figure 4-39** Time averaged CFD and smart proxy results for gas pressure, spatially averaged along the fluidized bed (time-steps = 1500 to 3400 and  $V_{in} = 1.02\text{m/s}$ )

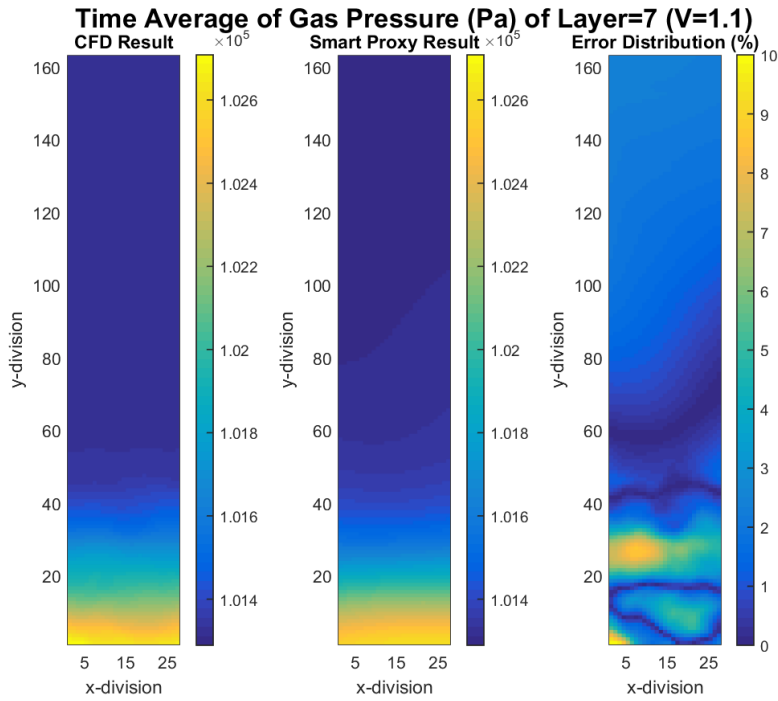


**Figure 4-40** CFD and smart proxy results for gas pressure averaged over time steps 1500 to 3400 at  $K=7$  cross-sectional plane with  $V_{in}=1.1\text{ m/s}$

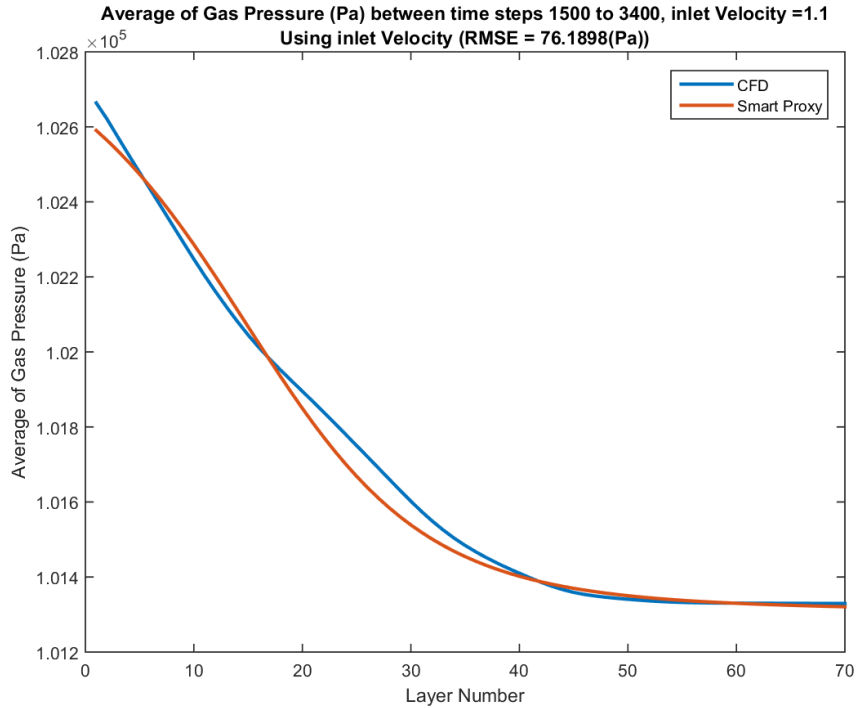


**Figure 4-41 Time averaged CFD and smart proxy results for gas pressure, spatially averaged along the fluidized bed (time-steps = 1500 to 3400 and  $V_{in} = 1.1$  m/s)**

#### 4.6 TRAINING FOR GAS VELOCITY AND GAS VOLUME FRACTION USING STATIC PARAMETERS

The same 11 static parameters that were used for the development of the smart proxy model for the gas pressure, were used to train a model to predict the behavior of a gas velocity and gas volume fraction using seven different inlet velocities. The gas velocity and gas volume fraction have more spatial variation than the gas pressure and this fact makes the training process more challenging.

Figure 4-42 and Figure 4-43 show the results of training for the gas velocity and gas volume fraction at  $K = 7$  cross-sectional plane and  $V_{in}=0.9$  m/s which is one of the inlet velocities in the training set. By comparing the CFD and Smart Proxy results, it is clear that the ANN is not training adequately. Results at different cross sectional plane are provided in Appendix V. Due to lack of agreement with CFD results, no blind test is carried out for this particular scenario.

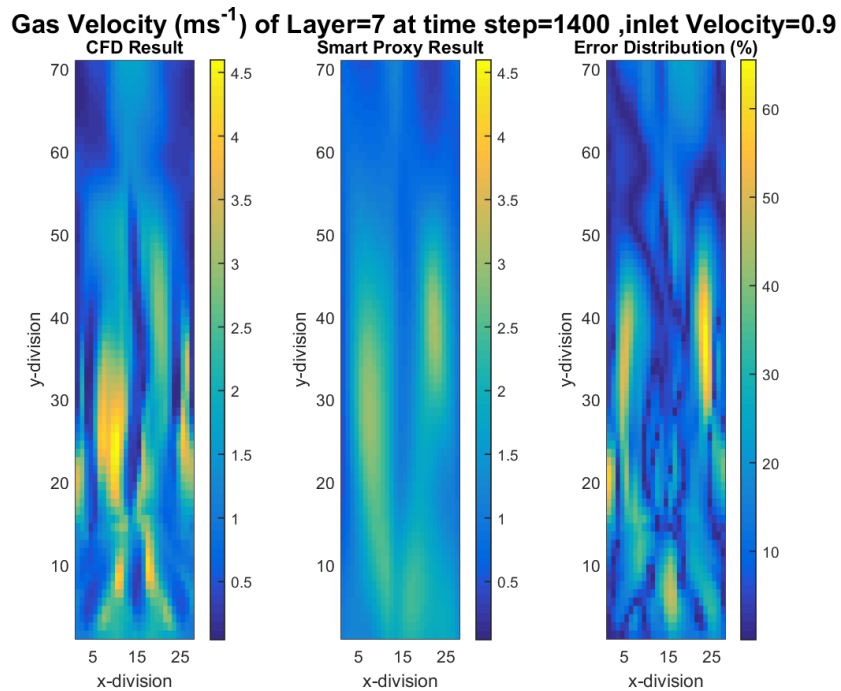


**Figure 4-42** CFD and smart proxy results for gas velocity at time step=1400,  $V_{\text{in}}=0.9$  m/s and  $K = 7$  cross-sectional plane, using 11 static parameters

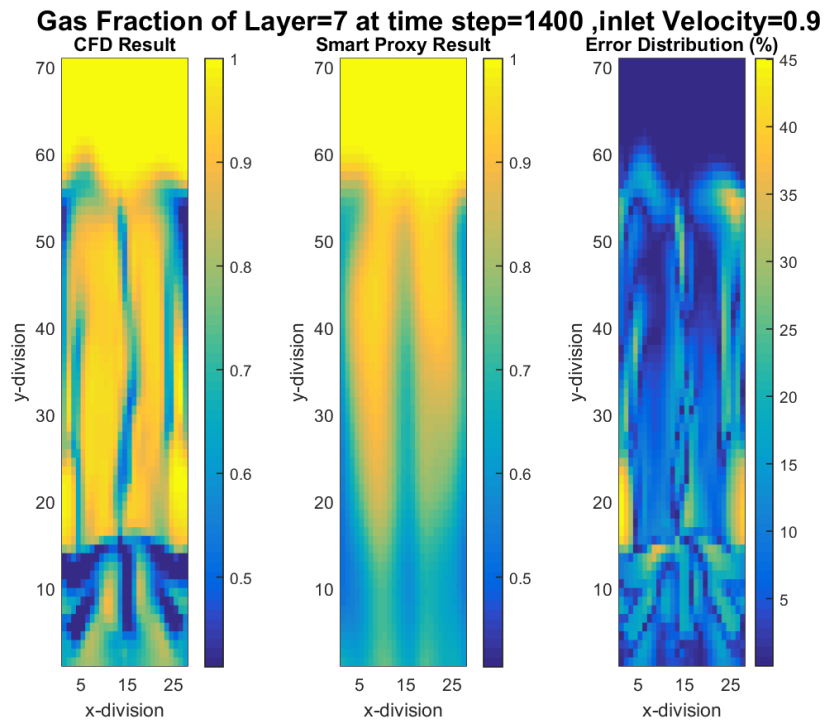


**Figure 4-43** CFD and smart proxy results for gas volume fraction at time step=1400,  $V_{\text{in}}=0.9$  m/s and  $K = 7$  cross-sectional plane, using 11 static parameters

### 4.7 SEQUENTIAL MODELING

It was observed in the previous section that high spatial variation in gas velocity and gas volume fraction led to a poor quality trained ANN. Sequential modeling is a potential remedy for this problem. First, an ANN is trained for gas pressure, then the output of gas pressure ANN is included as an input for training of gas velocity and finally, the trained ANNs for gas pressure and velocity are included as input in training of gas volume fraction.

Table 4-3 shows the training quality of ANN for gas velocity without and with using gas pressure as input respectively. There is not a noticeable improvement in the quality of the trained ANN for gas velocity. On the other hand, Table 4-3 shows an improvement in the quality of trained ANN when gas pressure and gas velocity are also included as the input parameters for training ANN for gas volume fraction. Since gas volume fraction is more trainable in this sequential approach than gas velocity, the order of the sequential modeling is changed, as shown in Figure 4-44. The gas pressure is used to train ANN for gas volume fraction first, as seen in Figure 4-45 and then gas pressure and gas volume fraction are used to train for gas velocity.

**Table 4-3 Quality of training  $R^2$  with and without using gas pressure**

<i>ANN's Output</i>	<i>without using pressure</i>	<i>with using pressure</i>
<i>Gas Velocity</i>	0.6663	0.6666
<i>Gas Volume Fraction</i>	0.8443	0.9473

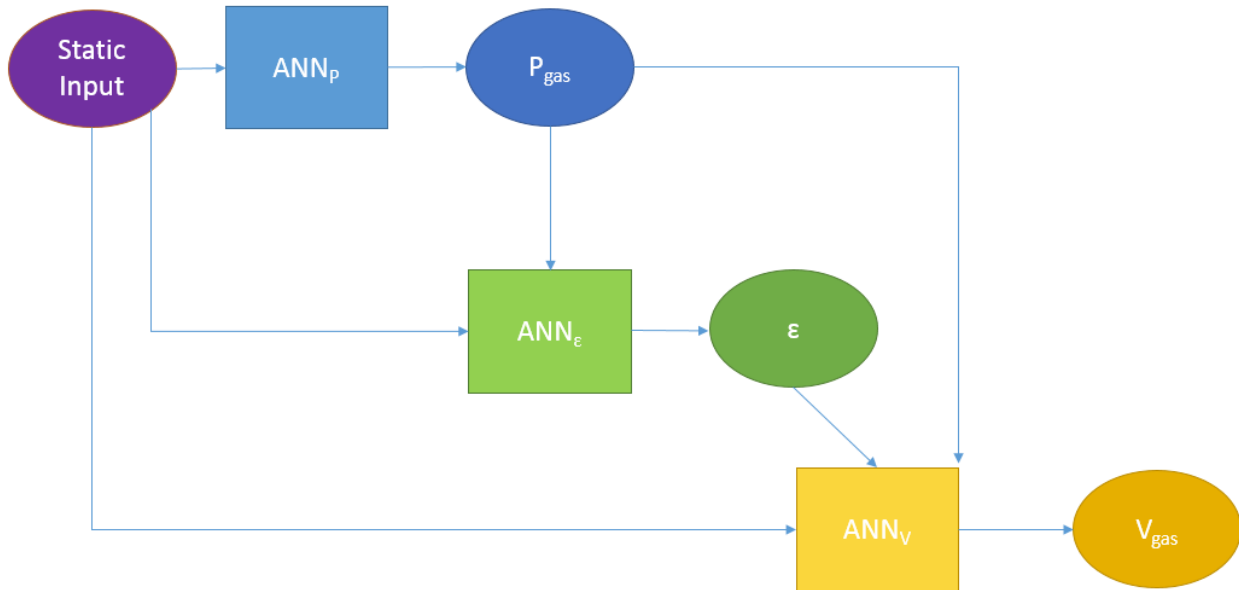


**Figure 4-44 Changing the order of sequential training algorithm**

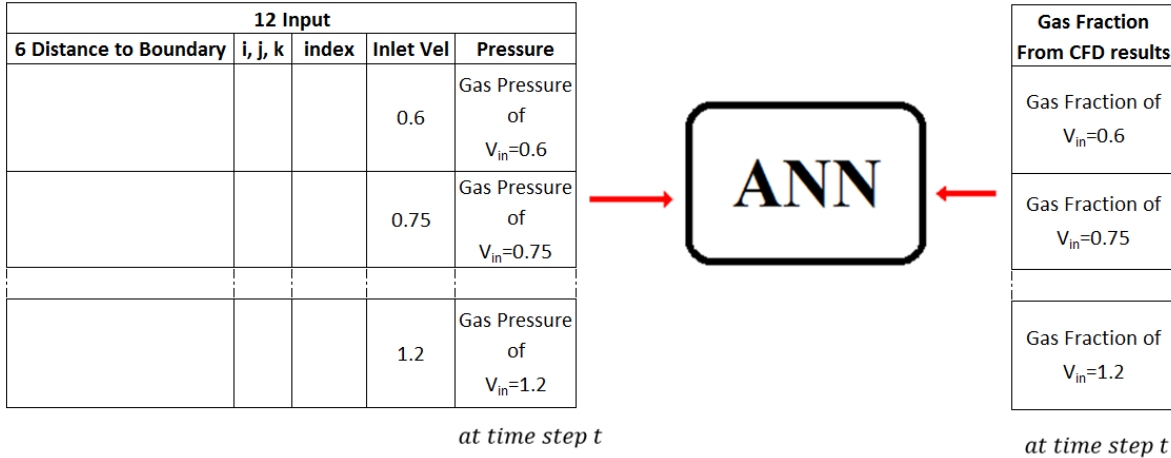


**Figure 4-45 Training for gas volume fraction using 11 static parameters and gas pressure**

A new ANN was trained with the architecture shown in Figure 4-45, using seven inlet velocities for time-step 1400. The spatially averaged result for the blind test condition of  $V_{in} = 0.825$  m/s at time step of 1400 is shown in Figure 4-46. Although the smart proxy prediction follows the same trend as CFD results, the predicted gas volume fraction field is under-predicted in the lower part of the bed, over-predicted in the upper region of the bed and under-predicted in the free board. To potentially improve the quality of ANN prediction, shown in Figure 4-45, the tier system is incorporated into the training process.

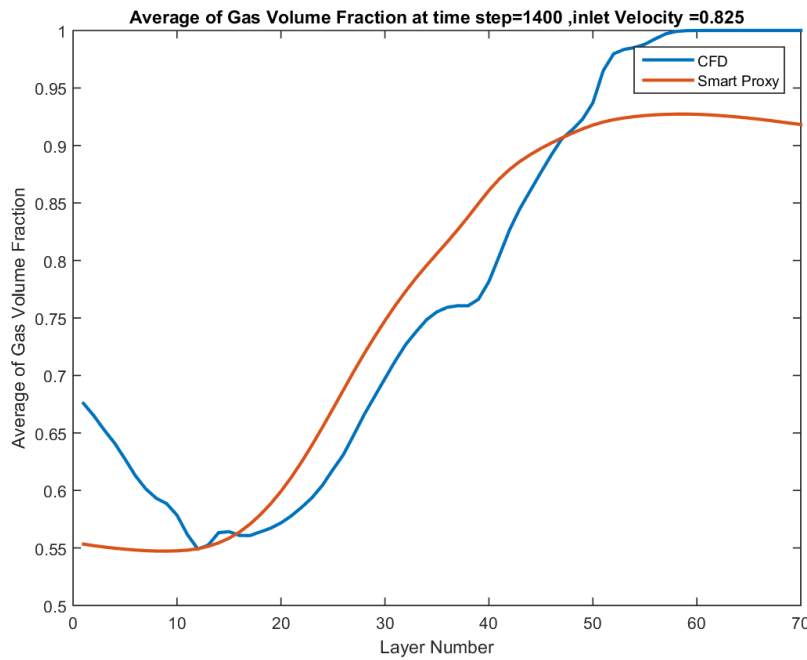


**Figure 4-46 Spatially averaged CFD and smart proxy results for gas volume fraction at time step = 1400 and  $V_{in}=0.825$  m/s**

### 4.8 SEQUENTIAL MODELING BY CONSIDERING TIER SYSTEM

A major advantage of the smart proxy methodology employed in this research is that an ANN is trained for each computational cell used in CFD, which provides the training data. As such, the tier system described in section 3.4.7 is incorporated into the training process for ANN. Figure 4-47 shows the training architecture of the ANN model for constructing an ANN for gas volume fraction using 18 inputs including static parameters and the gas pressure at a cell and its tier cells.

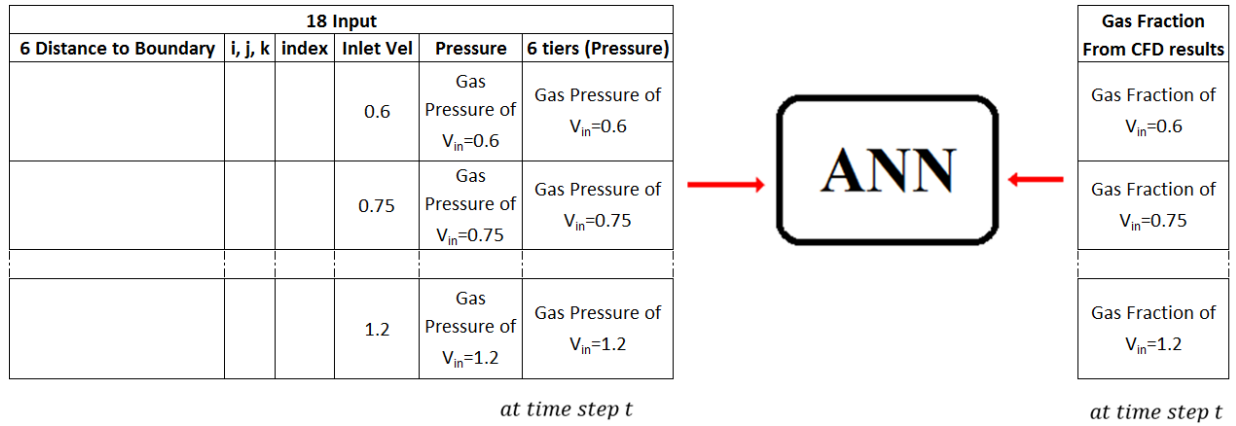


**Figure 4-47 Sequential training for gas volume fraction using gas pressure and tier cells**

The result of the spatial average of gas volume fraction along the fluidized bed, for a blind test at time step of 1400 and inlet velocity of  $V_{in}=0.825$  m/s is shown in Figure 4-48. This prediction shows a better agreement than the previous model prediction, shown in Figure 4-46. Since the results shown in Figure 4-48 look very promising, additional ANNs are constructed to compare time averaged gas volume fraction to CFD results, based on the sequential training approach outlined in Figure 4-47. To achieve this, 20 ANNs are trained using 7 inlet velocities for different time-steps according to Figure 4-34.

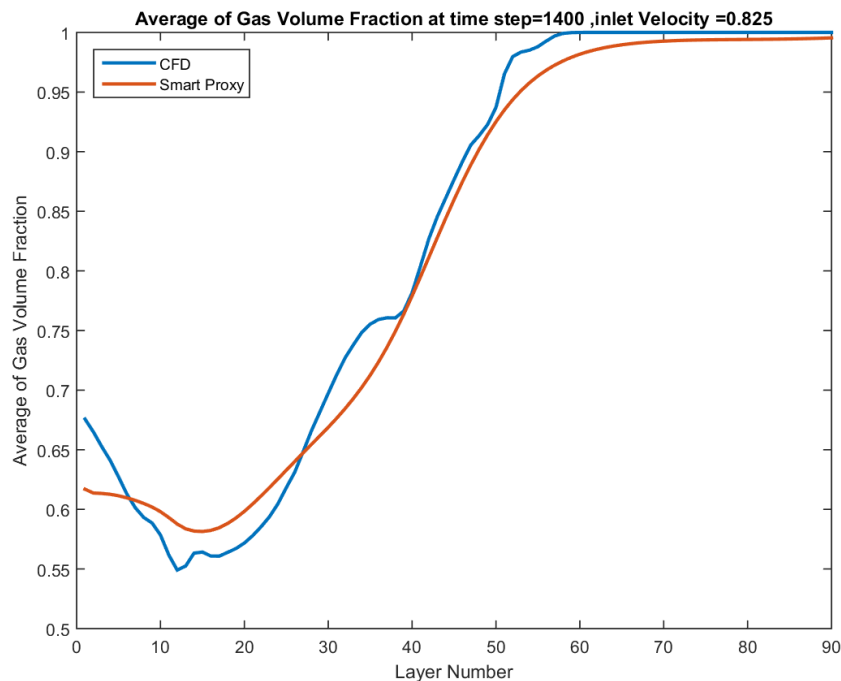


**Figure 4-48 Spatially averaged profile of CFD and smart proxy results for gas volume fraction at time step of 1400 and  $V_{in} = 0.825$  m/s, when tier cells are used**

To ensure the quality of the trained ANN, the predicted spatially averaged gas volume fraction over the time steps of 1500 to 3400 for the entire data set used for training (inlet velocities of 0.6, 0.69, 0.75, 0.9, 0.94, 1.05 and 1.2 m/s) are shown in Figure 4-49 through Figure 4-55 respectively. It can be seen that in the vicinity of inlet, ANN is under-predicting the average gas volume fraction. The under-prediction grows larger with increasing inlet gas velocity (in Figure 4-49 through Figure 4-55). At lower inlet velocity, the ANN predictions are in good agreement, with the CFD training data in the lower part of the fluidized bed (up to layer 20 in Figure 4-50 through Figure 4-51). However, as inlet velocity increases, ANN under-predicts the average gas volume fraction in the lower part of the fluidized bed (up to layer 20 in Figure 4-52 through Figure 4-55). In the upper portion of the fluidized bed (layer 20 to layer 40), ANN over-predicts the gas volume fraction, and as free board is approached (layer 40 and beyond), ANN under-predicts the gas volume fraction. Although the overall trend of predicted gas volume fraction by ANN is in agreement with the training data from CFD, clearly, further improvement in the training process is required. The trained ANN is now used in deployment mode for three blind tests, with inlet velocities of  $V_{in}=0.825$  m/s,  $V_{in}=1.02$  m/s, and  $V_{in}=1.1$  m/s, with results shown in Figure 4-56 through Figure 4-58 respectively. As expected, the same trends described above, are observed in ANN prediction, when ANN is used for blind tests. This reinforces the need for improvement in the training process.

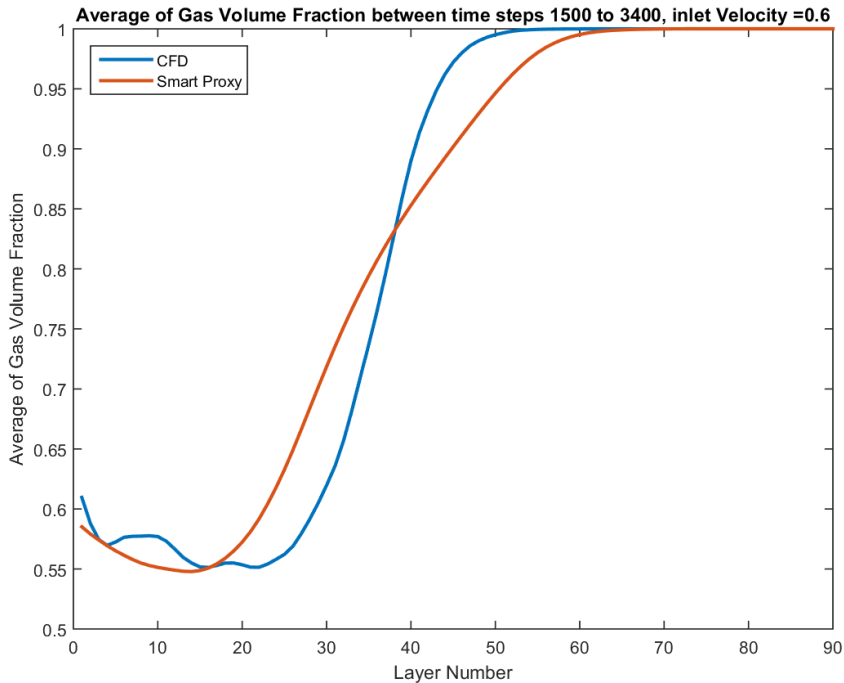


**Figure 4-49 Spatial average profile of CFD and smart proxy results for gas volume fraction, averaged over time steps 1500 to 3400 at inlet velocity of 0.6 m/s**

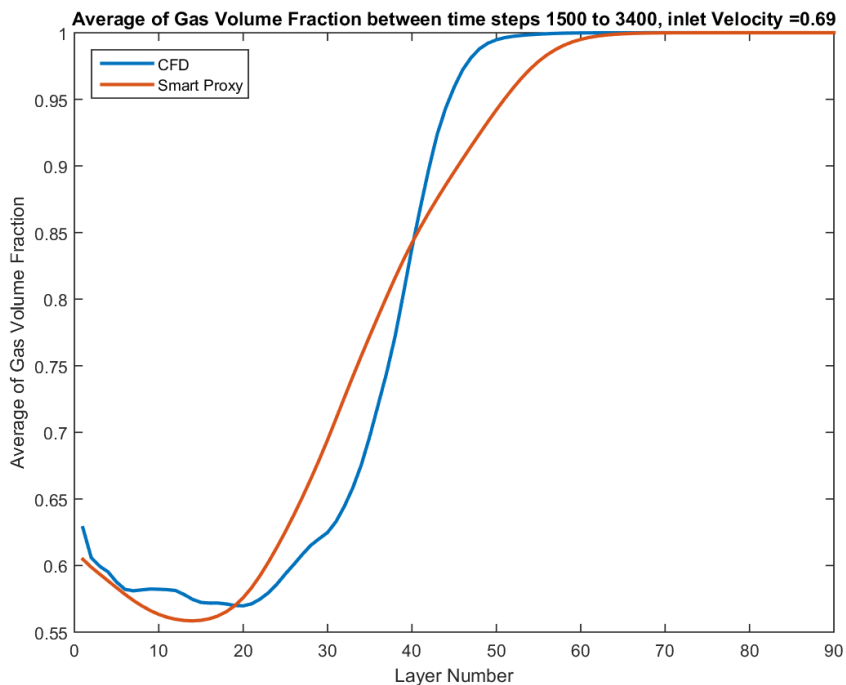


**Figure 4-50 Spatial average profile of CFD and smart proxy results for gas volume fraction, averaged over time steps 1500 to 3400 at inlet velocity of 0.69 m/s**

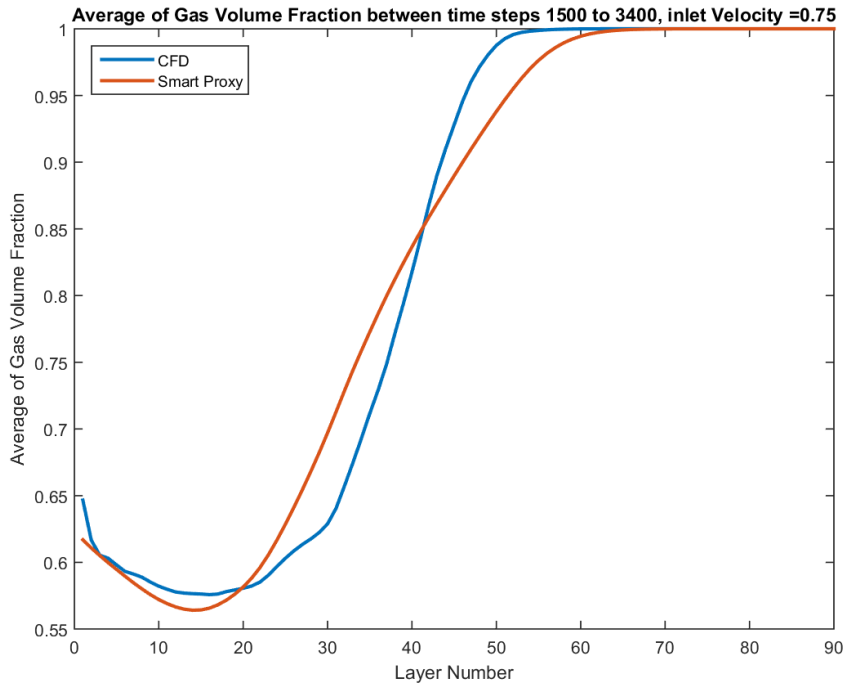


Figure 4-51 Spatial average profile of CFD and smart proxy results for gas volume fraction, averaged over time steps 1500 to 3400 at inlet velocity of 0.75 m/s

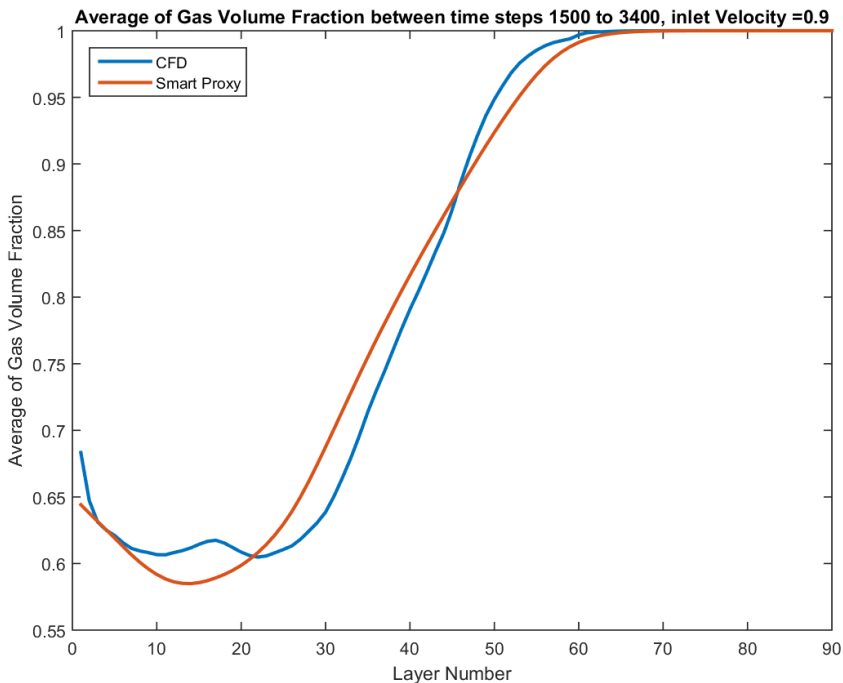
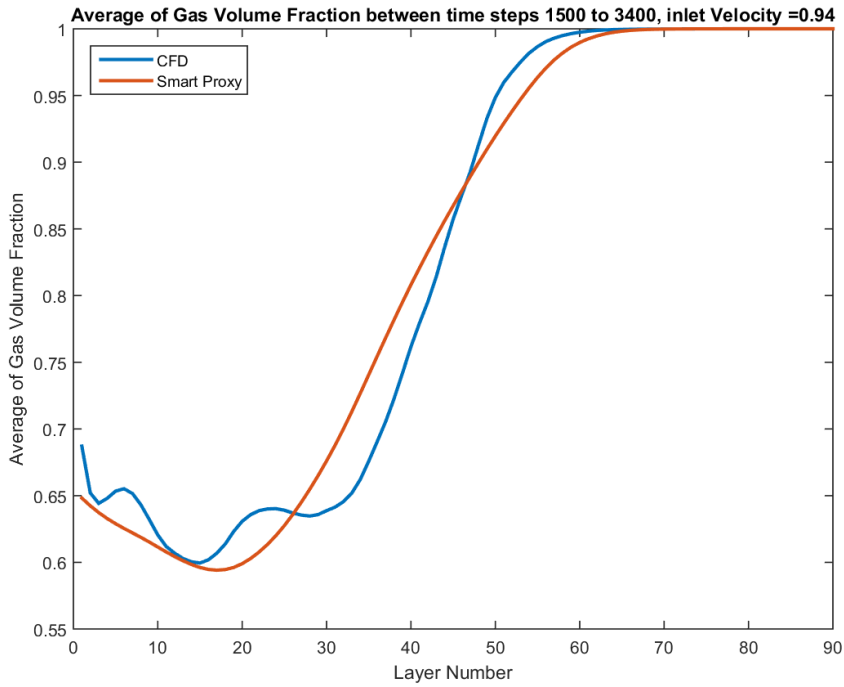
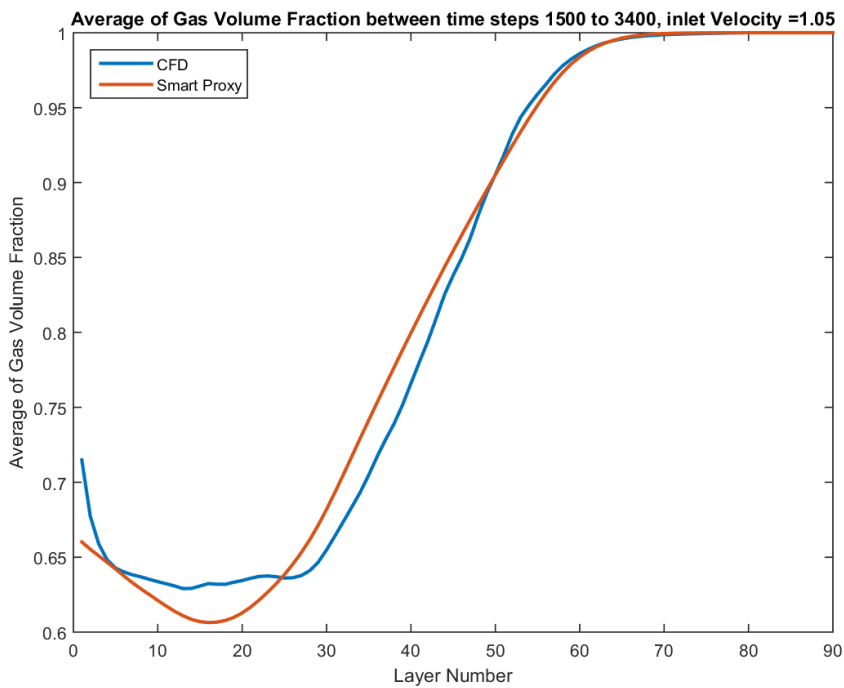


Figure 4-52 Spatial average profile of CFD and smart proxy results for gas volume fraction, averaged over time steps 1500 to 3400 at inlet velocity of 0.9 m/s



**Figure 4-53** Spatial average profile of CFD and smart proxy results for gas volume fraction, averaged over time steps 1500 to 3400 at inlet velocity of 0.94 m/s



**Figure 4-54** Spatial average profile of CFD and smart proxy results for gas volume fraction, averaged over time steps 1500 to 3400 at inlet velocity of 1.05 m/s

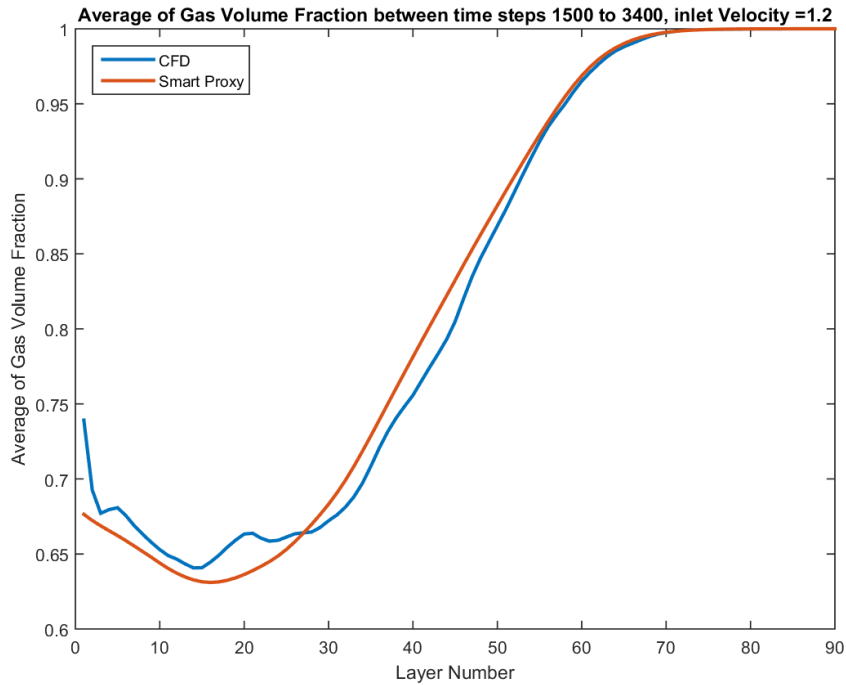


**Figure 4-55 Spatial average profile of CFD and smart proxy results for gas volume fraction, averaged over time steps 1500 to 3400 at inlet velocity of 1.2 m/s**

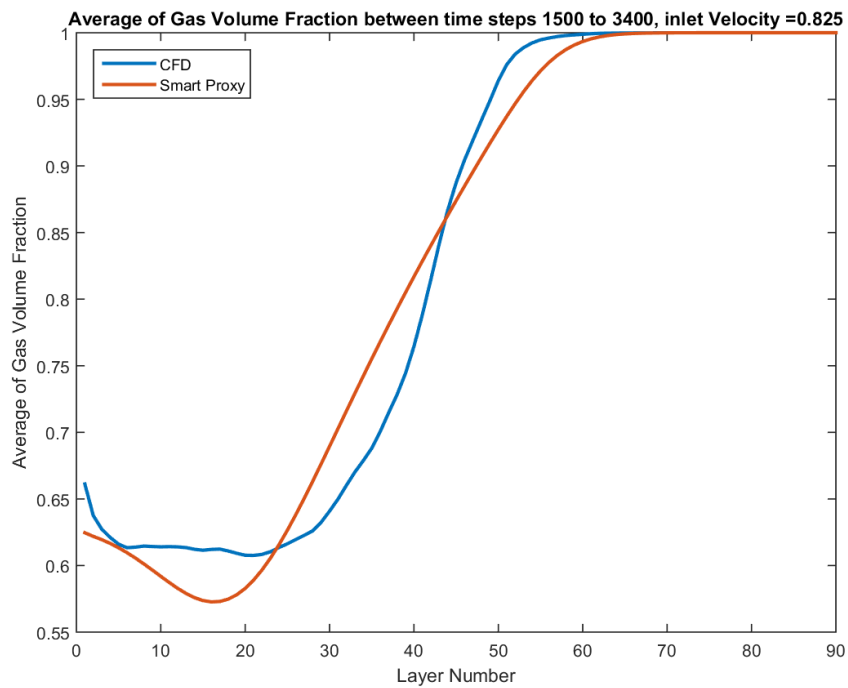


**Figure 4-56 Spatial average profile of CFD and smart proxy results for gas volume fraction, averaged over time steps 1500 to 3400 at inlet velocity of 0.825 m/s**

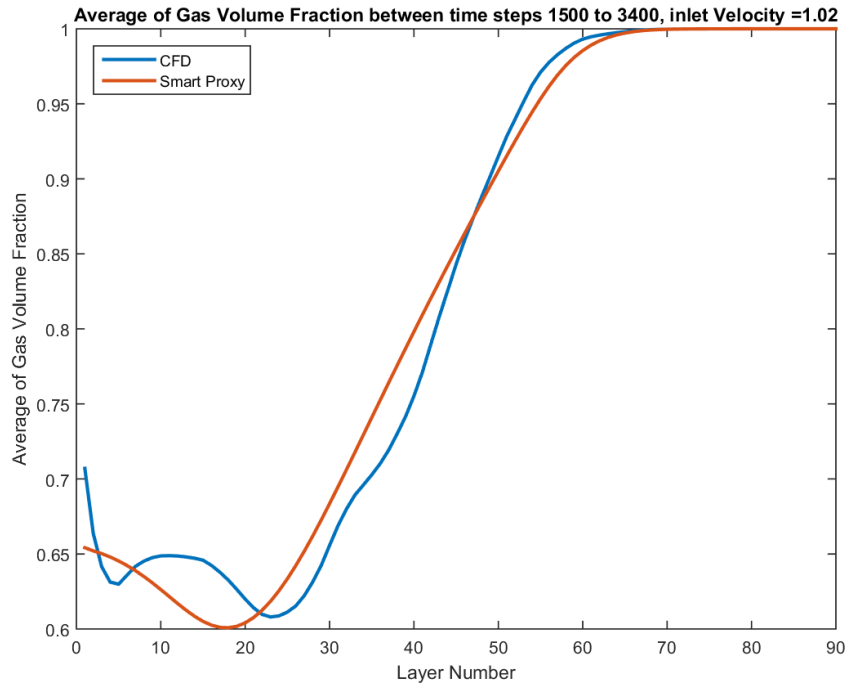


**Figure 4-57** Spatial average profile of CFD and smart proxy results for gas volume fraction, averaged over time steps 1500 to 3400 at inlet velocity of 1.02 m/s

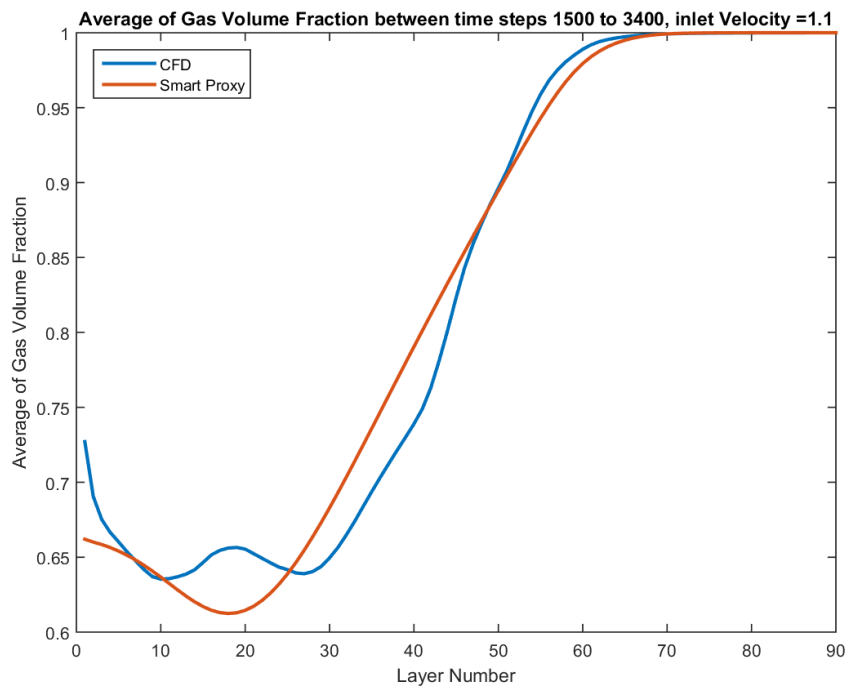


**Figure 4-58** Spatial average profile of CFD and smart proxy results for gas volume fraction, averaged over time steps 1500 to 3400 at inlet velocity of 1.1 m/s

## 5. CONCLUSIONS

A data-driven smart proxy has been developed to mimic CFD results for gas pressure and gas volume fraction in a fluidized bed, with a reasonable accuracy and faster execution time. Originally, the average time for training an ANN was about one hour. However, after improvement to the training process and training algorithm, the training time reduced to 2 to 3 minutes. The training time is strongly affected with the choice of hardware used. Table 5-1 shows the comparison of run time of multiphase CFD and smart proxy. This proxy requires incredibly less amount of time to execute than CFD simulation does, with a reasonable error (less than 10%). The results of this project are very promising and they show that artificial intelligence and machine learning can expedite application of non-intrusive uncertainty quantification techniques to CFD based multiphase flow modeling.

**Table 5-1 Execution time for CFD and smart proxy**

<i>Method</i>	<i>Execution Time</i>
<i>CFD</i>	<i>4 seconds simulation = 3 days on 4 CPUs</i>
<i>Smart Proxy</i>	<i>4 seconds simulation = 180 s = 3 min</i>

### 5.1 RECOMMENDATIONS AND FUTURE WORKS

This study showed that the smart proxy is a feasible technology to handle a complex, multi-physics, nonlinear gas-solid flow. Results in section 4.8 show that additional improvements are required in the training process, in order to increase the degree of fidelity of the constructed ANN. Some of ideas to be explored are:

1. Using additional tiers at each cell during the training process
2. Using gas velocity, alongside of gas pressure, when training an ANN for gas volume fraction. Higher values of gas volume fraction mean a more porous cell. This in turn leads to a lower gas velocity, compare to cells with lower gas volume fraction. Including gas velocity during the training could provide added learning opportunities for ANN.
3. Break down the fluidized bed to two separate zone of lower bed region and upper bed and free board regions.

Also train an ANN for gas velocity and solid velocity prediction. Additionally, the use of geometry as a model variable in training an ANN may be explored. This could expedite the process of scale up, which is very time consuming, when approached with CFD modeling.

## 6. REFERENCES

- [1] Gel, A., Garg, R., Tong, C., Shahnam, M., and Guenther, C., "Applying uncertainty quantification to multiphase flow computational fluid dynamics," *Powder Technology*, vol. 242, pp. 27-39, 2013.
- [2] Gel, A., Shahnam, M. and Subramaniyan, A.K., "Quantifying uncertainty of a reacting multiphase flow in a bench-scale fluidized bed gasifier. A Bayesian approach," *Powder Technology*, vol. 311, pp. 484-495, 2017.
- [3] Gel, A., Shahnam, M., Musser, J, Subramaniyan, A.K. and Dietiker, J.F., "Non-intrusive Uncertainty Quantification of Computational Fluid Dynamics Simulations of a Bench-scale Fluidized Bed Gasifier," *Industrial & Engineering Chemistry Research*, no. DOI: 10.1021/acs.iecr.6b02506, 2016.
- [4] Shahnam, M., Gel, A., Dietiker, J.-F., Subramaniyan, A. K. and Musser, J., "The Effect of Grid Resolution and Reaction Models in Simulation of a Fluidized Bed Gasifier through Non-intrusive Uncertainty Quantification Techniques," *ASME Journal of Verification, Validation and Uncertainty Quantification*, 2016.
- [5] Fullmer, W. and Hrenya, C., "Quantitative assessment of fine-grid kinetic theory based predictions of mean-slip in unbounded fluidization," *AIChE Journal*, Vols. DOI 10.1002/aic, 62, no. 2016, pp. 11-17.
- [6] Amini, S., Mohaghegh, S.D., Gaskari, R. and Bromhal, G.S., "Pattern Recognition and Data Driven Analytics for Fast and Accurate Replication of Complex Numerical Reservoir Models at Grid Block Level," in *SPE Intelligent Energy Conference and Exhibition*, Utrecht, The Netherlands, 2014.
- [7] Mohaghegh, S. D., "Converting Detail Reservoir Simulation Model into Effective Reservoir Management Tools Using SRMs: Case Study - Three Green Fields in Saudi Arabia," *International Journal of Oil, Gas and Coal Technology*, pp. 115-131, 2014.
- [8] Mohaghegh, S.D., Abdulla, F., Abdou, M., Gaskari, R. and Maysami, M., "Smart Proxy: An Innovative Reservoir Management Tool, Case Study of a Giant Mature Oilfield in UAE," in *Abu Dhabi International Petroleum Exhibition and Conference*, Abu Dubai, 2015.
- [9] Shahkarami, A., Mohaghegh, S.D., Gholami, V., Haghghat, A. and Moreno, D., "Modeling Pressure and Saturation Distribution in a CO<sub>2</sub> Storage Project Using a Surrogate Reservoir Model (SRM)," *Greenhouse Gas Science and Technology, Society of Chemical Industry, John Wiley & Sons, LTD*, pp. 289-315, doi:10.1002/ghg, 2013.
- [10] NETL Multiphase Flow Science, "MFiX software suite," National Energy Technology Laboratory, Morgantown, WV, 2016. [Online]. Available: <http://mfix.netl.doe.gov>.

- [11] Van der Hoef, M. A., Van Sint Annaland, M., Andrews, A. T., Sundaresan, S. and Kuipers, J. A. M., "Numerical Simulation of Dense Gas-Solid Fluidized Beds: A Multiscale Modeling Strategy," *Annual Review of Fluid Mechanics*, vol. 40, no. doi:10.1146/annurev.fluid.40111406.102130, pp. 47-70, 2008.
- [12] Van der Hoef, M. A., Ye, M., Van Sint Annaland, M., Andrews, A. T., Sundaresan, S. and Kuipers, J. A. M., "Multiscale Modeling of Gas-Fluidized Beds," *Advances in Chemical Engineering*, vol. 31, no. 6, pp. 65-149, 2006, doi:10.1016/S0065-2377(06)31002-2..
- [13] Deen, N. G., Van Sint Annaland, M., Van der Hoef, M. A. and Kuipers, J. A., M., "Review of Discrete Particle Modeling of Fluidized Beds," *Chemical Engineering Science*, doi:10.1016/j.ces.2006.08.014, vol. 62, no. 1-2, pp. 28-44, 2007.
- [14] Syamlal, M., Rogers, W., O'Brien, T. J., "MFiX Documentation Theory Guide," [Online]. Available: [https://mfix.netl.doe.gov/download/mfix/mfix\\_legacy\\_manual/Theory.pdf](https://mfix.netl.doe.gov/download/mfix/mfix_legacy_manual/Theory.pdf).
- [15] Benyahia, S., Syamlal, M., "Summary of MFiX Equations," 2012. [Online]. Available: [https://mfix.netl.doe.gov/download/mfix/mfix\\_current\\_documentation/MFIXEquations2012-1.pdf](https://mfix.netl.doe.gov/download/mfix/mfix_current_documentation/MFIXEquations2012-1.pdf).
- [16] A. Samuel, "Some Studies in Machine Learning using the Game Checkers," *IBM Journal*, vol. 3, no. 3, pp. 535-554, 1959.
- [17] Alpaydin, E., Introduction to Machine Learning, The MIT Press, second edition, 2010.
- [18] Haykin, S., Neural Networks - A Comprehensive Foundation, IEEE Press, 1994.
- [19] Mohaghegh, S., Ameri, S., Artificial Neural Network as a Valuable Tool for Petroleum Engineers, Network, 1995.
- [20] Mohaghegh, S., Arefi, R., Ameri, S., Rose, Deanna, "Design and Development of an Artificial Neural Network for Estimation of Formation Permeability," *SPE Computer Applications*, doi:10.2118/28237-PA, vol. 7, no. 6, pp. 151 - 155, 1995.
- [21] Alizadehdakhel, A., Rahimi, M., Sanjari, J., Abdulaziz, A., "CFD and Artificial Neural Network Modeling of Two-phase Flow Pressure Drop," *International Communication in Heat and Mass Transfer*, vol. 36, no. doi.org/10.1016/j.icheatmasstransfer.2009.05.005, pp. 850 - 856, 2009.
- [22] Esmaili, S., Mohaghegh, S., "Full Field Reservoir Modeling of Shale Assets using Advance Data-driven Analytics," *Geoscience Frontiers, Elsevier Ltd*, no. doi:10.1016/j.gsf.2014.12.006, 2015.
- [23] S. D. Mohaghegh, Data Driven Reservoir Modeling, Richardson, Texas: Society of Petroleum Engineers (SPE), 2017.

- [24] Kalantari-Dahaghi, A., Mohaghegh, S., Esmaili, S., "Coupling Numerical Simulation and Machine Learning to Model Shale Gas Production at Different Time Resolutions," *Journal of Natural Gas Science and Engineering*, vol. 25, pp. 380 - 392, 2015.
- [25] Kalantari-Dahaghi, A., Mohaghegh, S., Esmaili, S., "Data Driven Proxy at Hydraulic Fracture Cluster Level: A Technique for Efficient CO<sub>2</sub> Enhanced Gas Recovery and Storage Assessment in Shale Reservoir," *Journal of Natural Gas Science and Engineering*, vol. 27, no. doi:10.1016/j.jngse.2015.06.039, pp. 515 - 530, 2015.
- [26] Ansari, A., Mohaghegh, S., Shahnam, M., Dietiker, J.F., Takbiri Borujeni, A., Fathi, E., "Data Driven Smart Proxy for CFD, Application of Big Data Analytics & Machine Learning in Computational Fluid Dynamics, Part One: Proof of Concept," NETL-PUB-21574, 2017.

**7. APPENDIX I: GAS PRESSURE USING 7 STATIC PARAMETERS**

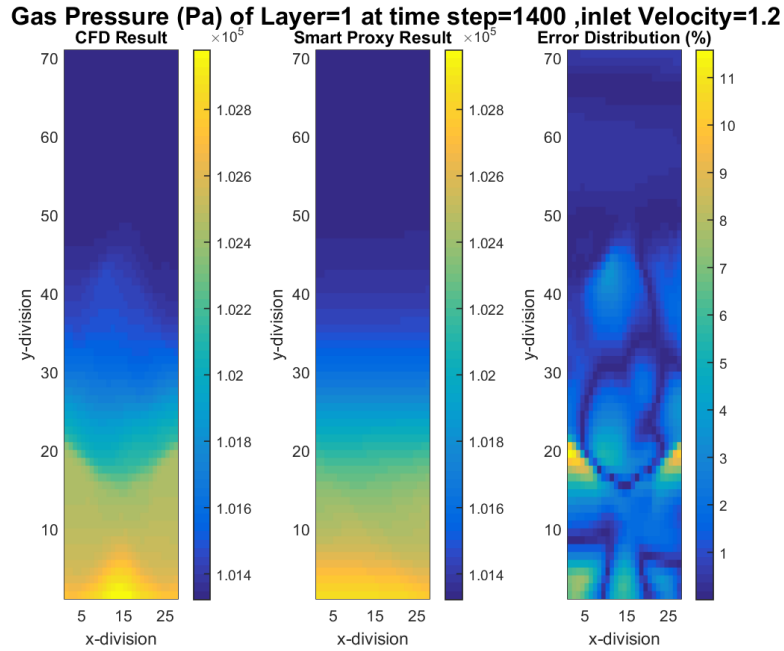


**Figure 7-1 CFD and smart proxy results for gas pressure at K=1 cross-sectional plane for time step of 1400 and  $V_{in}$  of 1.2 m/s, using 7 static parameters**

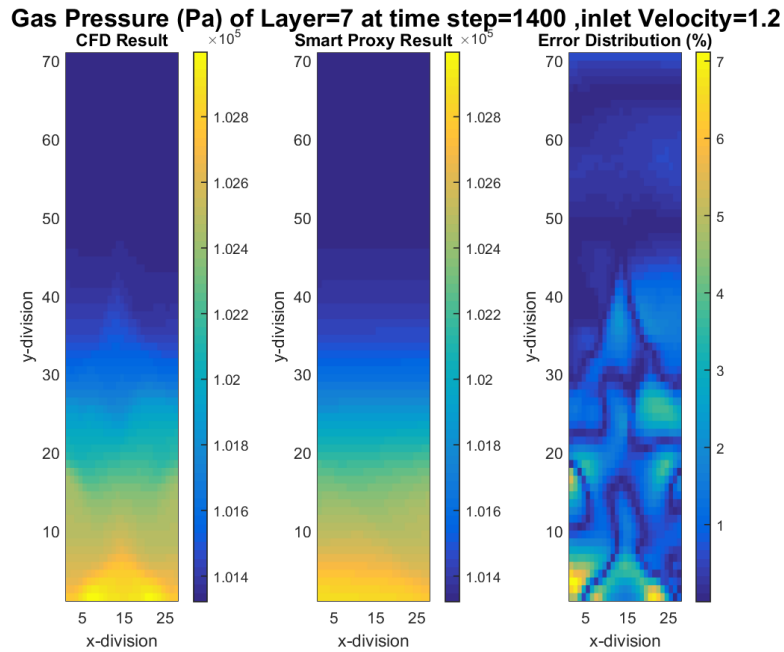


**Figure 7-2 CFD and smart proxy results for gas pressure at K=7 cross-sectional plane for time step of 1400 and  $V_{in}$  of 1.2 m/s, using 7 static parameters**

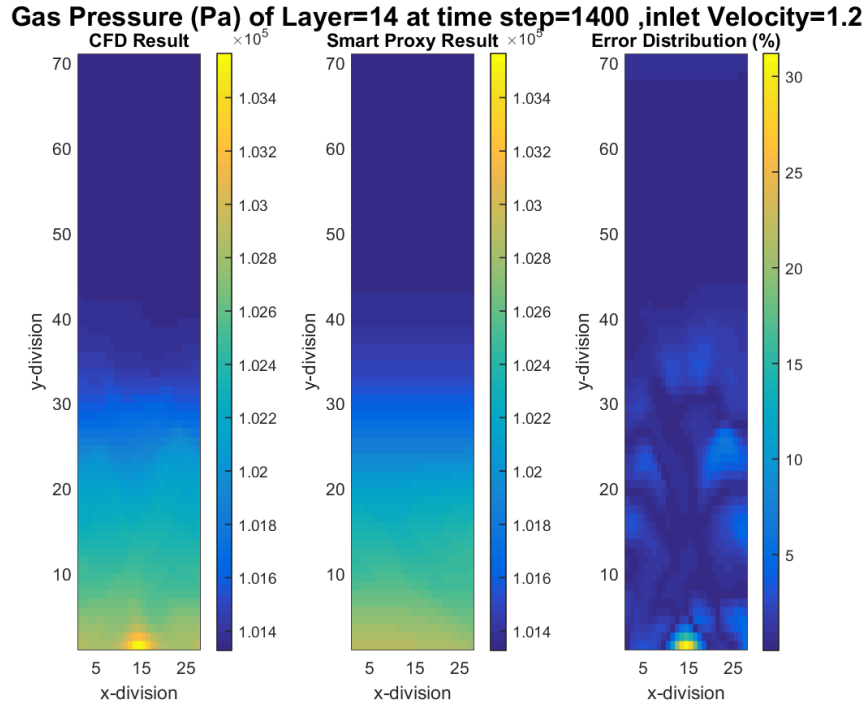


**Figure 7-3** CFD and smart proxy results for gas pressure at K=14 cross-sectional plane for time step of 1400 and  $V_{in}$  of 1.2 m/s, using 7 static parameters

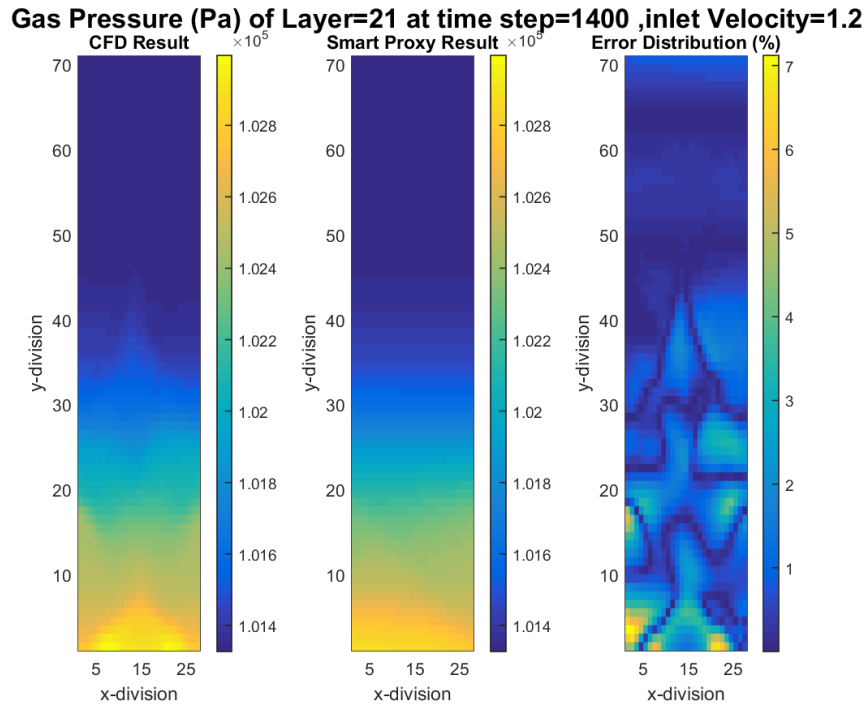


**Figure 7-4** CFD and smart proxy results for gas pressure at K=21 cross-sectional plane for time step of 1400 and  $V_{in}$  of 1.2 m/s, using 7 static parameters

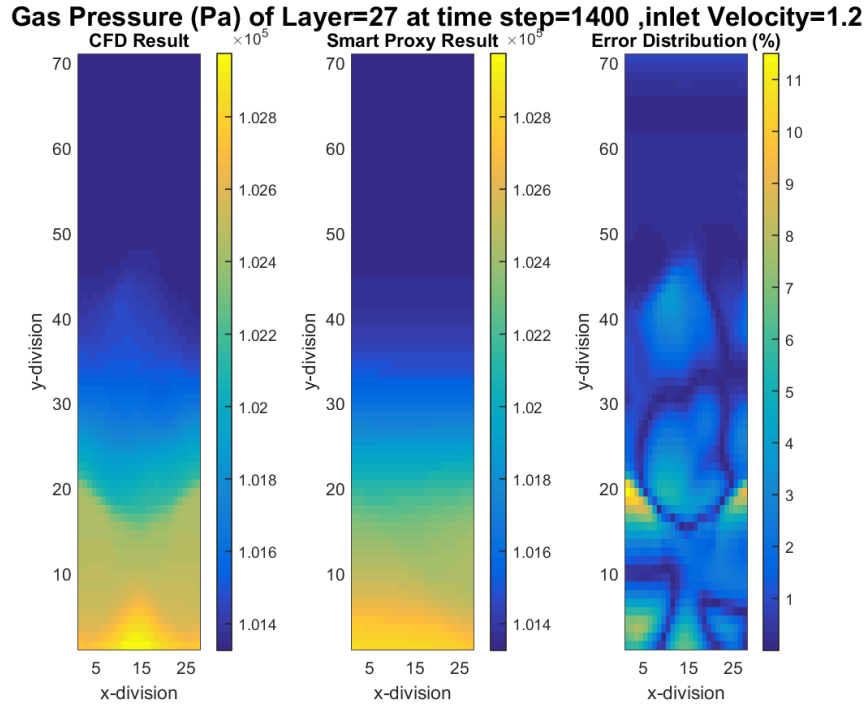


Figure 7-5 CFD and smart proxy results for gas pressure at K=27 cross-sectional plane for time step of 1400 and  $V_{in}$  of 1.2 m/s, using 7 static parameters

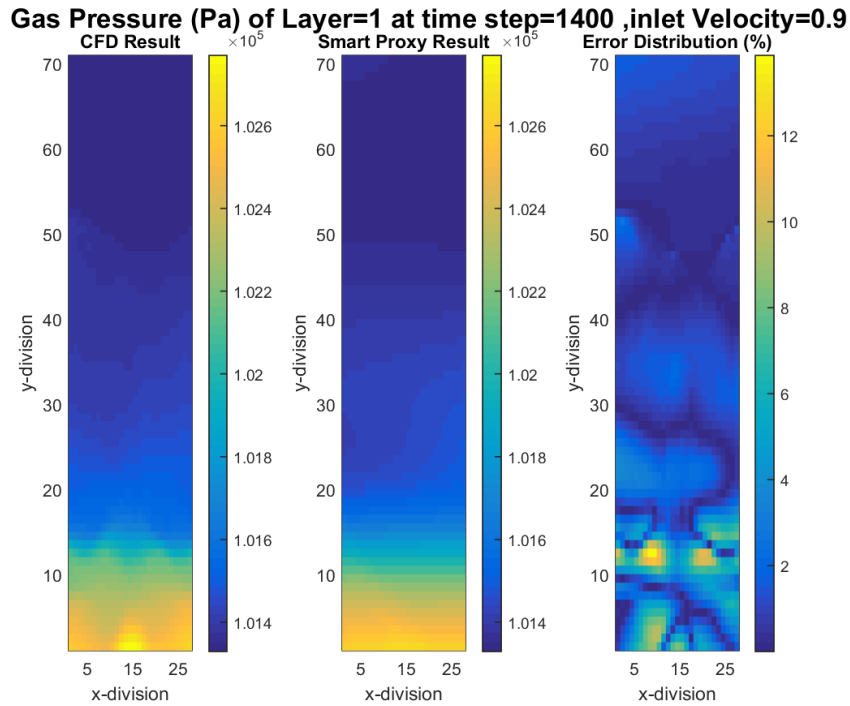
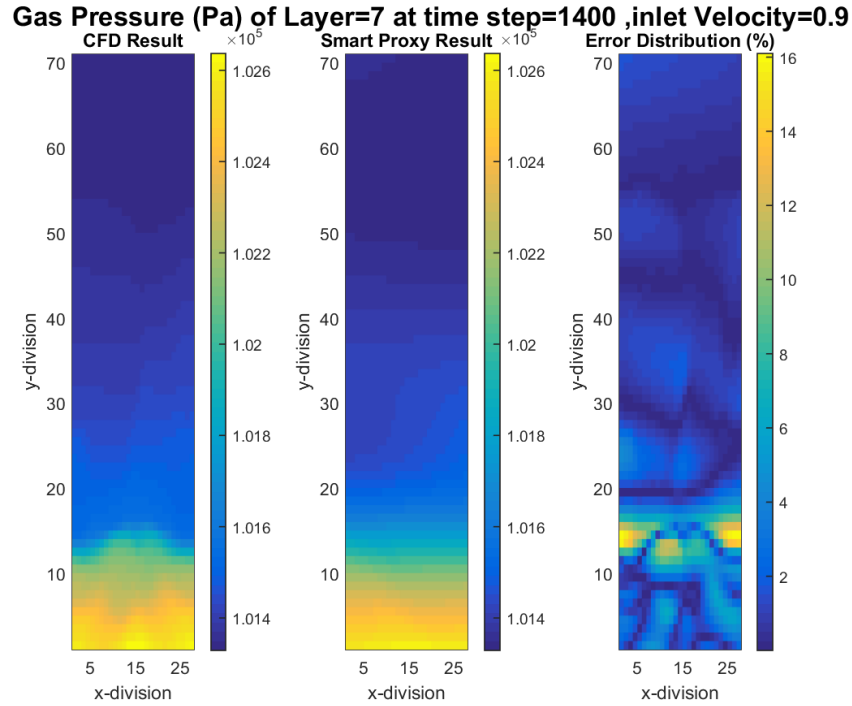
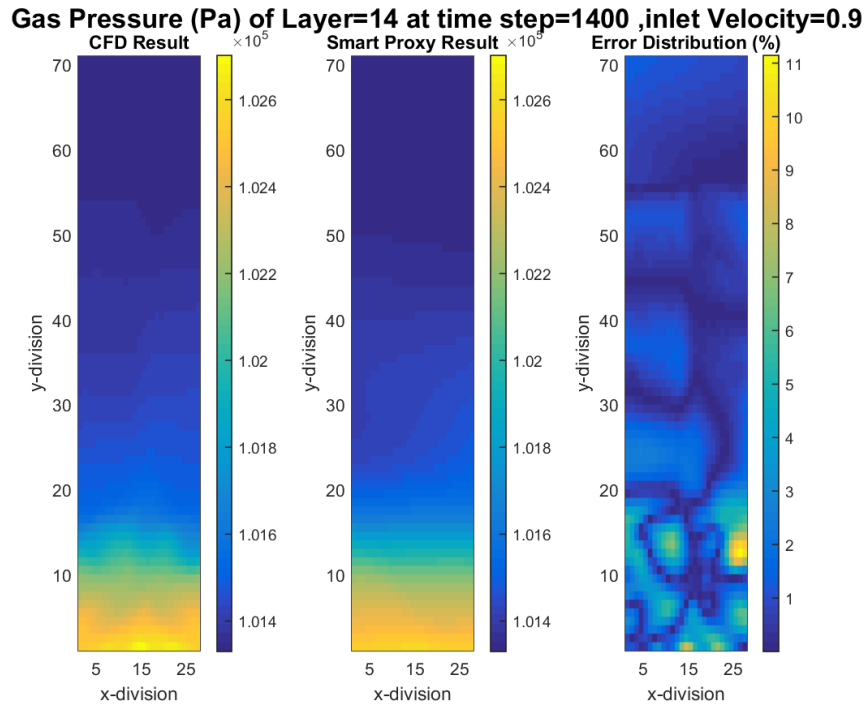


Figure 7-6 CFD and smart proxy results for gas pressure at K=1 cross-sectional plane for time step of 1400 and  $V_{in}$  of 0.9 m/s, using 7 static parameters



**Figure 7-7** CFD and smart proxy results for gas pressure at K=7 cross-sectional plane for time step of 1400 and  $V_{in}$  of 0.9 m/s, using 7 static parameters



**Figure 7-8** CFD and smart proxy results for gas pressure at K=14 cross-sectional plane for time step of 1400 and  $V_{in}$  of 0.9 m/s, using 7 static parameters

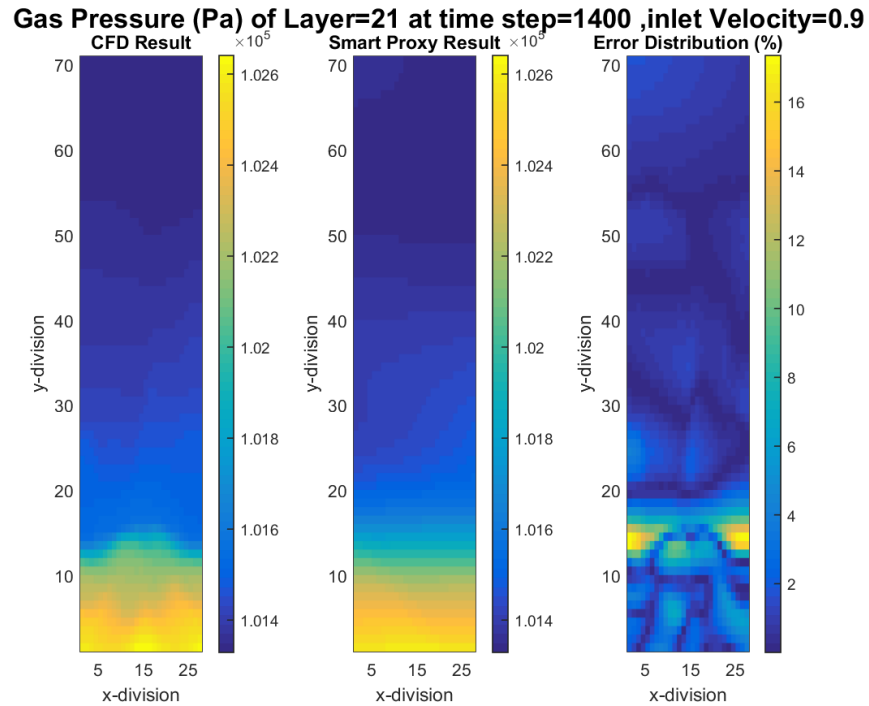


**Figure 7-9** CFD and smart proxy results for gas pressure at K=21 cross-sectional plane for time step of 1400 and  $V_{in}$  of 0.9 m/s, using 7 static parameters

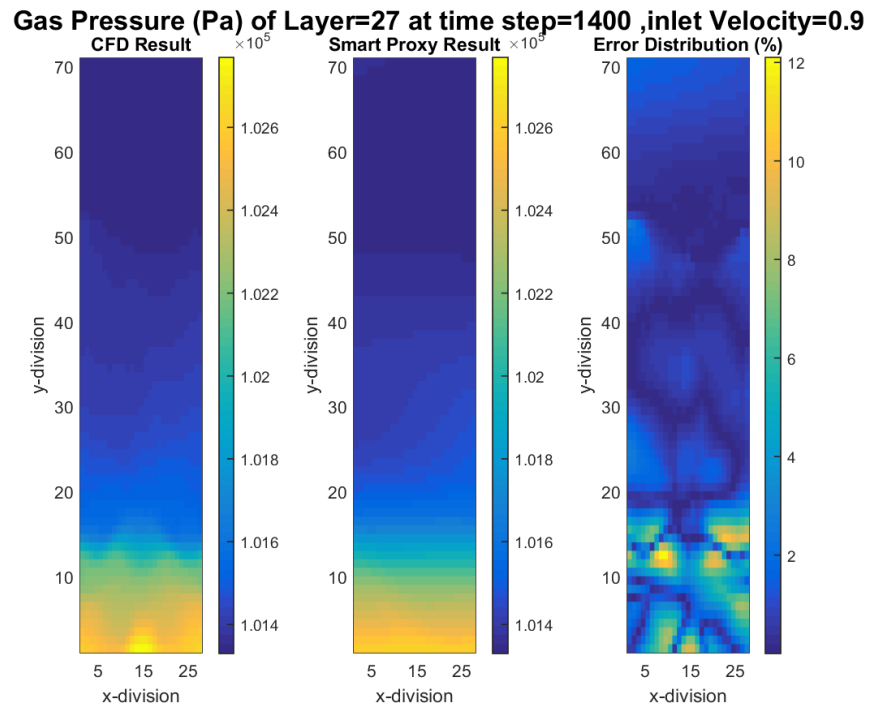


**Figure 7-10** CFD and smart proxy results for gas pressure at K=27 cross-sectional plane for time step of 1400 and  $V_{in}$  of 0.9 m/s, using 7 static parameters

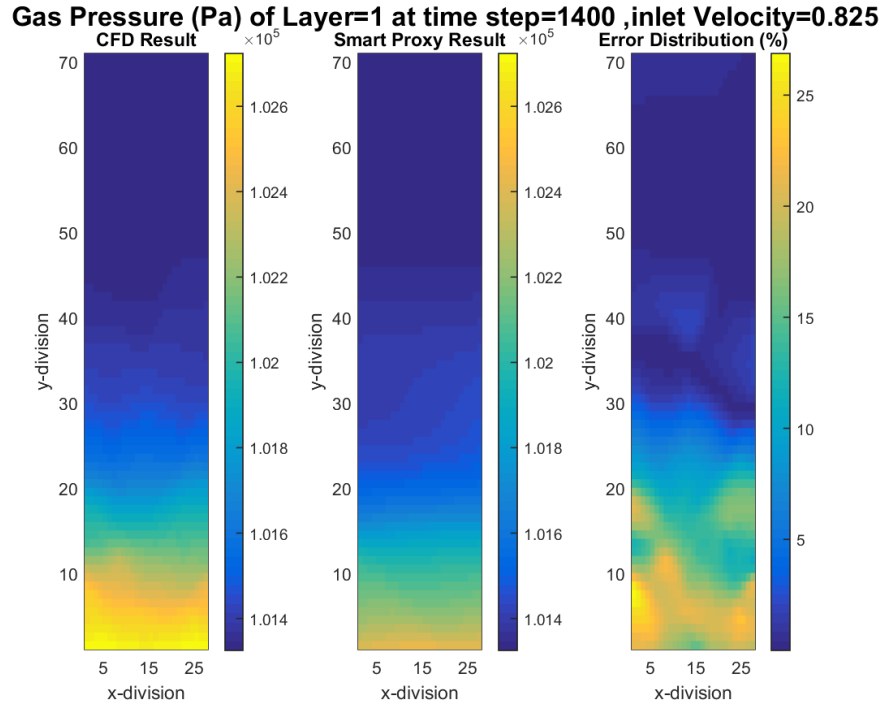


**Figure 7-11** CFD and smart proxy results for gas pressure at  $K=1$  cross-sectional plane for time step of 1400 and  $V_{in}$  of 0.825 m/s, using 7 static parameters

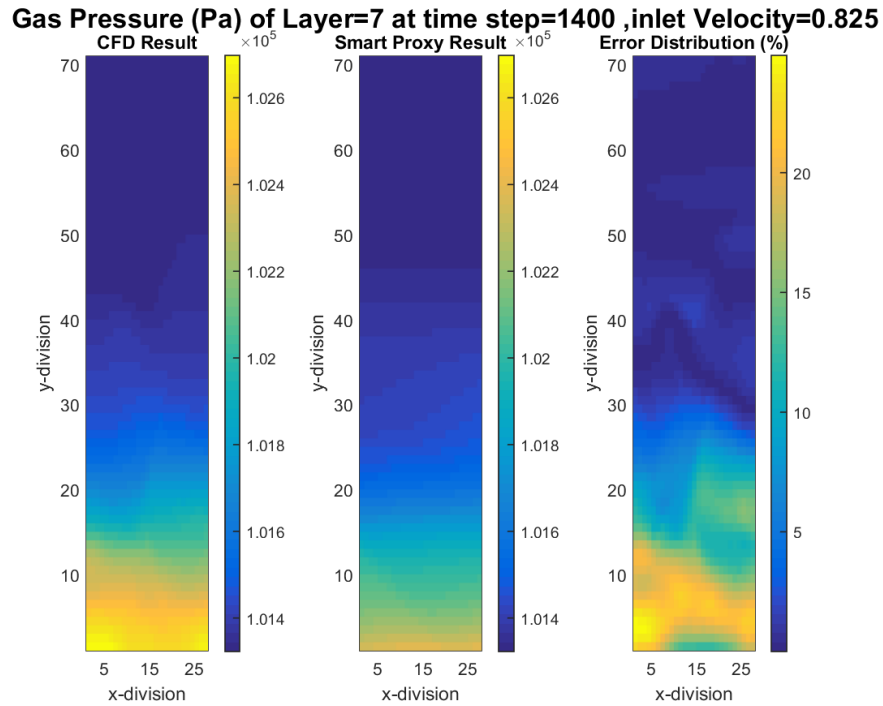


**Figure 7-12** CFD and smart proxy results for gas pressure at  $K=7$  cross-sectional plane for time step of 1400 and  $V_{in}$  of 0.825 m/s, using 7 static parameters

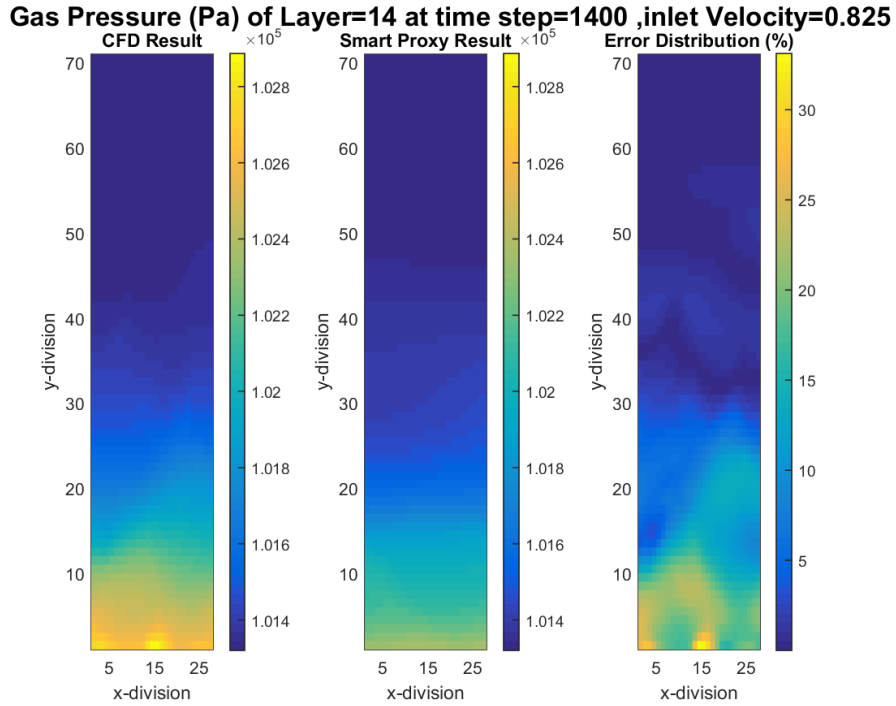


**Figure 7-13** CFD and smart proxy results for gas pressure at  $K=14$  cross-sectional plane for time step of 1400 and  $V_{in}$  of 0.825 m/s, using 7 static parameters

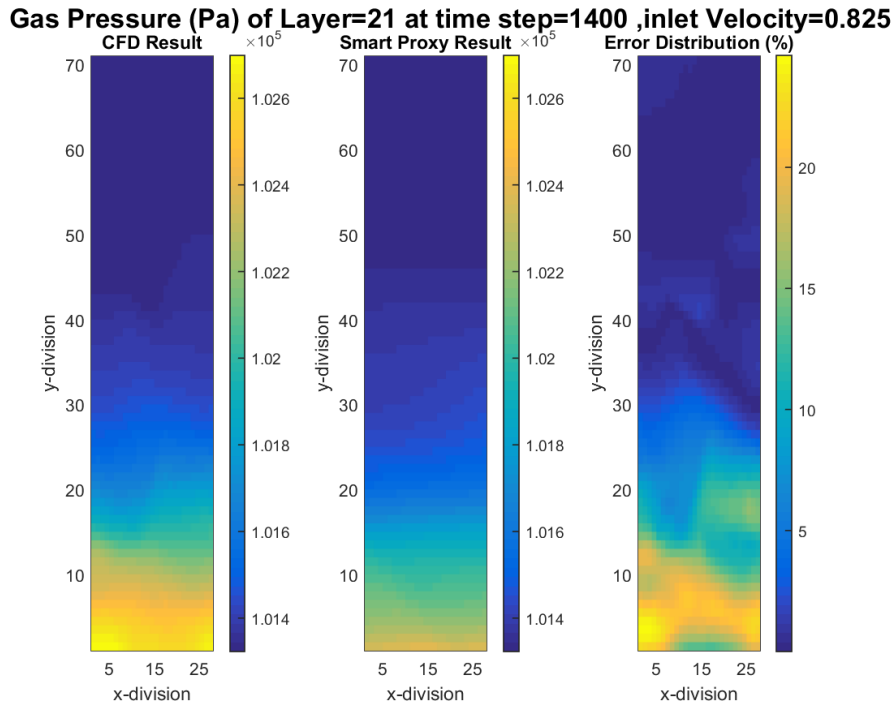


**Figure 7-14** CFD and smart proxy results for gas pressure at  $K=21$  cross-sectional plane for time step of 1400 and  $V_{in}$  of 0.825 m/s, using 7 static parameters

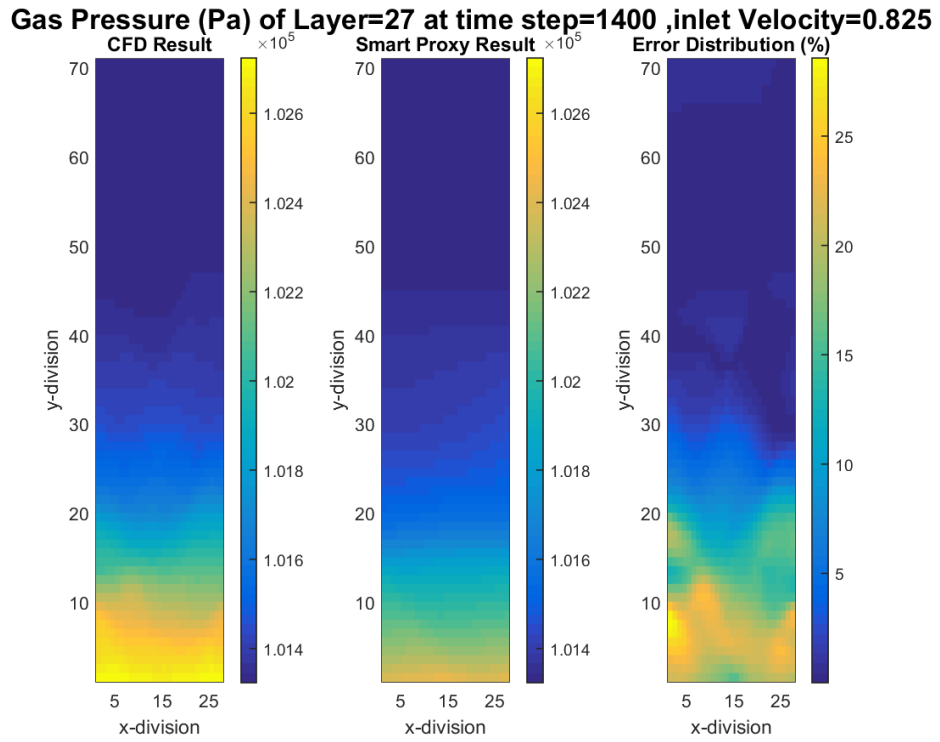


**Figure 7-15 CFD and smart proxy results for gas pressure at K=27 cross-sectional plane for time step of 1400 and  $V_{in}$  of 0.825 m/s, using 7 static parameters**

**8. APPENDIX II: GAS PRESSURE USING 11 STATIC PARAMETERS**

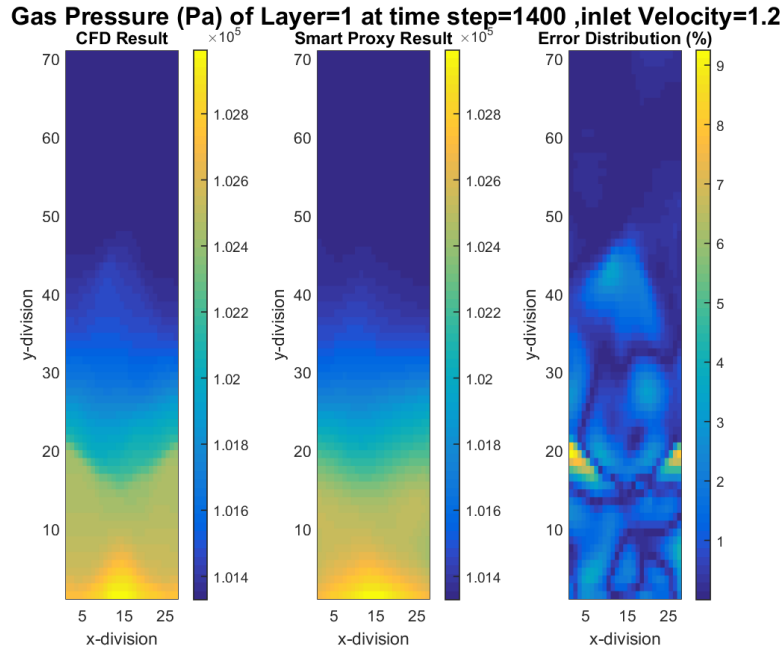


**Figure 8-1** CFD and smart proxy results for gas pressure at K=1 cross-sectional plane for time step of 1400 and  $V_{in}$  of 1.2 m/s, using 11 static parameters

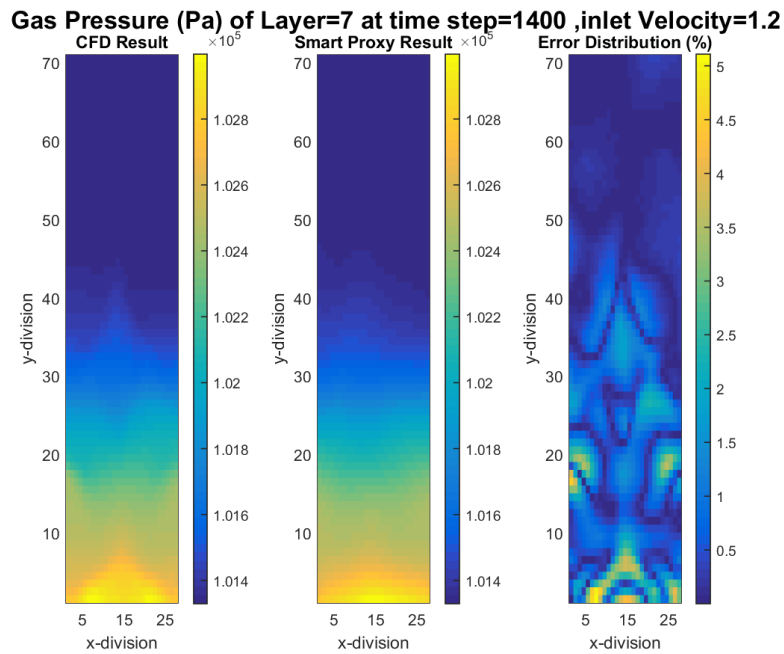


**Figure 8-2** CFD and smart proxy results for gas pressure at K=7 cross-sectional plane for time step of 1400 and  $V_{in}$  of 1.2 m/s, using 11 static parameters

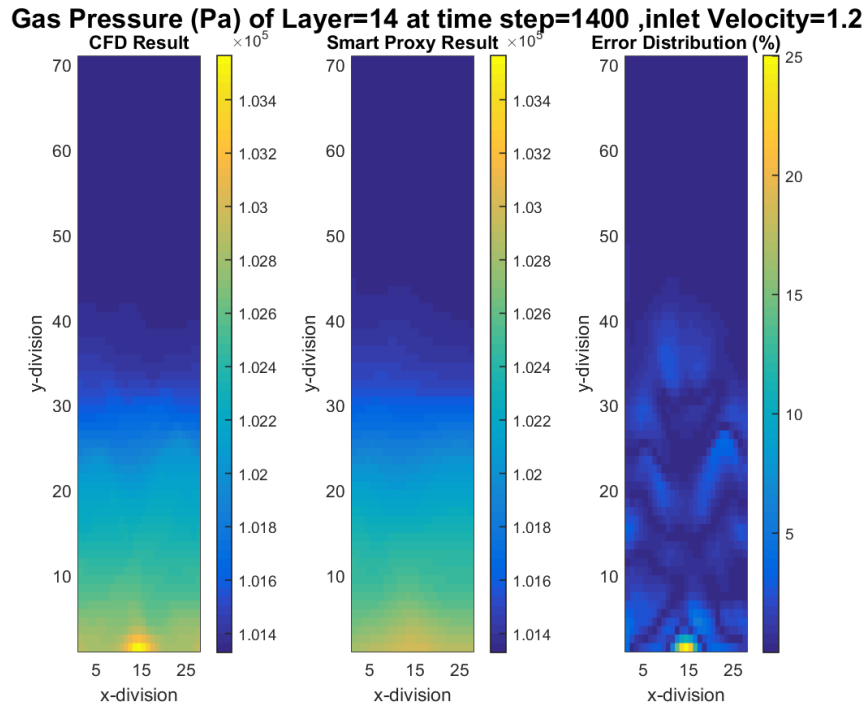


**Figure 8-3** CFD and smart proxy results for gas pressure at K=14 cross-sectional plane for time step of 1400 and  $V_{in}$  of 1.2 m/s, using 11 static parameters

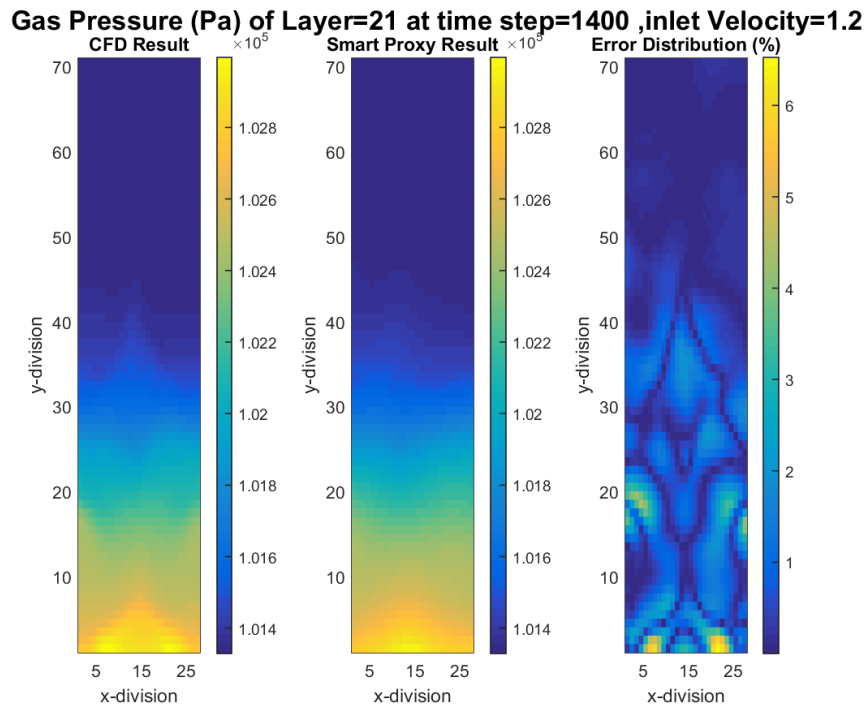


**Figure 8-4** CFD and smart proxy results for gas pressure at K=21 cross-sectional plane for time step of 1400 and  $V_{in}$  of 1.2 m/s, using 11 static parameters

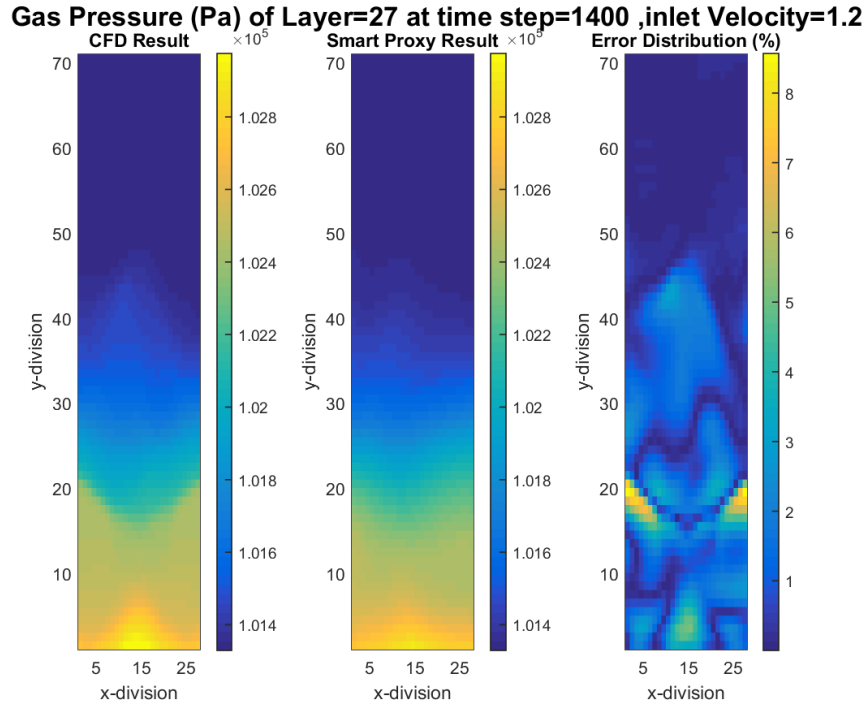


**Figure 8-5** CFD and smart proxy results for gas pressure at  $K=27$  cross-sectional plane for time step of 1400 and  $V_{in}$  of 1.2 m/s, using 11 static parameters

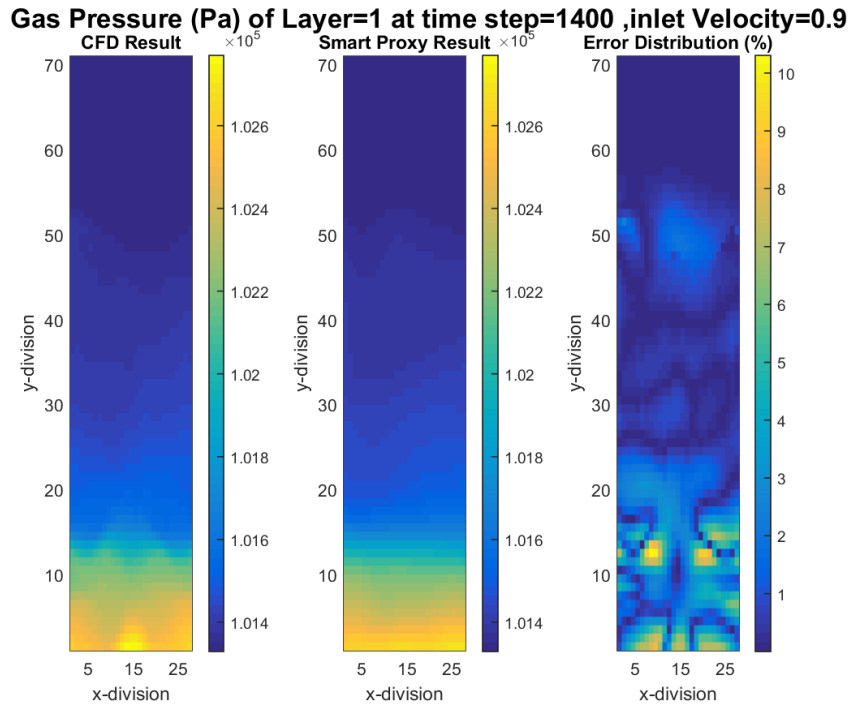


**Figure 8-6** CFD and smart proxy results for gas pressure at  $K=1$  cross-sectional plane for time step of 1400 and  $V_{in}$  of 0.9 m/s, using 11 static parameters

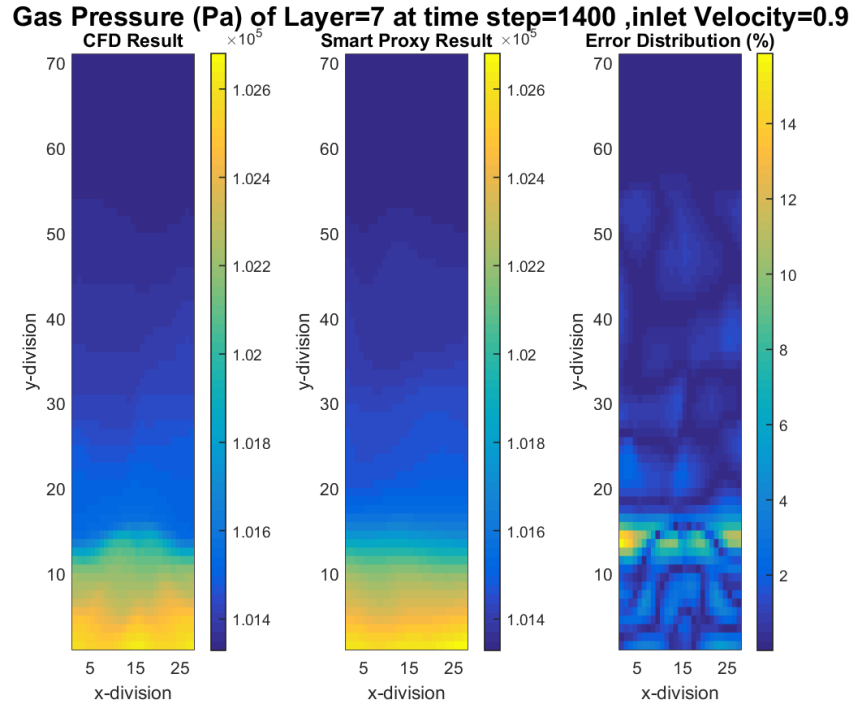


**Figure 8-7** CFD and smart proxy results for gas pressure at K=7 cross-sectional plane for time step of 1400 and  $V_{in}$  of 0.9 m/s, using 11 static parameters

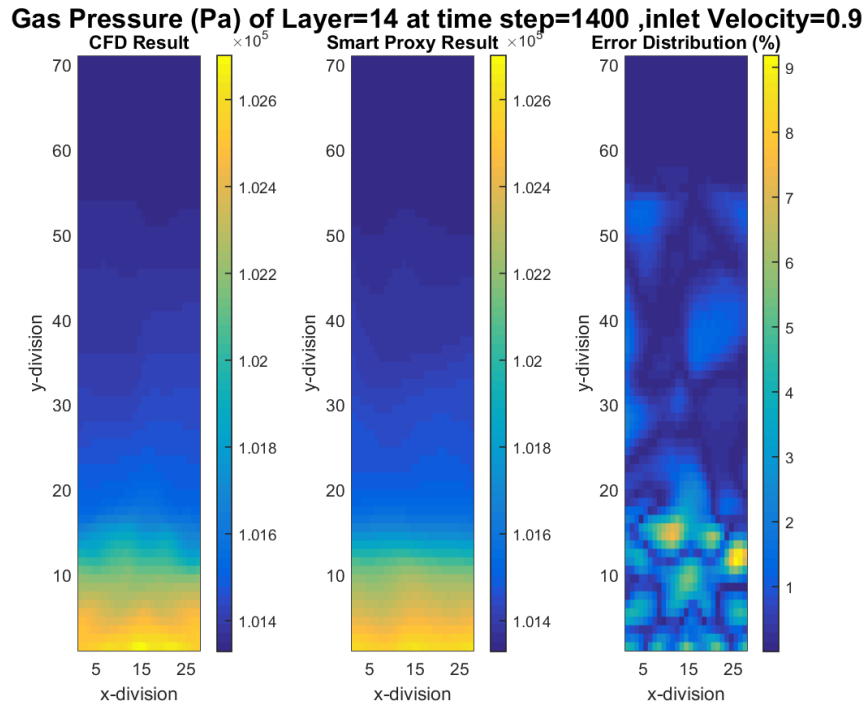


**Figure 8-8** CFD and smart proxy results for gas pressure at K=14 cross-sectional plane for time step of 1400 and  $V_{in}$  of 0.9 m/s, using 11 static parameters

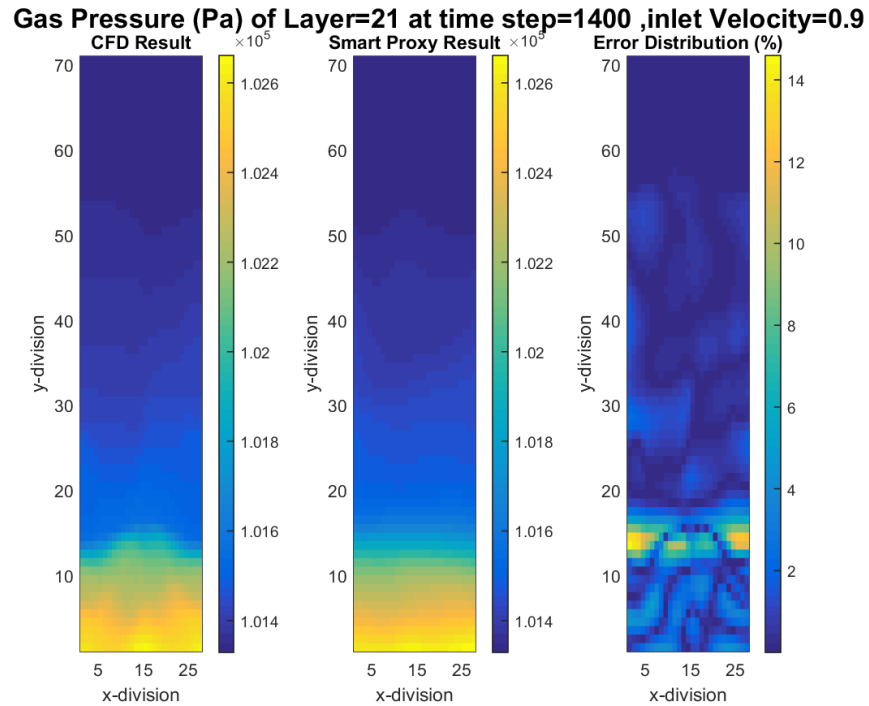


**Figure 8-9** CFD and smart proxy results for gas pressure at K=21 cross-sectional plane for time step of 1400 and  $V_{in}$  of 0.9 m/s, using 11 static parameters

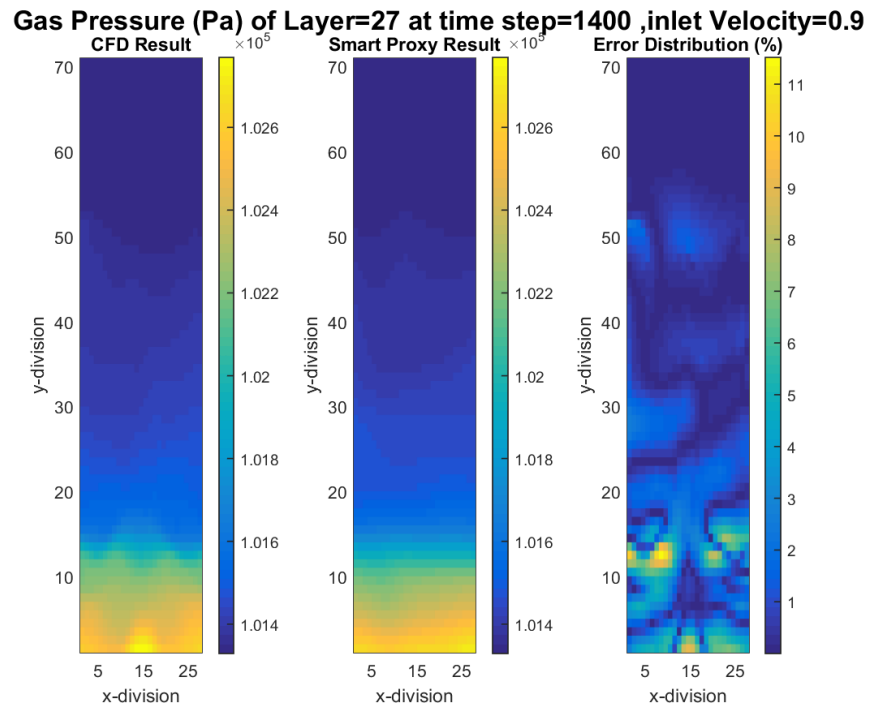


**Figure 8-10** CFD and smart proxy results for gas pressure at K=27 cross-sectional plane for time step of 1400 and  $V_{in}$  of 0.9 m/s, using 11 static parameters

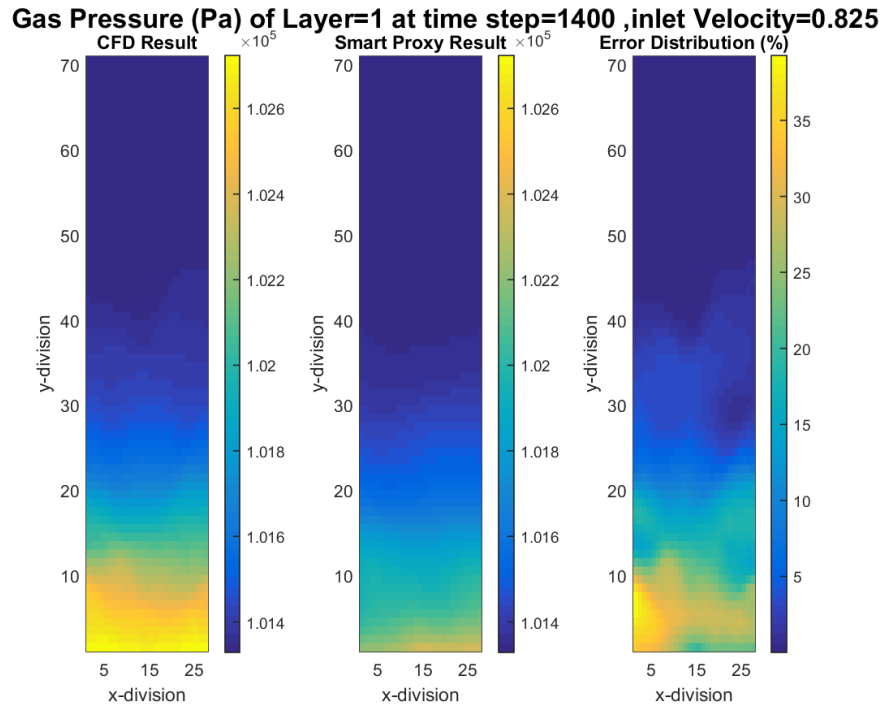


**Figure 8-11** CFD and smart proxy results for gas pressure at  $K=1$  cross-sectional plane for time step of 1400 and  $V_{in}$  of 0.825 m/s, using 11 static parameters

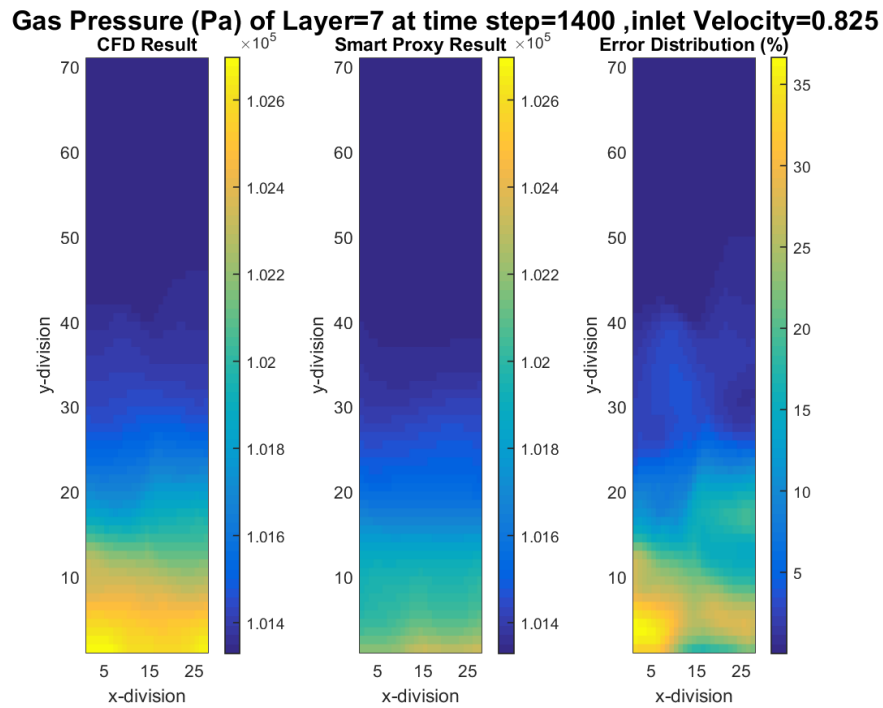


**Figure 8-12** CFD and smart proxy results for gas pressure at  $K=7$  cross-sectional plane for time step of 1400 and  $V_{in}$  of 0.825 m/s, using 11 static parameters

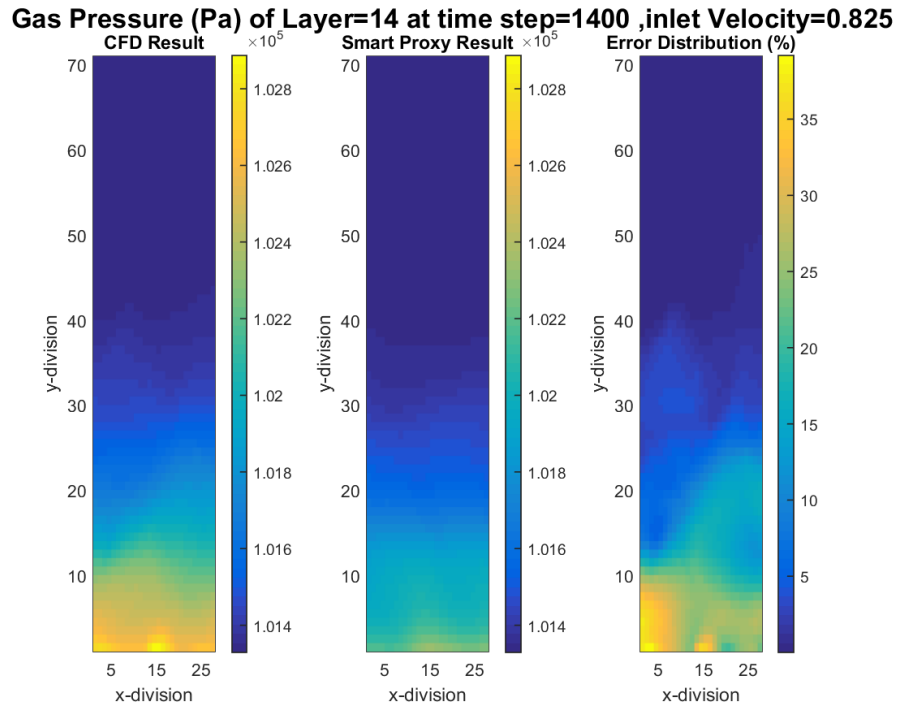


**Figure 8-13** CFD and smart proxy results for gas pressure at K=14 cross-sectional plane for time step of 1400 and  $V_{in}$  of 0.825 m/s, using 11 static parameters

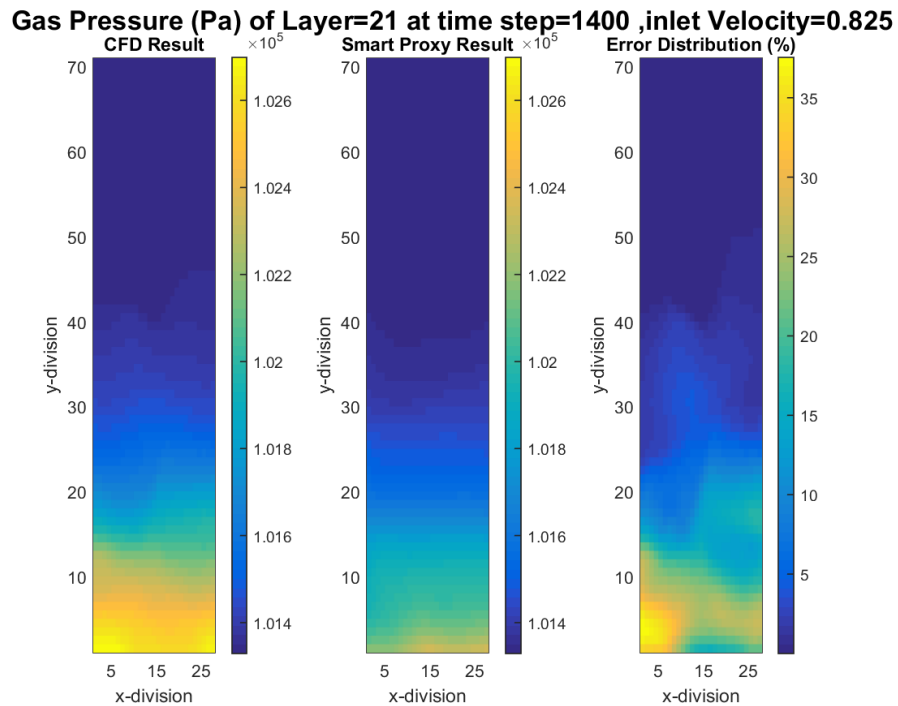


**Figure 8-14** CFD and smart proxy results for gas pressure at K=21 cross-sectional plane for time step of 1400 and  $V_{in}$  of 0.825 m/s, using 11 static parameters

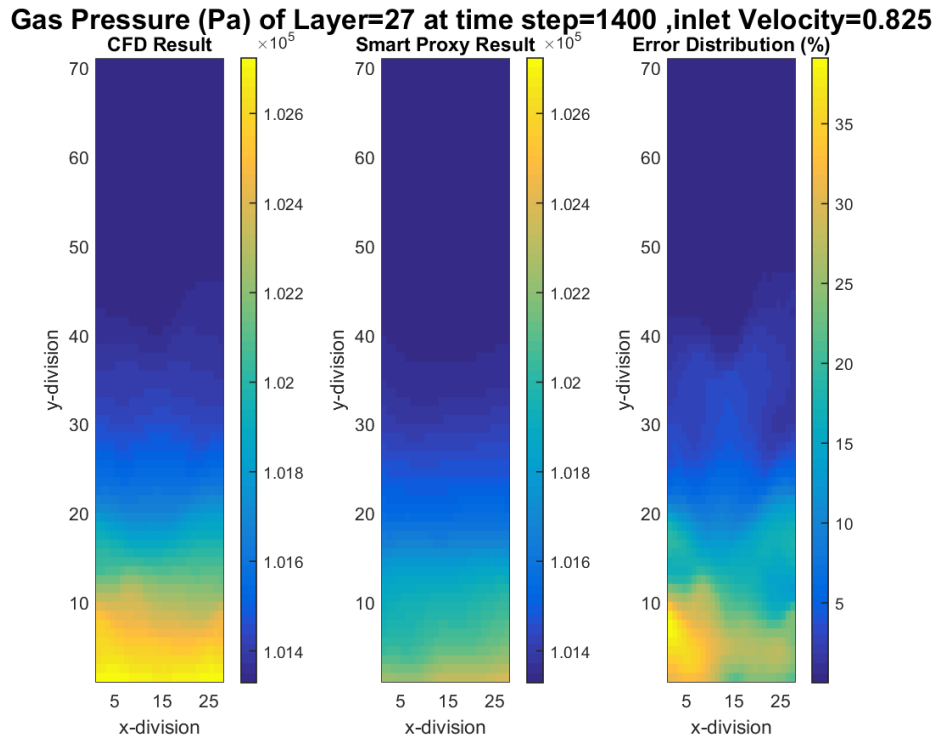


**Figure 8-15 CFD and smart proxy results for gas pressure at K=27 cross-sectional plane for time step of 1400 and  $V_{in}$  of 0.825 m/s, using 11 static parameters**

**9. APPENDIX III: TIME AVERAGE OF GAS PRESSURE BETWEEN TIME STEP 500 TO 1400**

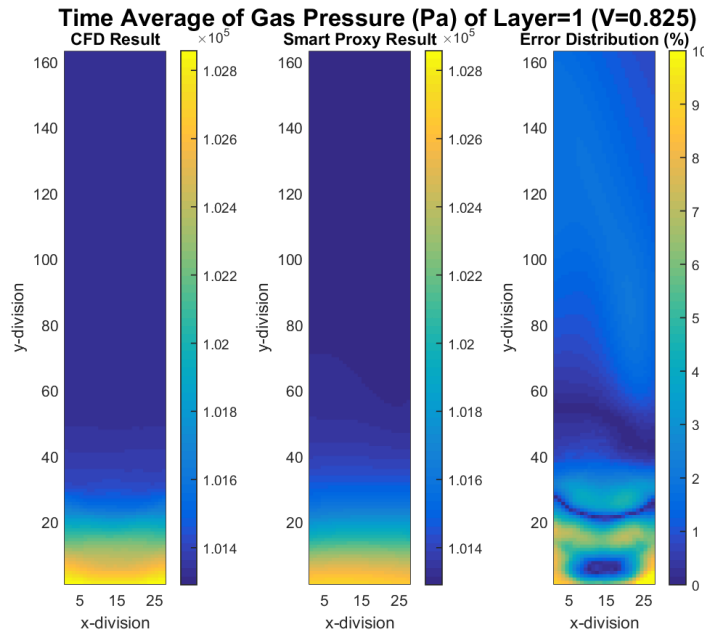


**Figure 9-1** CFD and smart proxy results for gas pressure averaged over time steps 500 to 1400 at K=1 cross-sectional plane and  $V_{in}=0.825$  m/s

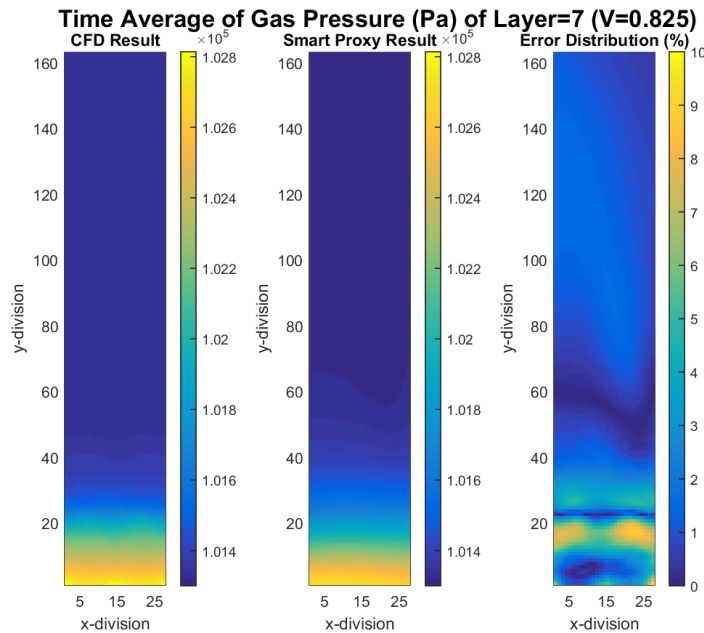


**Figure 9-2** CFD and smart proxy results for gas pressure averaged over time steps 500 to 1400 at K=7 cross-sectional plane and  $V_{in}=0.825$  m/s

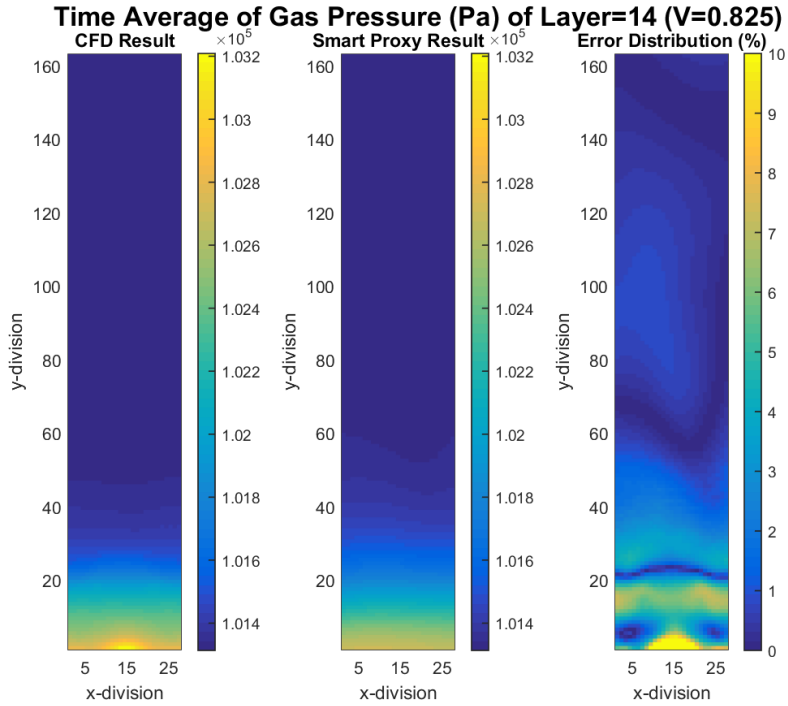


**Figure 9-3** CFD and smart proxy results for gas pressure averaged over time steps 500 to 1400 at K=14 cross-sectional plane and  $V_{in}=0.825$  m/s

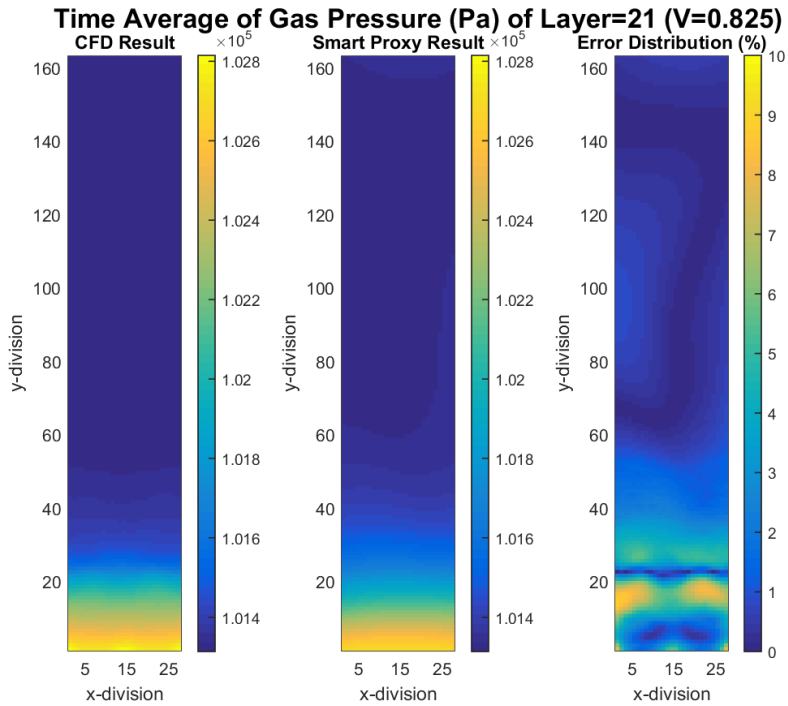


**Figure 9-4** CFD and smart proxy results for gas pressure averaged over time steps 500 to 1400 at K=21 cross-sectional plane and  $V_{in}=0.825$  m/s

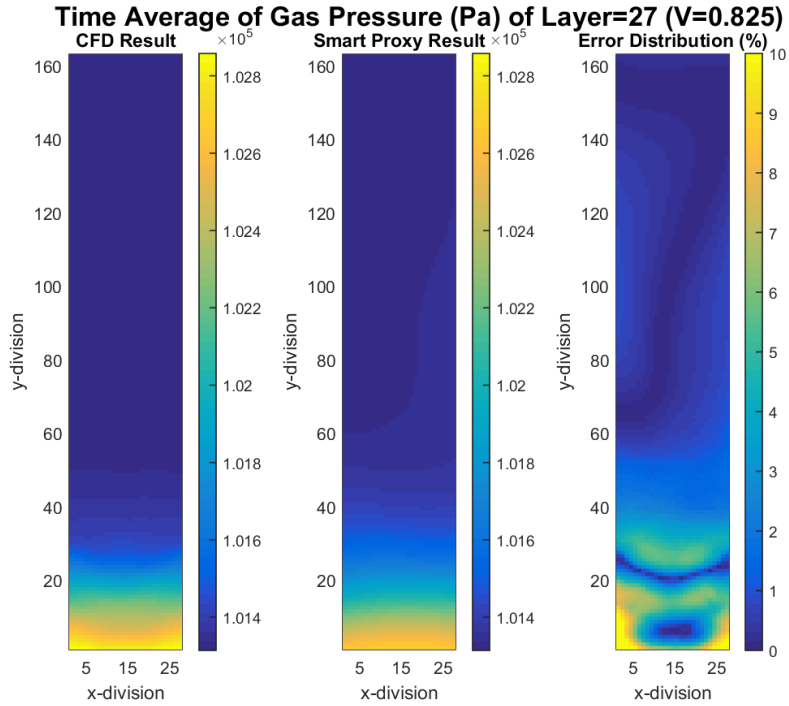


**Figure 9-5** CFD and smart proxy results for gas pressure averaged over time steps 500 to 1400 at K=27 cross-sectional plane and  $V_{in}=0.825$  m/s

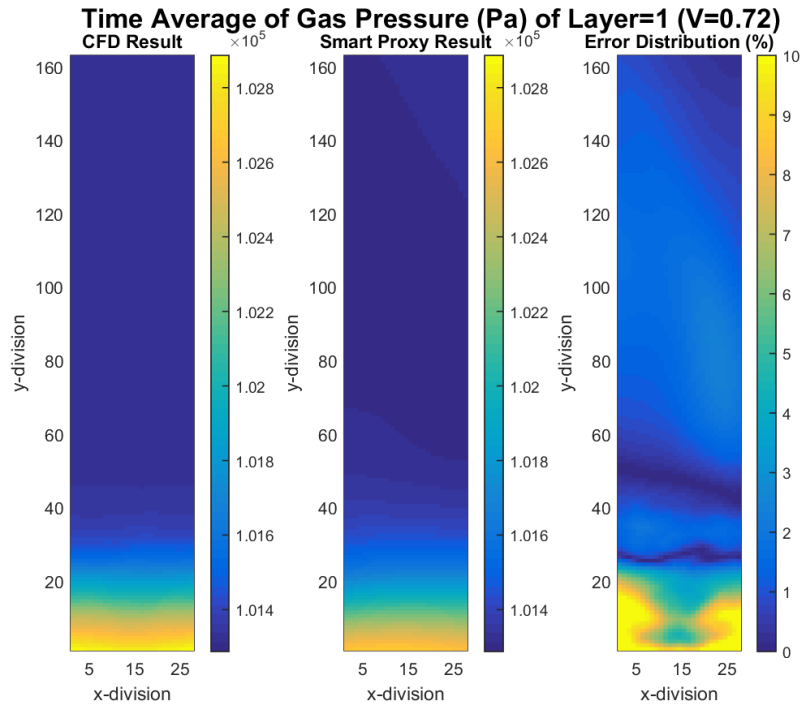


**Figure 9-6** CFD and smart proxy results for gas pressure averaged over time steps 500 to 1400 at K=1 cross-sectional plane and  $V_{in}=0.72$  m/s

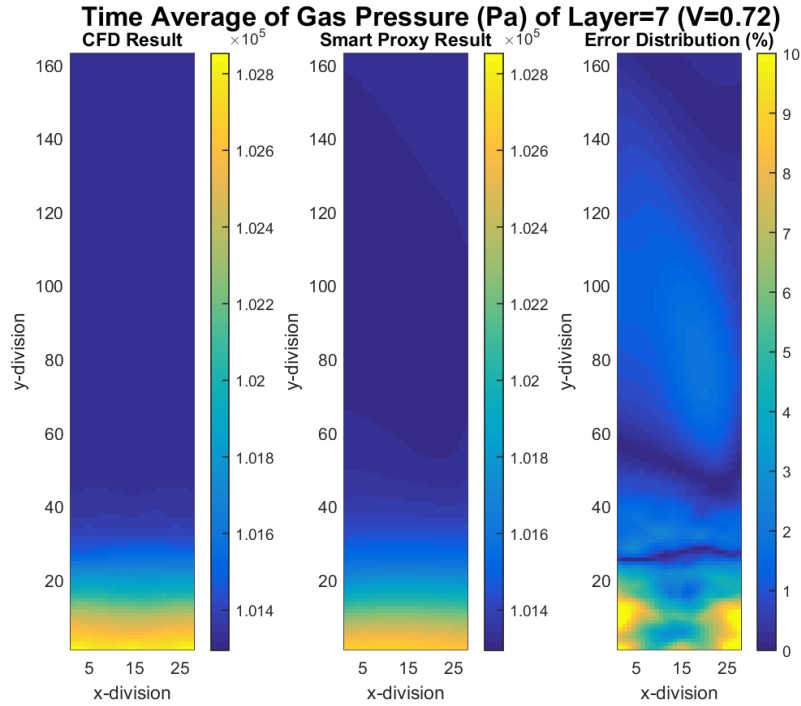


**Figure 9-7** CFD and smart proxy results for gas pressure averaged over time steps 500 to 1400 at K=7 cross-sectional plane and  $V_{in}=0.72$  m/s

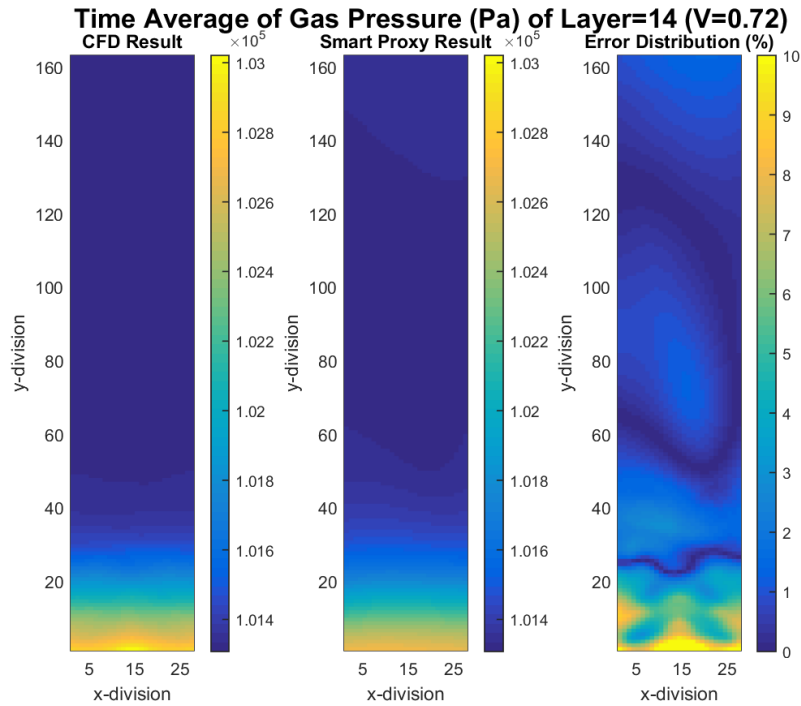


**Figure 9-8** CFD and smart proxy results for gas pressure averaged over time steps 500 to 1400 at K=17 cross-sectional plane and  $V_{in}=0.72$  m/s

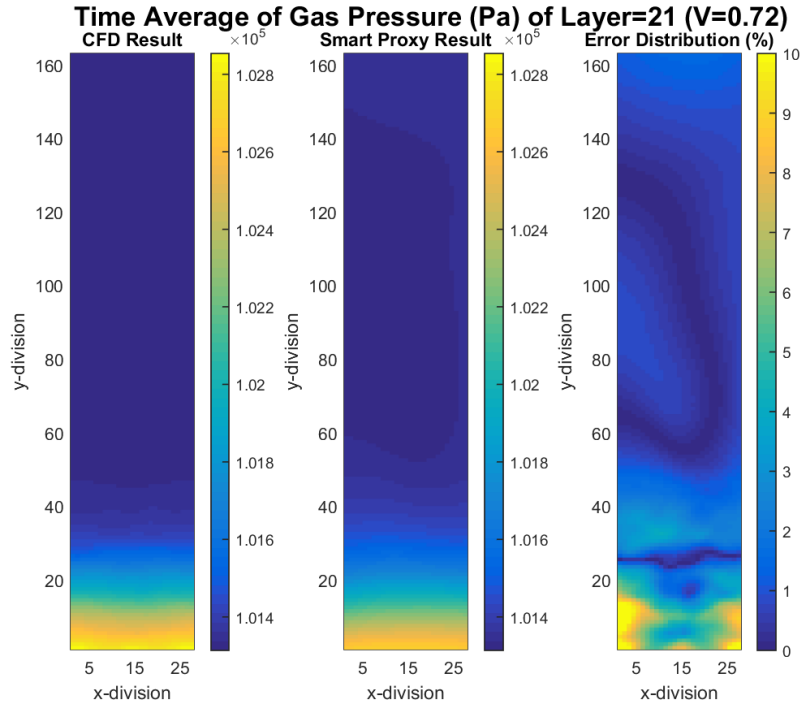


**Figure 9-9** CFD and smart proxy results for gas pressure averaged over time steps 500 to 1400 at K=21 cross-sectional plane and  $V_{in}=0.72$  m/s

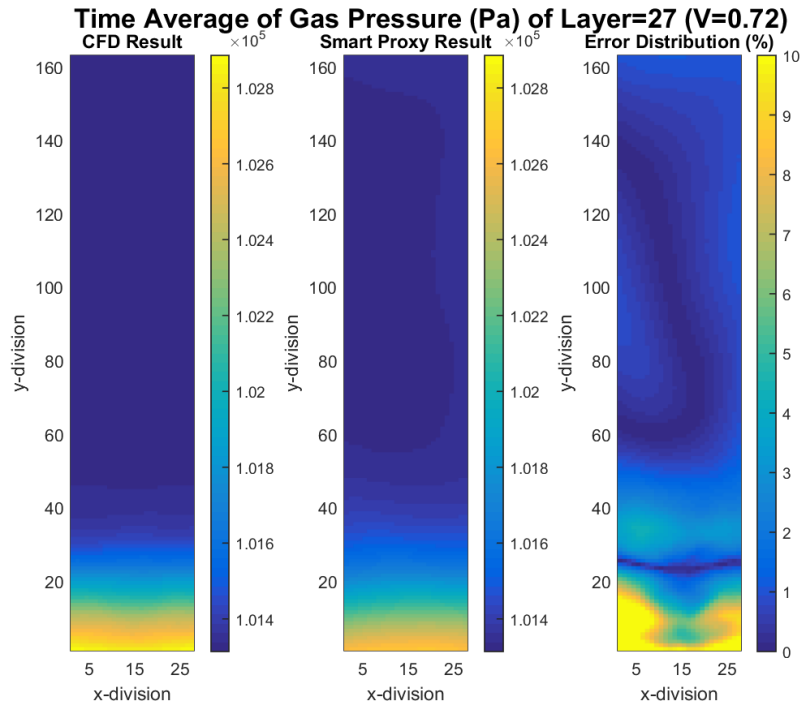


**Figure 9-10** CFD and smart proxy results for gas pressure averaged over time steps 500 to 1400 at K=27 cross-sectional plane and  $V_{in}=0.72$  m/s

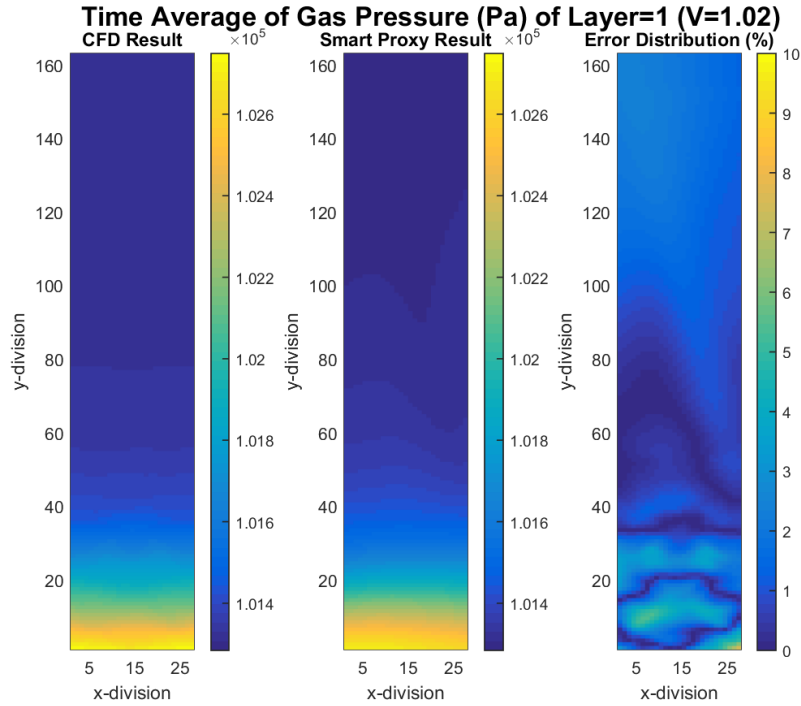


**Figure 9-11** CFD and smart proxy results for gas pressure averaged over time steps 500 to 1400 at K=1 cross-sectional plane and  $V_{in}=1.02$  m/s

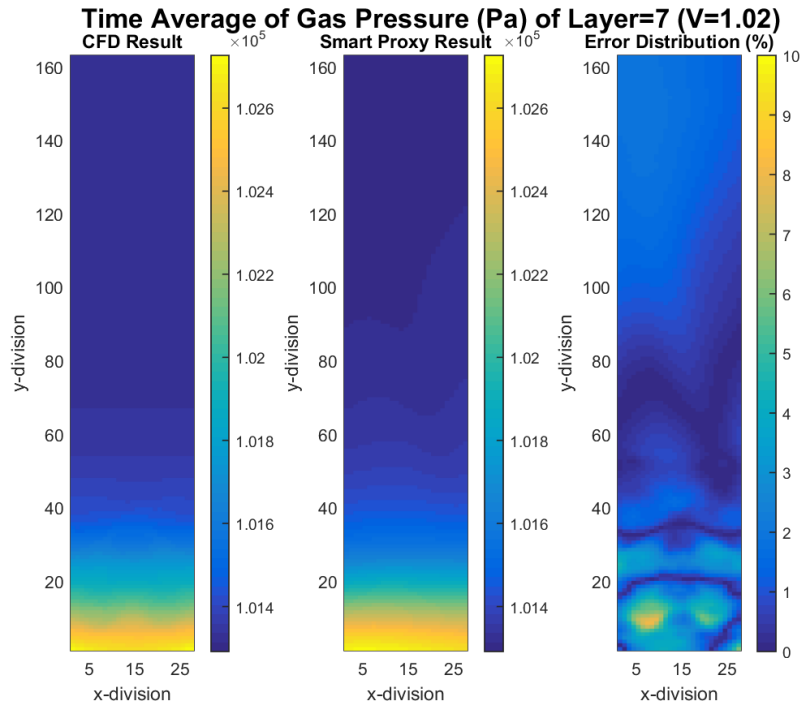


**Figure 9-12** CFD and smart proxy results for gas pressure averaged over time steps 500 to 1400 at K=7 cross-sectional plane and  $V_{in}=1.02$  m/s

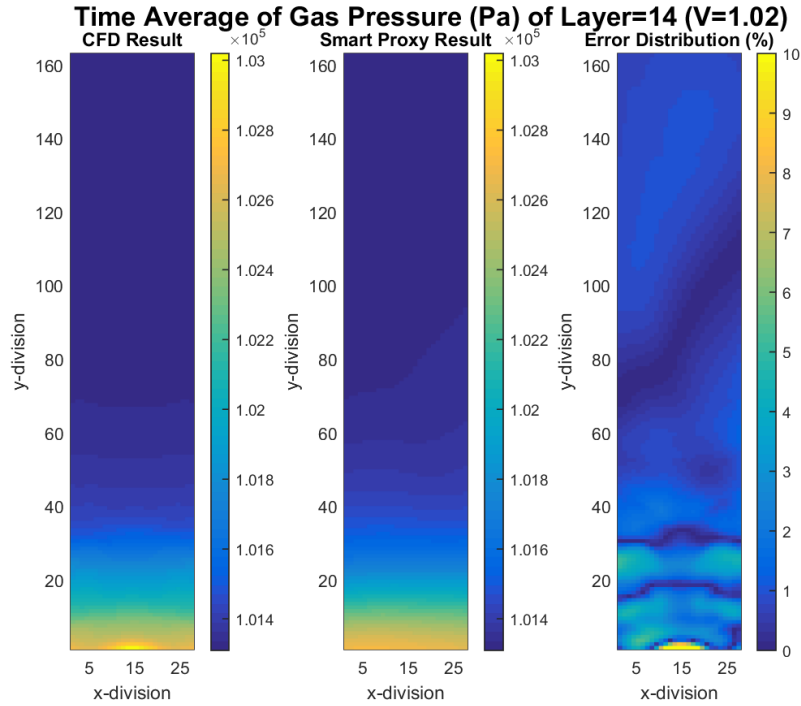


**Figure 9-13** CFD and smart proxy results for gas pressure averaged over time steps 500 to 1400 at K=14 cross-sectional plane and  $V_{in}=1.02$  m/s

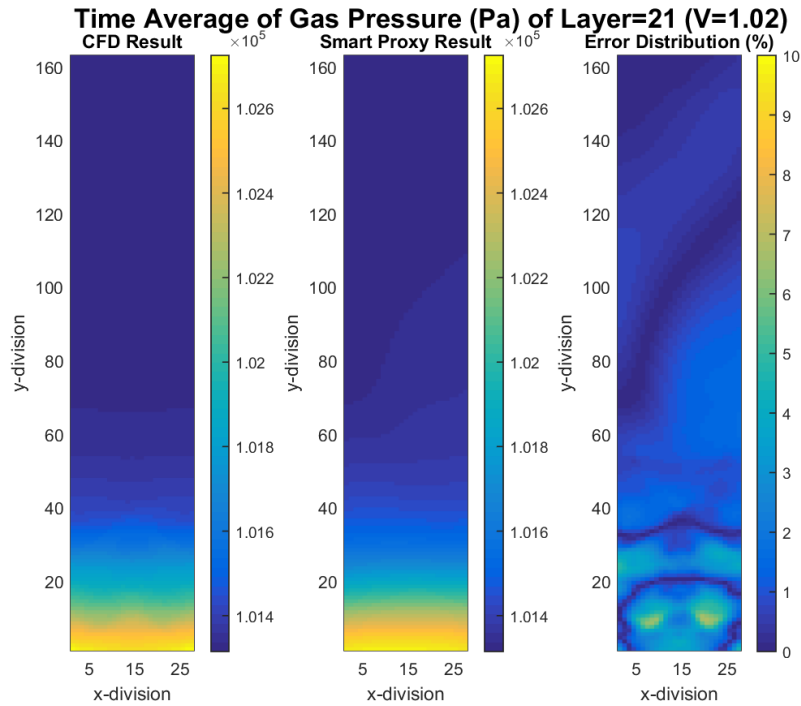


**Figure 9-14** CFD and smart proxy results for gas pressure averaged over time steps 500 to 1400 at K=21 cross-sectional plane and  $V_{in}=1.02$  m/s

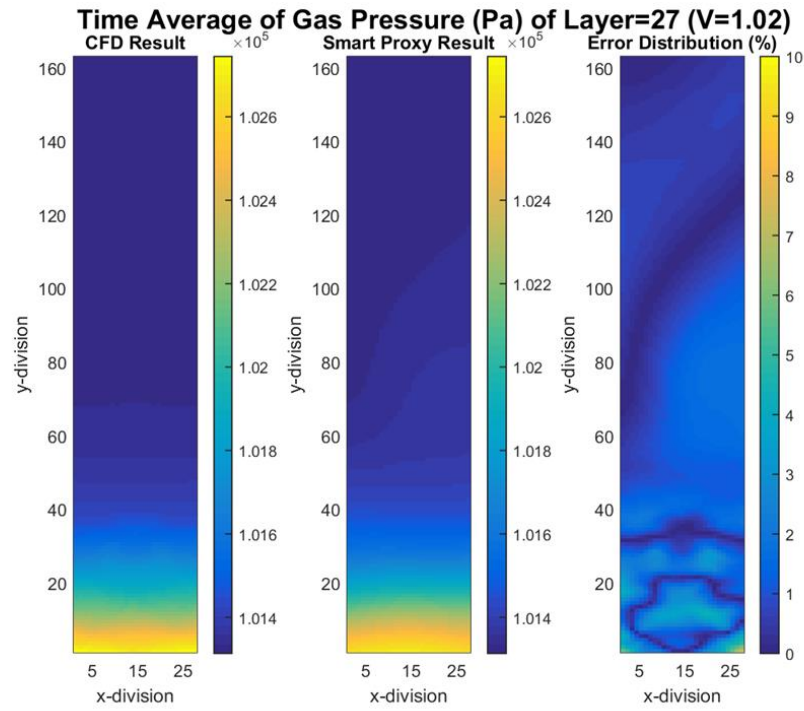


**Figure 9-15** CFD and smart proxy results for gas pressure averaged over time steps 500 to 1400 at  $K=27$  cross-sectional plane and  $V_{in}=1.02$  m/s

**10. APPENDIX IV: BLIND TEST RESULTS FOR TIME AVERAGE OF GAS PRESSURE BETWEEN TIME STEP 1500 TO 3400**

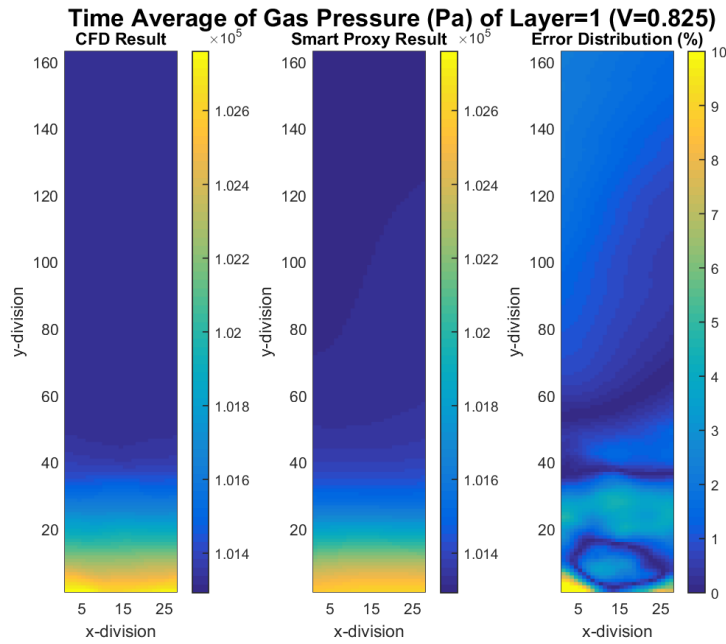


**Figure 10-1 CFD and smart proxy results for gas pressure averaged over time steps 1500 to 3400 at K=1 cross-sectional plane and  $V_{in}=0.825$  m/s**

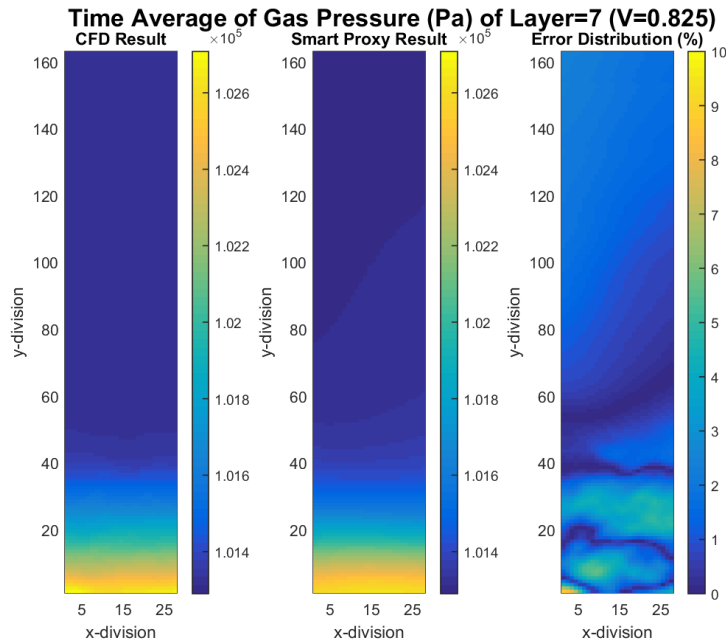


**Figure 10-2 CFD and smart proxy results for gas pressure averaged over time steps 1500 to 3400 at K=7 cross-sectional plane and  $V_{in}=0.825$  m/s**

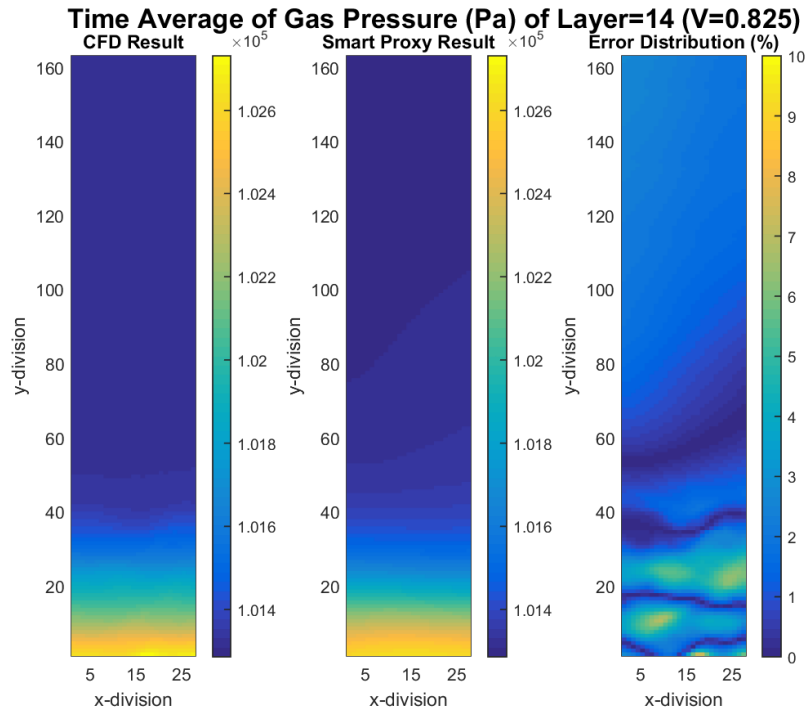


**Figure 10-3** CFD and smart proxy results for gas pressure averaged over time steps 1500 to 3400 at K=14 cross-sectional plane and  $V_{in}=0.825$  m/s

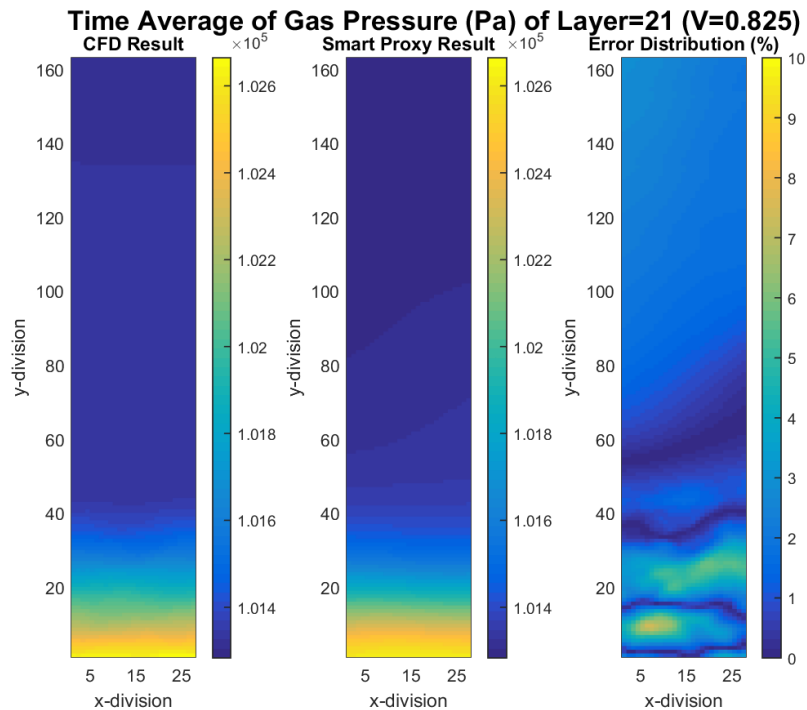


**Figure 10-4** CFD and smart proxy results for gas pressure averaged over time steps 1500 to 3400 at K=21 cross-sectional plane and  $V_{in}=0.825$  m/s

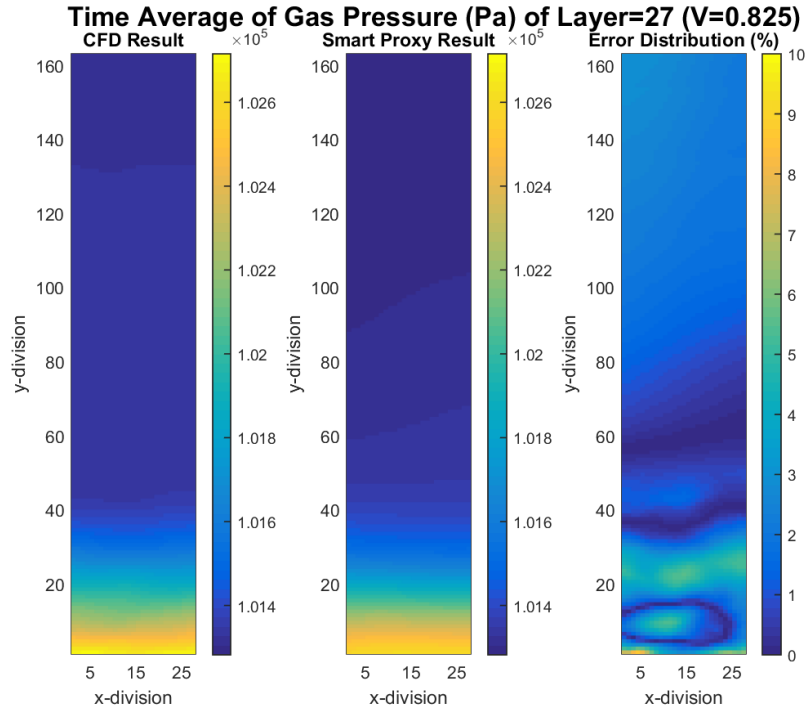


**Figure 10-5** CFD and smart proxy results for gas pressure averaged over time steps 1500 to 3400 at K=27 cross-sectional plane and  $V_{in}=0.825$  m/s

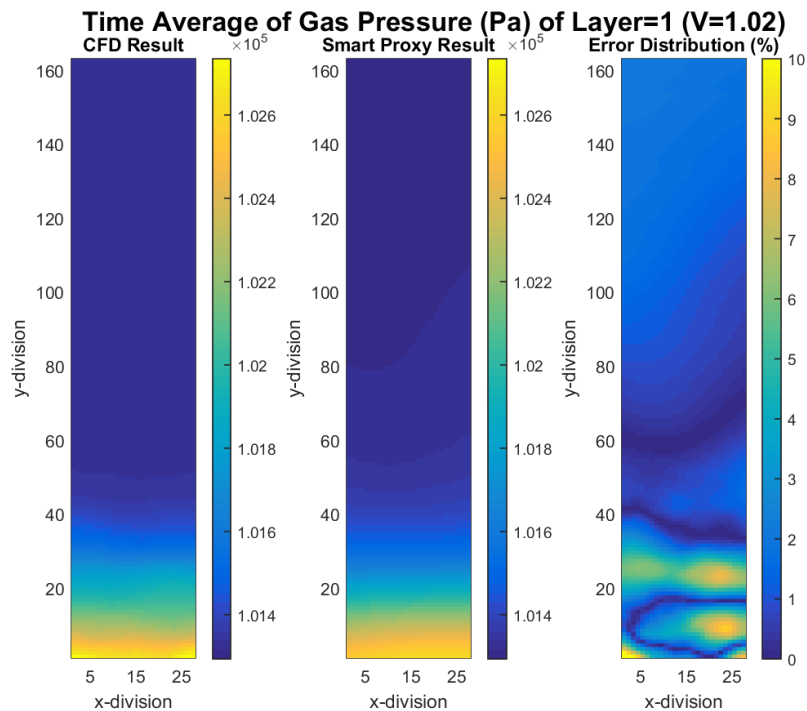


**Figure 10-6** CFD and smart proxy results for gas pressure averaged over time steps 1500 to 3400 at K=1 cross-sectional plane and  $V_{in}=1.02$  m/s

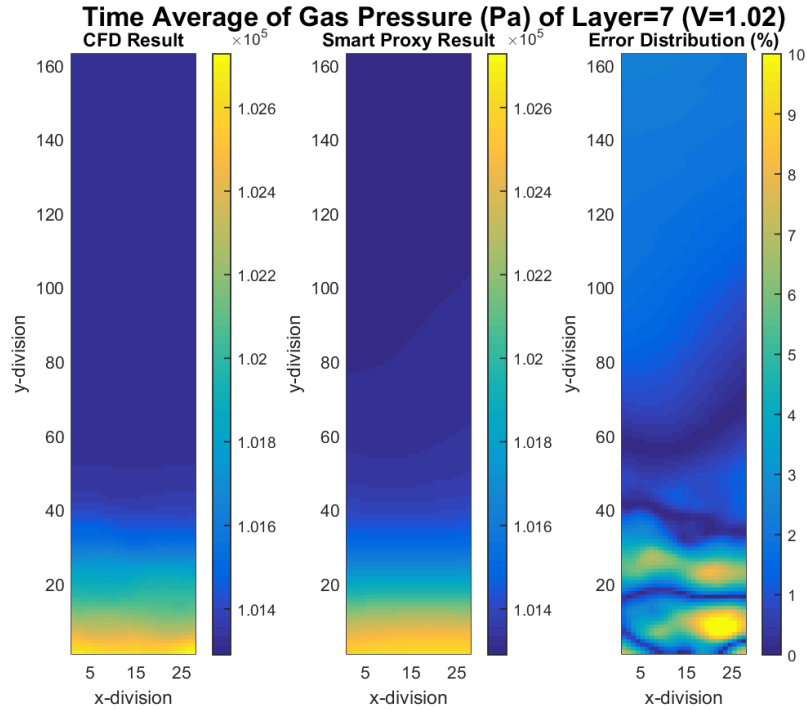


**Figure 10-7** CFD and smart proxy results for gas pressure averaged over time steps 1500 to 3400 at K=7 cross-sectional plane and  $V_{in}=1.02$  m/s

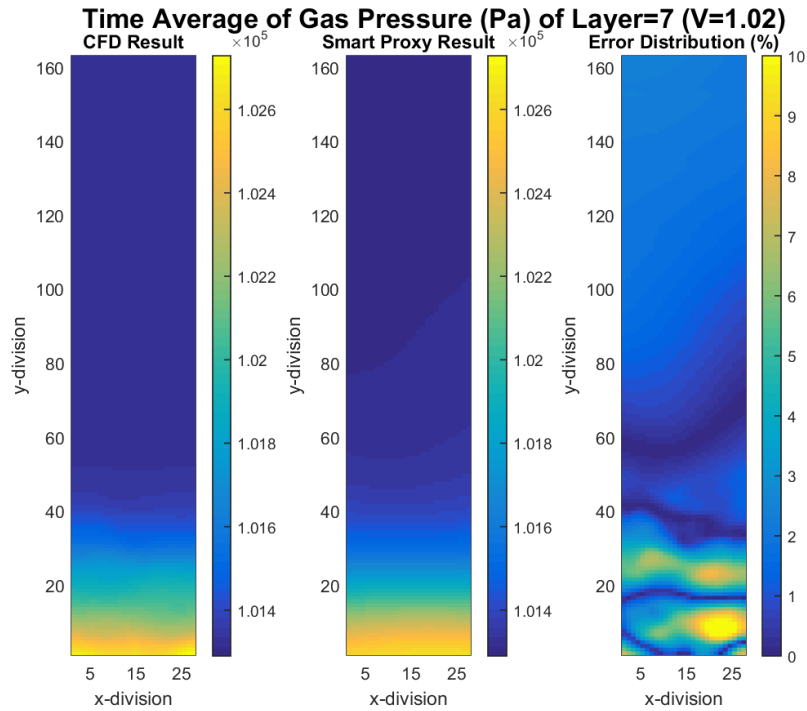


**Figure 10-8** CFD and smart proxy results for gas pressure averaged over time steps 1500 to 3400 at K=7 cross-sectional plane and  $V_{in}=1.02$  m/s

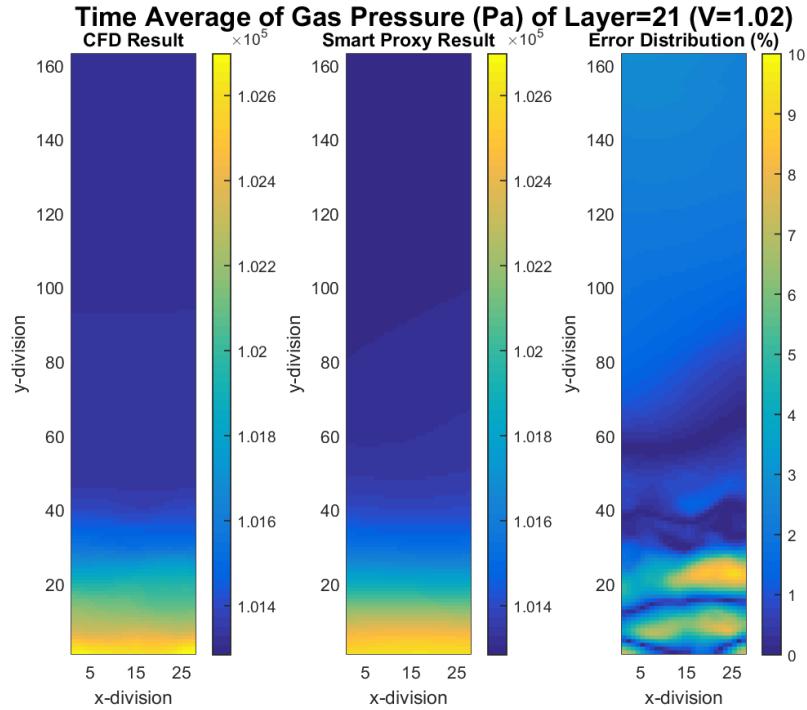


**Figure 10-9** CFD and smart proxy results for gas pressure avergaed over time steps 1500 to 3400 at K=21 cross-sectional plane and  $V_{in}=1.02$  m/s

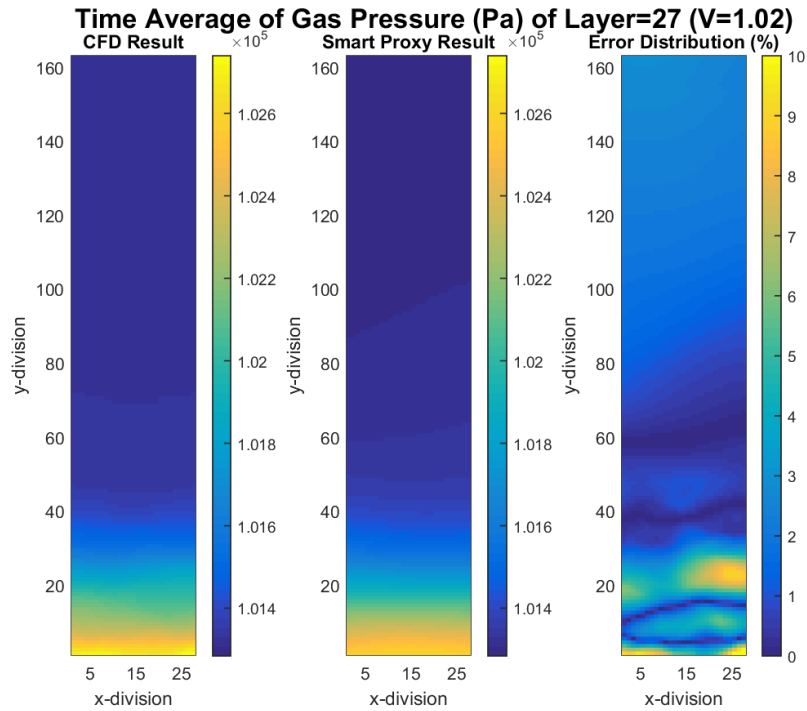


**Figure 10-10** CFD and smart proxy results for gas pressure avergaed over time steps 1500 to 3400 at K=27 cross-sectional plane and  $V_{in}=1.02$  m/s

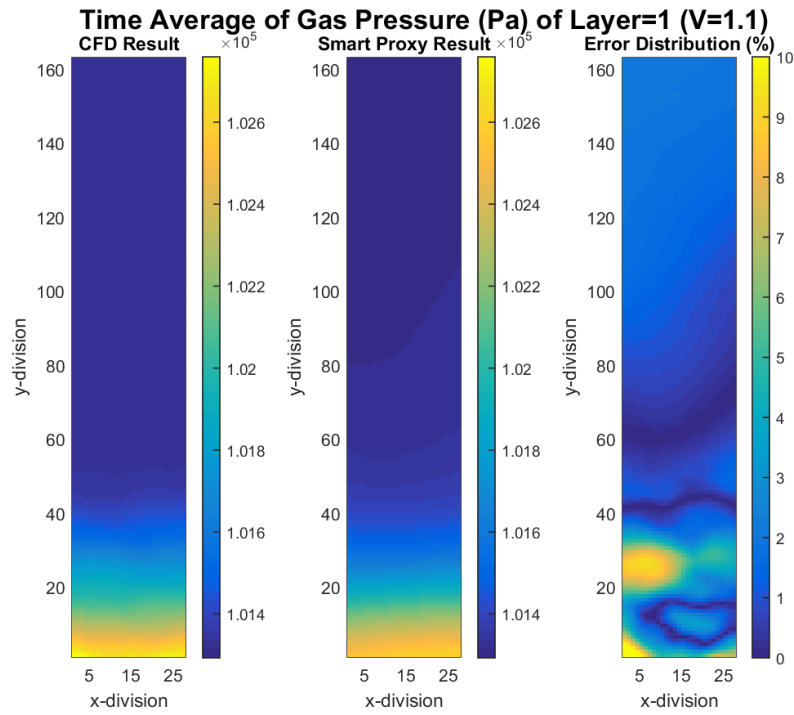


**Figure 10-11 CFD and smart proxy results for gas pressure averaged over time steps 1500 to 3400 at K=1 cross-sectional plane and  $V_{in}=1.1$  m/s**

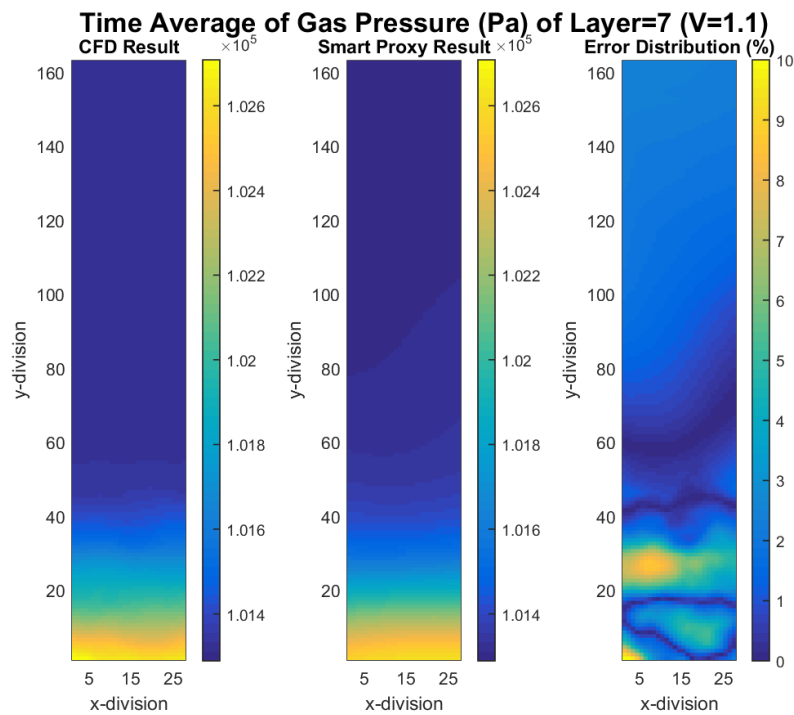


**Figure 10-12** CFD and smart proxy results for gas pressure averaged over time steps 1500 to 3400 at K=7 cross-sectional plane and  $V_{in}=1.1$  m/s

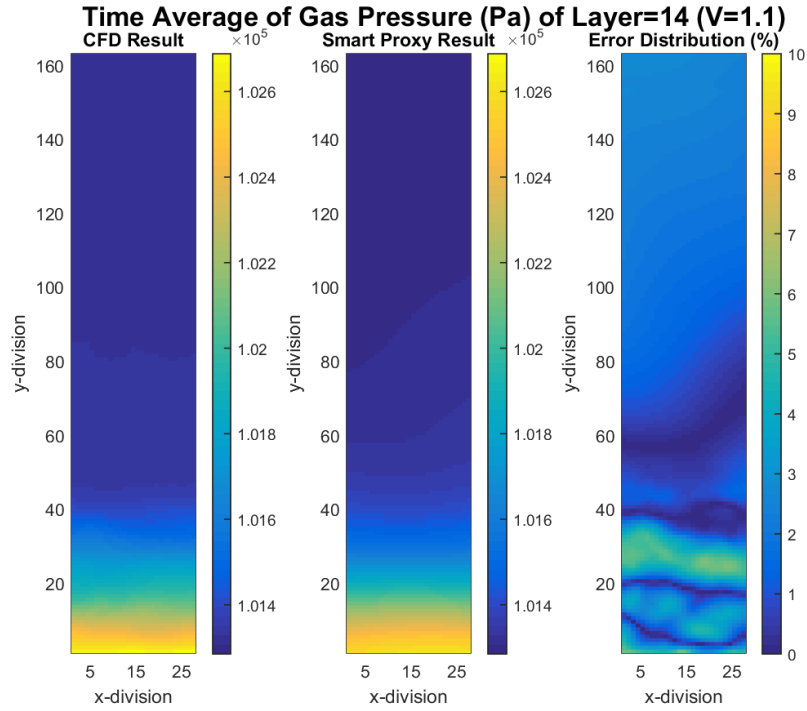


**Figure 10-13** CFD and smart proxy results for gas pressure averaged over time steps 1500 to 3400 at K=14 cross-sectional plane and  $V_{in}=1.1$  m/s

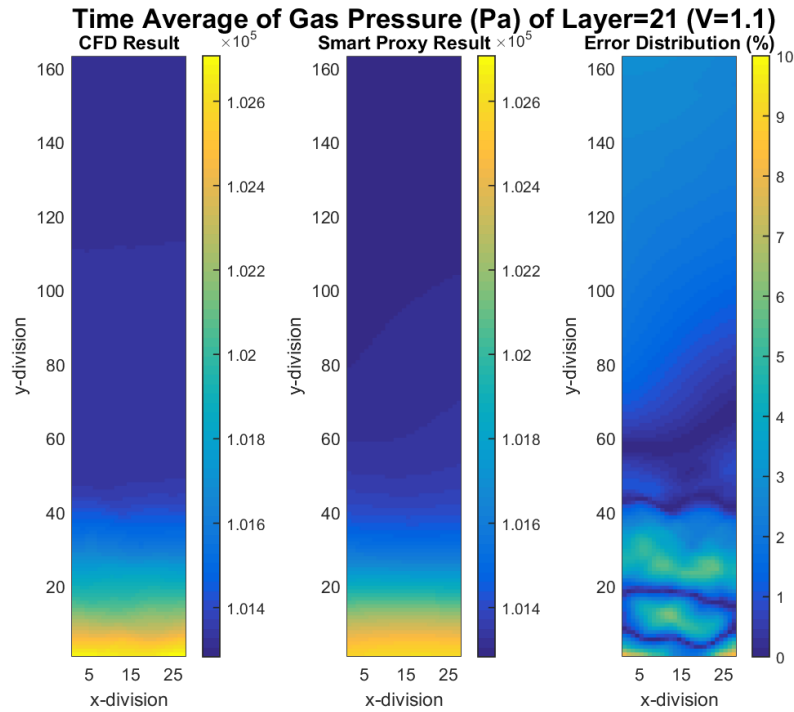


**Figure 10-14** CFD and smart proxy results for gas pressure averaged over time steps 1500 to 3400 at K=21 cross-sectional plane and  $V_{in}=1.1$  m/s

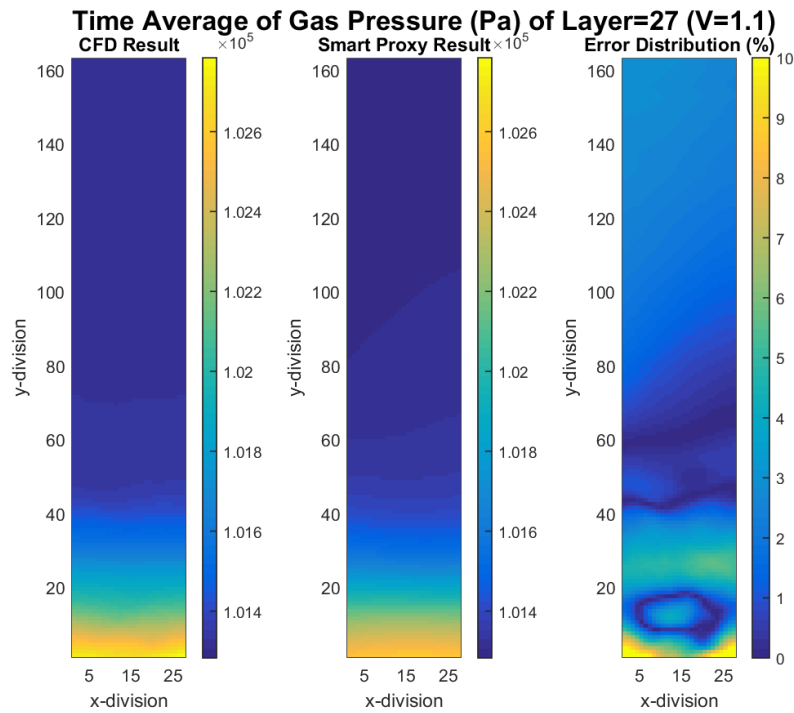


**Figure 10-15** CFD and smart proxy results for gas pressure averaged over time steps 1500 to 3400 at K=27 cross-sectional plane and  $V_{in}=1.1$  m/s

**11. APPENDIX V: GAS VELOCITY AND GAS VOLUME FRACTION USING STATIC PARAMETERS**

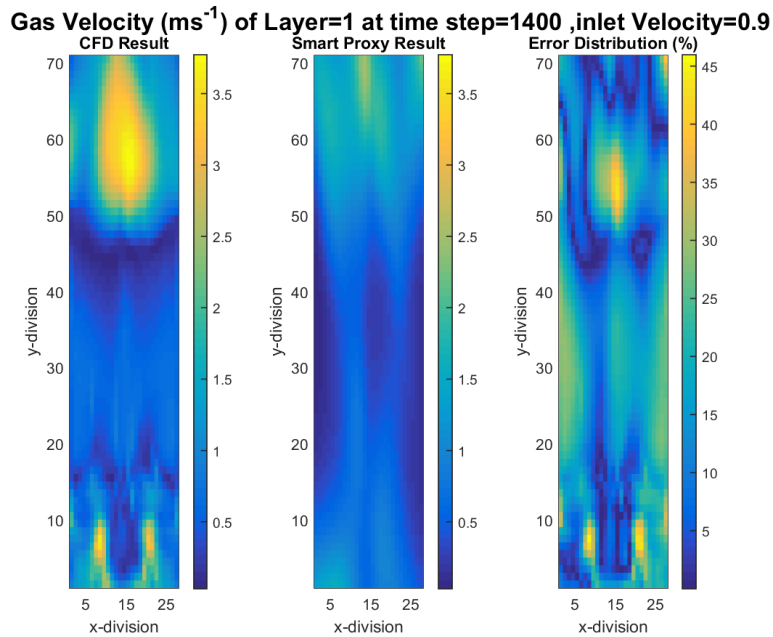


**Figure 11-1** CFD and smart proxy results for gas velocity at time step=1400,  $V_{in}=0.9$  m/s and  $K=1$  cross-sectional plane, using 11 static parameters

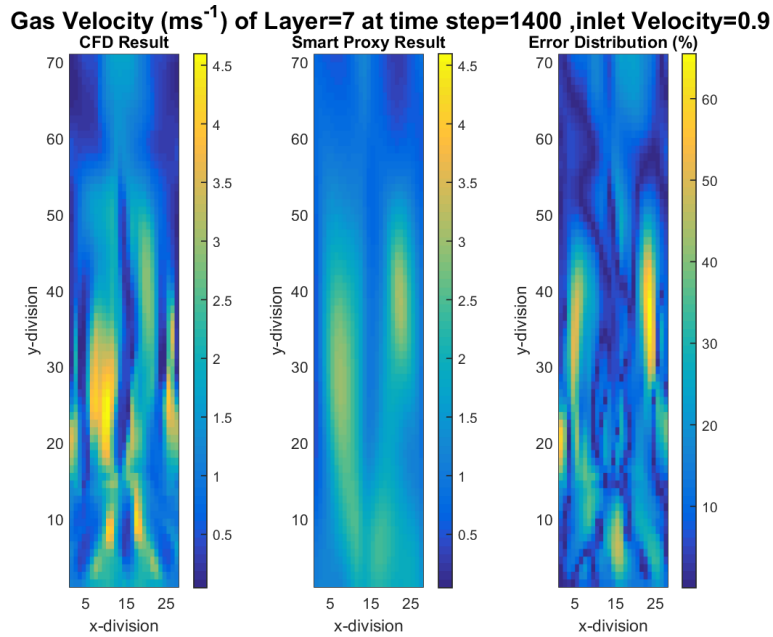


**Figure 11-2** CFD and smart proxy results for gas velocity at time step=1400,  $V_{in}=0.9$  m/s and  $K=7$  cross-sectional plane, using 11 static parameters

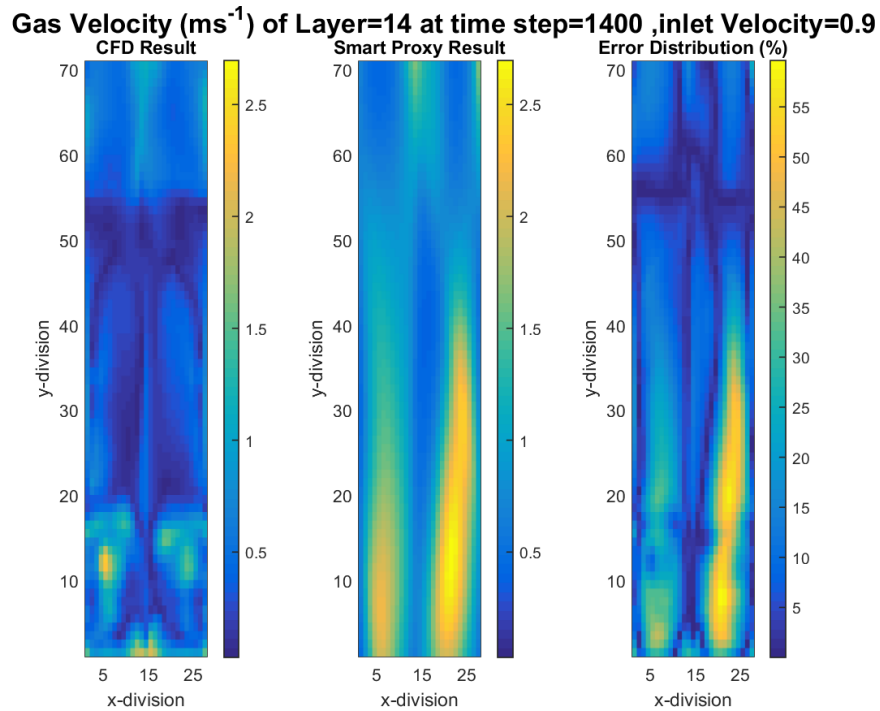


**Figure 11-3** CFD and smart proxy results for gas velocity at time step=1400,  $V_{\text{in}}=0.9$  m/s and  $K=4$  cross-sectional plane, using 11 static parameters

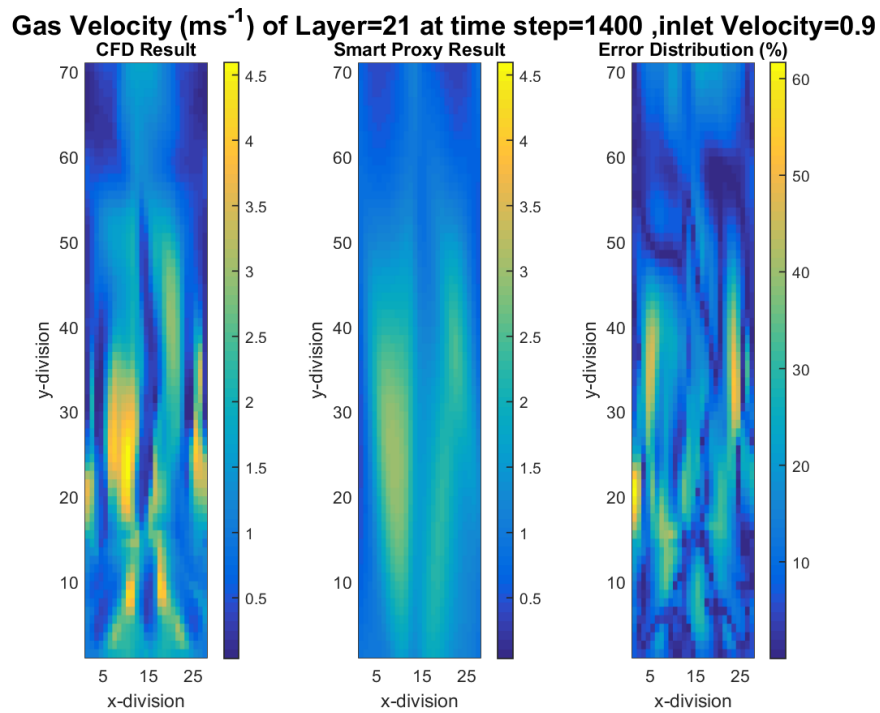


**Figure 11-4** CFD and smart proxy results for gas velocity at time step=1400,  $V_{\text{in}}=0.9$  m/s and  $K=21$  cross-sectional plane, using 11 static parameters

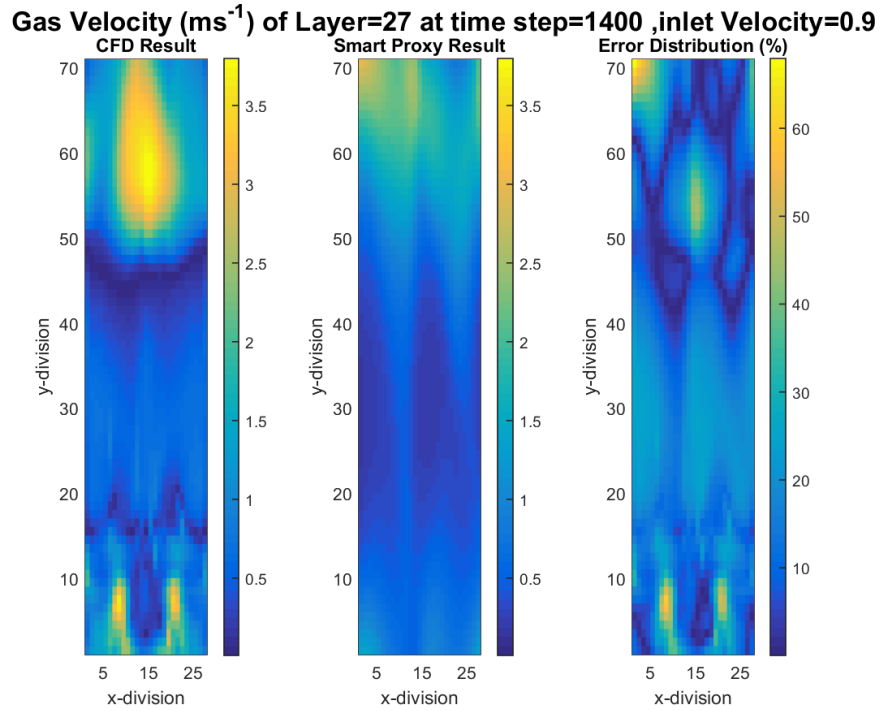


**Figure 11-5** CFD and smart proxy results for gas velocity at time step=1400,  $V_{in}=0.9$  m/s and  $K=27$  cross-sectional plane, using 11 static parameters

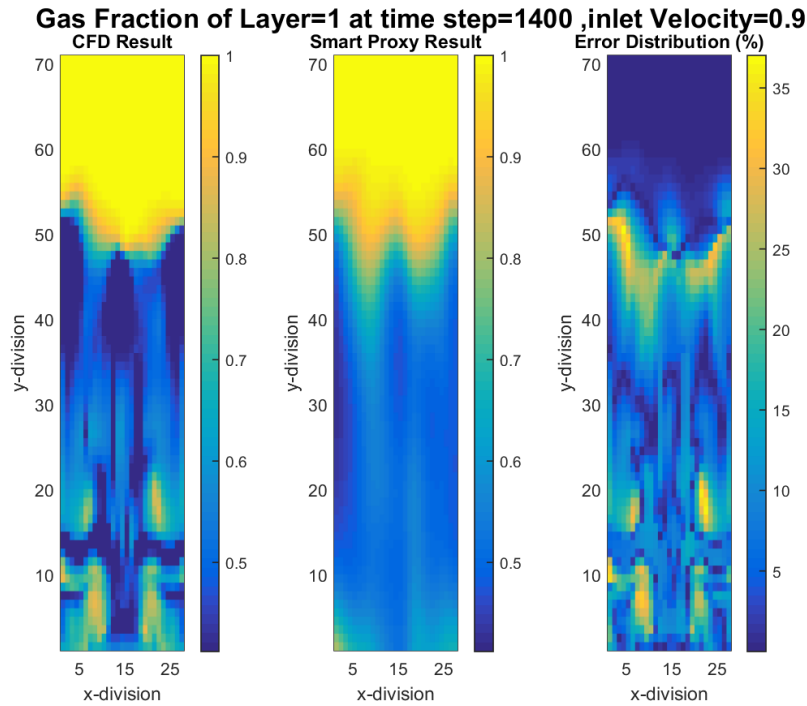


**Figure 11-6** CFD and smart proxy results for gas volume fraction at time step=1400,  $V_{in}=0.9$  m/s and  $K=1$  cross-sectional plane, using 11 static parameters

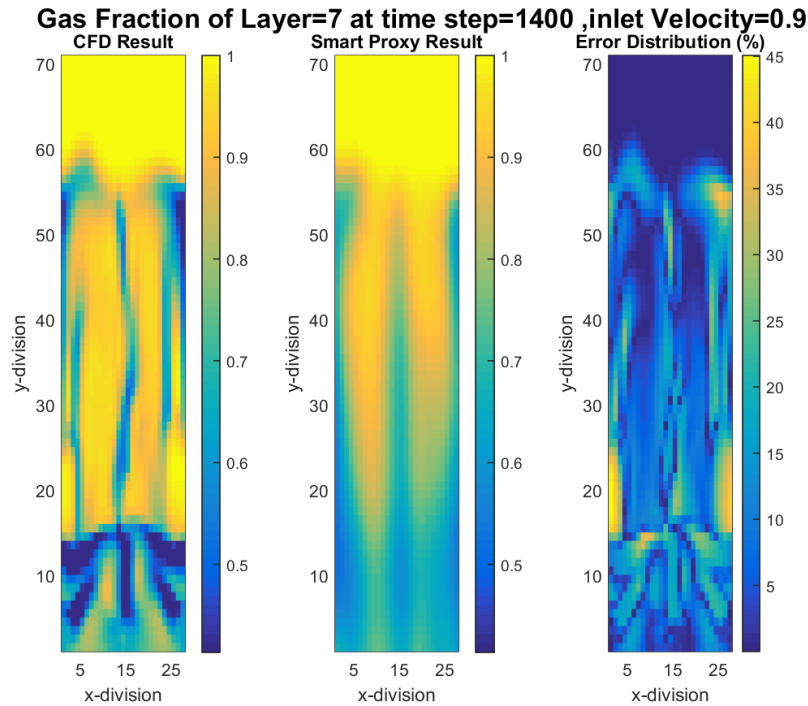


Figure 11-7 CFD and smart proxy results for gas volume fraction at time step=1400,  $V_{in}=0.9$  m/s and  $K=7$  cross-sectional plane, using 11 static parameters

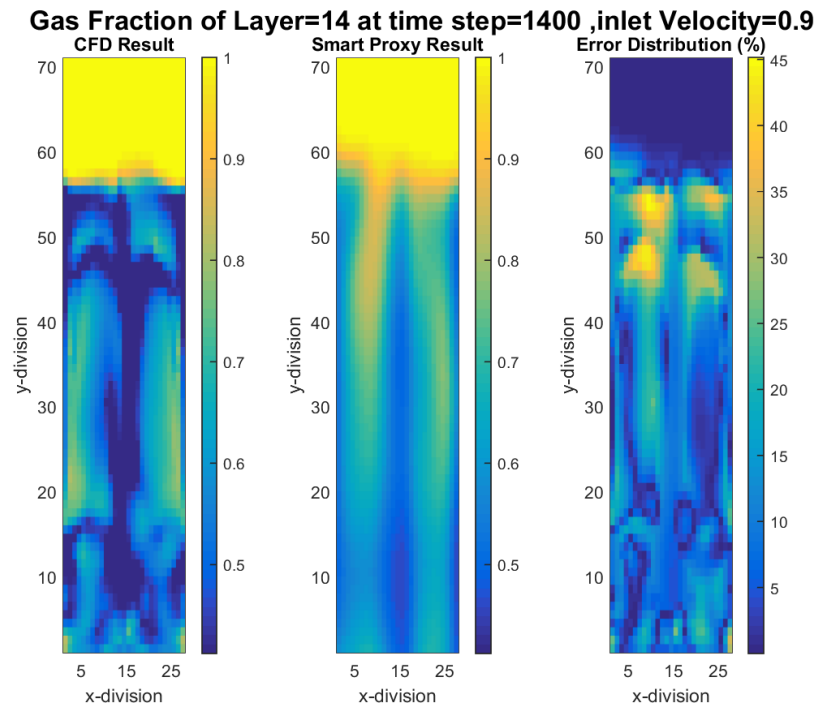


Figure 11-8 CFD and smart proxy results for gas volume fraction at time step=1400,  $V_{in}=0.9$  m/s and  $K=14$  cross-sectional plane, using 11 static parameters

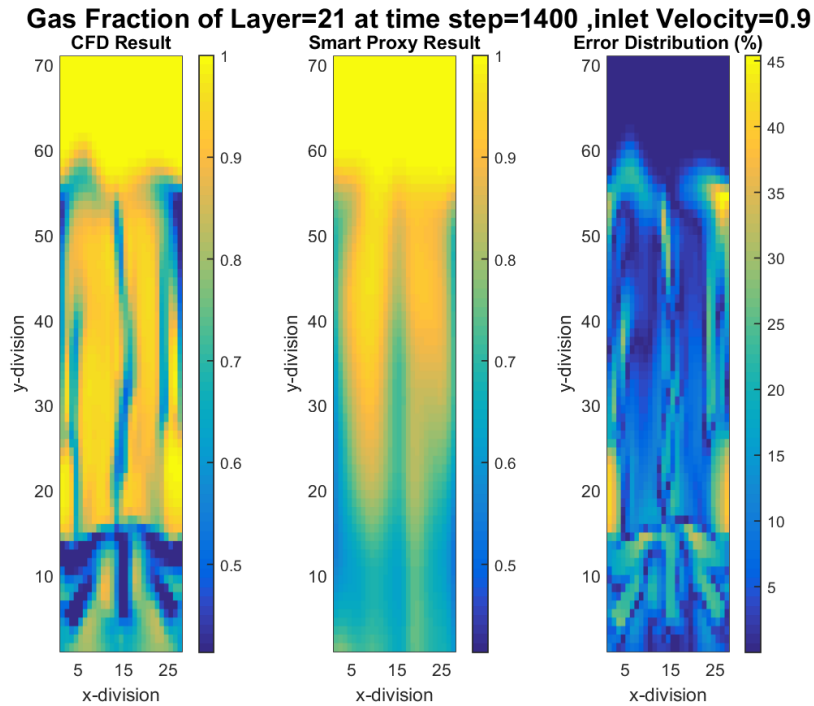


Figure 11-9 CFD and smart proxy results for gas volume fraction at time step=1400,  $V_{in}=0.9$  m/s and  $K=21$  cross-sectional plane, using 11 static parameters

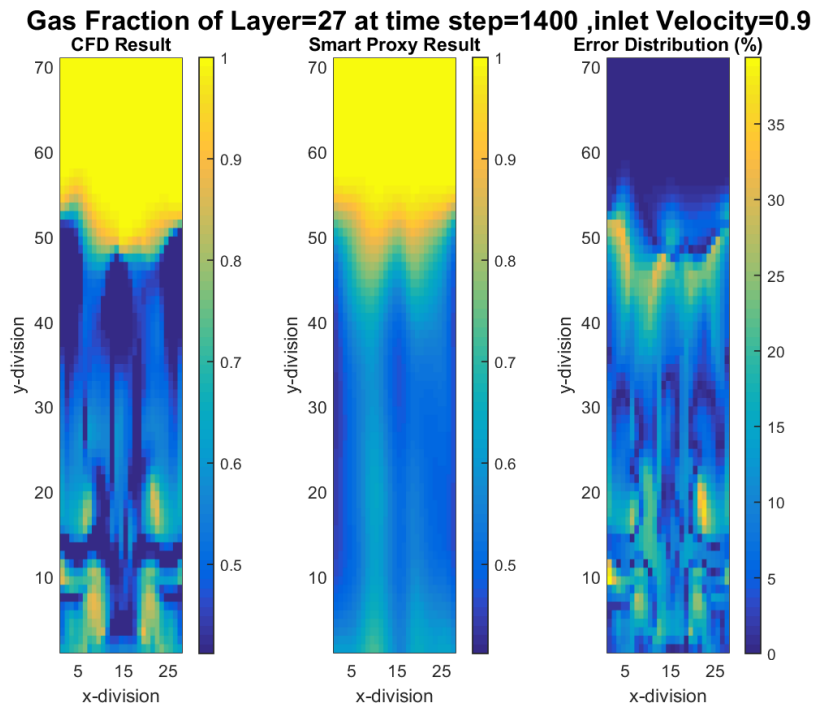


Figure 11-10 CFD and smart proxy results for gas volume fraction at time step=1400,  $V_{in}=0.9$  m/s and  $K=27$  cross-sectional plane, using 11 static parameters



**Sean Plasynski**

Executive Director  
Technology Development & Integration  
Center  
National Energy Technology Laboratory  
U.S. Department of Energy

**John Wimer**

Associate Director  
Strategic Planning  
Science & Technology Strategic Plans &  
Programs  
National Energy Technology Laboratory  
U.S. Department of Energy

**David Alman**

Executive Director  
Research & Innovation Center  
National Energy Technology Laboratory  
U.S. Department of Energy

